

On the relevance of optimization methods for
the systematic improvement of combustion
reaction mechanisms

DISSERTATION

submitted to the Combined Faculties for the Natural Sciences and for
Mathematics of Rupertus Carola University of Heidelberg, Germany for the
degree of Doctor of Natural Sciences

submitted by M.Sc. Marc Fischer born in Metz, France

**Ruprecht-Karls-Universität Heidelberg Interdisziplinäres Zentrum
für Wissenschaftliches Rechnen 2011**

On the relevance of optimization methods for
the systematic improvement of combustion
reaction mechanisms

DISSERTATION

submitted to the Combined Faculties for the Natural Sciences and for
Mathematics of Rupertus Carola University of Heidelberg, Germany for the
degree of Doctor of Natural Sciences

presented by M.Sc. Marc Fischer born in Metz, France

**Ruprecht-Karls-Universität Heidelberg Interdisziplinäres Zentrum
für Wissenschaftliches Rechnen 2011**

**On the relevance of optimization
methods for the systematic
improvement of combustion reaction
mechanisms**

Supervisor: Prof. Dr. Uwe Riedel
Reviewer: _____

Abstract

This work concerns the use of optimization methods to systematically improve the agreement of chemical kinetic combustion models with available experimental profiles. Under many circumstances, chemical kinetic parameters can neither be evaluated analytically from experiments nor accurately calculated through quantum chemistry methods. Thus, optimization methods relying on the numerical solution of the underlying differential equations (accounting for the experiments) are needed [14].

The program package Kinefit has been developed in C++. Based on the software Homrea, for the simulation of gas phase homogeneous systems, it allows the optimization/estimation of parameters against experimental data. It uses four optimization methods, namely an adaptive Random Search (RS), a Genetic Algorithm (GA) and CONDOR and BOBYQA, two optimization programs based on trust regions. Since in many cases several sub-optimal local minima exist, the three local optimization methods (RS, BOBYQA and CONDOR) were globalized through the introduction of random restarts in the parameter space.

The classical analysis methods for reaction mechanisms (sensitivity analyses and reaction flow analysis) have proven to be insufficient for identifying the influential parameters suitable for the optimization. Thus, a new method, called "reaction significance analysis" has been developed. It shows the influence of all parameters on the global distance between model prediction and experimental values. Only the parameters having a significant influence are candidates for the optimization. Box constraints on each parameter are often not sufficient if several parameters of the same reaction are optimized simultaneously. Consequently, penalty terms were implemented to put constraints on the whole reaction rate coefficient.

Numerical tests were created to validate the optimization methods. They use the $\text{H}_2 - \text{O}_2$ sub-mechanism of the GRI-mechanism [54]. Artificial experimental profiles were generated using all initial values of the parameters. The most influential parameters were then identified and modified in such a way to introduce great discrepancies with the "experimental" profiles. One cause of the oscillations of the distance as a function of separately varied parameters was identified: it is related to the exponential decrease of concentrations due to self-ignition. Optimization problems based on six experiments with respectively three profiles were constructed. The optimization methods were first validated for problems without self ignition. It was shown that they can reliably identify optimal parameter sets for problems involving respectively 6

pre-exponential factors, six pre-exponential factors located on bounds while using the penalty terms and 6 pre-exponential factors, temperature coefficients and activation energies. The optimization methods were then validated for problems where a significant amount of oscillations occur. All methods were able to solve a problem involving seven parameters, all methods except one could solve a problem with 7 temperature coefficients and activation energies. All optimization methods failed for a complex problem involving seven pre-exponential factors, temperature coefficients and activation energies.

The program package Kinefit was then used to evaluate whether or not the GRI-mechanism is refuted by real experiments involving the pyrolysis of CH_3 and C_2H_6 [47]. With the initial parameter values, considerable discrepancies exist whereas after the optimization good agreements were achieved.

Mechanism reduction methods are often utilized for chemical kinetic optimization and can be relevant for problems pertaining to soot formation, always characterized by very large reaction mechanisms. As a consequence a C++ reduction program was developed during this work. The reliability of reduction approaches in the context of parameter optimization was evaluated on an example involving the experiments of CH_3 and C_2H_6 pyrolysis to which the GRI-mechanism was optimized [47]. The results indicate that reduction methods are only reliable for optimization problems where parameters are varied within narrow ranges.

Finally, the program package Kinefit was employed for an optimization problem involving a semi-detailed reaction mechanism accounting for the pyrolyses of the propargyl radical and 1,5-hexadiene [59]. Propargyl is a vital species for accurate simulations of PAH (PolyAromatic Hydrocarbons) and soot formation since it plays a crucial role for the formation of the first aromatic ring [33].

Zusammenfassung

Diese Arbeit betrifft die Verwendung von Optimierungsmethoden, um systematisch die Übereinstimmung zwischen kinetischen Verbrennungsmodellen und verfügbaren experimentellen Verläufen zu verbessern. Oft können chemische kinetische Parameter weder aus Experimenten analytisch eingeschätzt noch durch quantenchemische Methoden berechnet werden. Deswegen werden Optimierungsverfahren benötigt, die auf der numerischen Lösung von den die Experimente beschreibenden Differentialgleichungen beruhen. [14].

Das Programm-Paket Kinefit wurde in C++ entwickelt. Es beruht auf der Software Homrea, für die Simulation von homogenen Systemen der Gasphase, und erlaubt die Optimierung/Schätzung von Parametern in Bezug auf experimentelle Daten. Es benutzt vier Optimierungsverfahren, nämlich eine adaptive Randomssuche (RS), einen genetischen Algorithmus (GA) und CONDOR und BOBYQA, zwei Trust-Region basierte Optimierungsprogramme. Da in vielen Fällen mehrere suboptimale lokale Minima existieren, werden die drei lokalen Optimierungsmethoden (RS, BOBYQA und CONDOR) globalisiert, indem zufällige Neustarts im Parameterraum eingeführt werden.

Die klassischen Analysemethoden für Reaktionsmechanismen (Sensitivitätsanalysen und Reaktionsflußanalysen) haben sich als ungenügend herausgestellt, um die für die Optimierung geeigneten sensitiven Parameter zu identifizieren. Deswegen wurde eine neue Methode, die Reaktionsignifikanzanalyse, entwickelt. Sie zeigt den Einfluß von allen Parametern auf die globale Distanz zwischen den Vorhersagen des Modells und den experimentellen Werten. Lediglich die Parameter, die einen bedeutsamen Einfluß haben sind Kandidaten für die Optimierung.

Box constraints für jeden Parameter reichen oft nicht aus, wenn mehrere Parameter der selben Reaktion gleichzeitig optimiert werden müssen. Deshalb werden Strafterme implementiert, um Nebenbedingungen dem gesamten Reaktionsgeschwindigkeitskoeffizient zu erzwingen.

Numerische Tests wurden zur Validierung der Optimierungsverfahren ausgeführt. Sie beruhen auf dem $\text{H}_2 - \text{O}_2$ Teilsystem des GRI-Mechanismus. [54]. Künstliche experimentelle Verläufe wurden durch Verwendung aller ursprüngliche Parameterwerte generiert. Die sensitivsten Parameter wurden dann identifiziert und so modifiziert, dass große Diskrepanzen mit den pseudo-experimentellen Verläufen eingeführt wurden. Eine Ursache der Oszillationen der Distanz als Funktion von getrennt variierten Parametern wurde identifiziert: es hängt mit der exponentialen Abnahme von Konzentrationen wegen der Selbstzündung zusammen. Optimierungsprobleme wurden konstruiert, die

auf sechs Experimenten mit jeweils drei Verläufen beruhen. Die Optimierungsverfahren wurden zuerst für Probleme ohne Selbstzündung validiert. Es wurde gezeigt, dass sie zuverlässig sind, um optimale Parametersätze für Probleme zu identifizieren, die jeweils 6 prä-exponentiale Faktoren, 6 sich auf Grenzen befindenden prä-exponentialen Faktoren und 6 prä-exponentialen Faktoren, Temperaturkoeffizienten und Aktivierungsenergien involvieren. Die Optimierungsmethoden wurden dann für Probleme validiert, wo viele Oszillationen auftreten. Alle Methoden waren im Stande, ein Problem mit sieben prä-exponentialen Faktoren zu lösen. Alle Methoden außer eine konnten ein Problem mit 7 Temperaturkoeffizienten und Aktivierungsenergien lösen. Alle Optimierungsverfahren scheiterten an einem komplexen Problem, das 7 prä-exponentielle Faktoren, Temperaturkoeffizienten und Aktivierungsenergien involvierte.

Das Programm-Paket Kinefit wurde dann verwendet, um herauszufinden, ob der GRI-Mechanismus von realen Experimenten widerlegt wird, die die Pyrolyse von CH_3 und C_2H_6 [47] involvieren. Während erhebliche Diskrepanzen mit den ursprünglichen Parameterwerten vorlagen, wurde eine gute Übereinstimmung durch die Optimierung erreicht. Reduktionsmethoden für Reaktionsmechanismen werden oft für die chemische kinetische Optimierung benutzt und können relevant für die die Rußbildung betreffenden Probleme sein, da solche Probleme immer durch sehr breite Reaktionsmechanismen charakterisiert werden. Als Konsequenz wurde ein C++ Reaktionsprogramm im Laufe dieser Arbeit entwickelt. Die Zuverlässigkeit von Reduktionsverfahren im Rahmen von Parameteroptimierung wurde an einem Beispiel eingeschätzt, das die oben genannten Experimente mit CH_3 und C_2H_6 Pyrolyse involvierte. Die Resultate weisen darauf hin, dass Reduktionsmethoden nur für Optimierungsprobleme zuverlässig sind, wo Parameter innerhalb engen Grenzen optimiert werden.

Letzlich, das Programm Packet Kinefit wurde für ein Optimierungsproblem verwendet, das einen halbdetaillierten Mechanismus involviert, der die Pyrolyse von Propargyl und 1,5-Hexadyne beschreibt [59]. Propargyl ist eine wesentliche Spezies für präzisen Simulationen der PAK (PolyAromatischen Kohlenwasserstoffe)- und Rußbildung, da es eine entscheidende Rolle für die Bildung des ersten aromatischen Ringes spielt.

Danksagung

Vor allem will ich Professor Jürgen Warnatz danken, der mich vor mehr als vier Jahren als Doktorand angenommen hatte. Von seinem Tod wurde ich zutiefst erschüttert und hätte gewünscht, diesen hervorragenden Wissenschaftler ein zweites Mal zu treffen. Ich bin Uwe Riedel und Elke Goos äußerst dankbar, die Betreuung übernommen zu haben, und mich durch zahlreiche Ratschläge und Hinweise ermutigt zu haben, ohne eure Hilfe würde dieses Projekt nicht vollendet sein. Meine Dankbarkeit gilt auch besonders meinen Kollegen Jens Marquetand und Iliyana Naydenova, deren wertvollen Meinungen ich hochgeschätzt habe. Die zahlreichen Diskussionen mit Thomas Hoffmann und Georgiana Baldea haben häufig meine Stimmung erhoben und mir die Motivation für die bevorstehenden Aufgaben aufgebracht. Ich will mich auch bei Stefan Körkel und Mario Mommer bedanken, deren Fachkenntnisse in Optimierung und Parameterschätzung sehr nützlich waren. Das ständige gute Gemüt von Stefan war mir auch besonders angenehm. Natürlich will ich auch meinen Eltern und meinen Freunden in Heidelberg vom ganzen Herzen danken.

Contents

1	Introduction	7
2	Basics of chemical kinetics applied to combustion problems	11
2.1	Chemical Kinetics	11
2.1.1	Thermochemistry	11
2.1.2	Elementary reactions	13
2.1.3	Pressure dependent reactions	16
2.2	Simplified Combustion systems	19
2.2.1	General characteristics	19
2.2.2	Shock tubes	20
2.2.3	Rapid Compression Machines	21
2.2.4	Plug Flow reactors	21
2.3	Mathematical handling and analysis of the problem	21
2.3.1	Formulation of the underlying ODE system	21
2.3.2	Sensitivity analyses	23
2.3.3	Reaction flow analyses	25
3	Optimization and estimation of kinetic parameters	26
3.1	Theoretical bases	26
3.1.1	Motivation	26
3.1.2	Choice of the norm	28
3.1.3	Mathematical formulation of a kinetic parameter optimization problem	32
3.1.4	Statistical interpretation of an optimization problem	33
3.2	The optimization program library Kinefit	35
3.2.1	General characteristics of the optimization interface	35
3.2.2	Optimization methods used by Kinefit	36
3.2.3	Consideration of non-linear constraints	39
3.2.4	Analyses of reaction significances	42

4	Numerical tests	43
4.1	Oscillation of the distance	44
4.2	Optimization when no oscillations happen	50
4.2.1	Optimization of six pre-exponential factors	50
4.2.2	Optimization of six pre-exponential factors located on bounds	56
4.2.3	Optimization of six pre-exponential factors, tempera- ture coefficients and activation energies	58
4.3	Optimization when fluctuations take place	60
4.3.1	Optimization of seven pre-exponential factors	60
4.3.2	Optimization of seven temperature coefficients and seven activation energies	68
4.3.3	Optimization of seven pre-exponential factors, temper- ature coefficients and activation energies	73
4.4	Experimental information and parameter accuracy	81
4.5	Conclusion of the validation of the optimization methods	88
5	Application of the optimization methods to the GRI-mechanism	90
6	Mechanism reduction	103
6.1	Motivation	103
6.2	Overview of existing approaches	104
6.3	Description and validation of the program Mechacut	105
6.4	Application to the optimization of large reaction mechanisms	109
7	Parameter estimation for benzene formation during propargyl pyrolysis	116
7.1	Relevance for soot formation and characterization of the sys- tem	116
7.2	First trial to determine an optimal propargyl-subsystem	117
7.2.1	Structure of the mechanism	117
7.2.2	Comparison between Tang's mechanism and mechanisms Ma and Mb	123
7.3	Optimization of the mechanism Ma	128
7.3.1	Use of the chi-squares Norm	129
7.3.2	Use of a new customized norm	136
7.3.3	Sucessive optimization of Ma	142
7.4	Addition of two isomerization reactions to the mechanism Ma	153
7.5	Conclusion of the optimization trials	156
8	Conclusion	158

Chapter 1

Introduction

Ever since the first industrial revolution, combustion technologies have proven a crucial driver of development, from the global economy point of view to the every day life of billions of people all over the Earth, whose environment has been heavily impacted. Among others, combustion has been used for heating, for car engine locomotive energy, for producing electricity and incinerating non-recyclable wastes. Two major concerns have arisen with respect to the use of combustion processes. On the one hand, optimizing the combustion conditions is highly desirable from an economical standpoint in such a way that greater quantities can be produced at a lesser cost. Optimal conditions include among others fuel and oxidant with their initial concentrations, shape and size of the reactor, initial temperature and pressure, and duration of the process. On the other hand, it has become quite clear over the last century that combustion processes also release many harmful compounds for both the environment and the health of human beings. Among those, soot particles and their precursors PAH (Polycyclic Aromatic Hydrocarbons) can penetrate deeply into the lungs and be absorbed on their surfaces. There, they become important factors of heart attacks, strokes, cardiovascular deaths [11] and lung cancer [42]. However noxious, soot can also be a useful product in the form of carbon black [19] which is employed among others in the production of automotive tires as a reinforcing agent for rubbers or to provide colour for printing ink, painting, paper, and plastics.

To find good combustion conditions, which ideally should both maximize the desired outcome and minimize the amount of pollution emitted, the past traditional method would carry out great numbers of actual experiments in complex practical systems like car engines in such a manner that better conditions could be identified. This approach proves however to be very expensive, thus driving to developing models capable of simulating the combustion processes under various conditions. If a model were able to accurately reproduce

realistic situations, calibration would need only a limited number of experiments to estimate parameters of the model, which would then bring about optimal initial conditions in terms of efficiency and pollutants. All these rely on mathematical optimization methods instead of numerous costly experiments. Such models for the simulation of combustion processes are basically composed of two highly interacting parts:

1. the physical description of the systems including flow and diffusion effects, heat transport and thermodynamics,
2. the chemical description of the systems which consists in reaction mechanisms accounting for the chemistry going on under the conditions of the process.

Since the computation time required for the simulation of real three-dimensional industrial systems is extremely high, the reaction mechanisms used in such cases are extremely simplified. To decouple the study of the physical aspects of the problem from the chemical description, experiments targeting the chemistry alone are carried out on simplified systems such as shock tubes, rapid compression machines, laminar flow reactors, and pre-mixed flames where the concentrations and other variables depend only on either time or distance. Since simplified empirical reaction mechanisms for intensive CFD calculations cannot describe the real chemistry under every possible situation, fitting their parameters through a series of practical experiments is enough as long as they encompass all conditions of the real system. It is however universally recognized among researchers that the development of micro-kinetic detailed reaction mechanisms has been a great step forward for both the chemical understanding and the predictability of combustion systems. Such reaction mechanisms include all possible elementary reactions that can occur with certain combustibles under a wide variety of conditions. They allow a detailed description of the chemical processes taking place on a molecular level.

The determination of parameters corresponding to the chemical reality is a complex task. Traditionally, it has been realized under three different manners

1. By designing experiments isolating some reactions in such a way that the model concentrations corresponding to the measured ones can be expressed analytically as a function of parameters of interest. The optimal values can then mathematically be identified through a least-squares regression.

2. By using methods from theoretical chemistry such as Density Functional Theory (DFT) calculations [64] coupled with Transition State Theory (TST). Depending on the assumptions and simplifications done, eg. through limited computer resources, some methods, especially semi-empirical methods, can lead to great uncertainties with respect to the evaluated parameters.
3. By analogy with similar reactions with known rate coefficients. An unknown uncertainty is also introduced by this approach.

If the reaction mechanism contains all possible reactions playing a role in the experiments and enough profiles are available for an unambiguous estimation, the first method is the most promising for obtaining parameter values with great accuracy. Nevertheless, most chemical kinetic system cannot be simplified enough to provide analytical expressions within a reasonable accuracy suitable for the parameter estimation. In such a case, an optimization method minimizing the distance $d(p)$ between experimental results and model predictions by solving numerically the underlying system of differential equations for different set of parameter values must be engaged.

Many researchers in the chemical kinetics community are sceptical of the greedy use of optimization techniques, for good reasons. If they are employed only for fitting some parameters to a small number of experimental profiles, it is extremely likely that the resulting parameters will prove false. This in turn will lead to apparent discrepancies for other profiles which were previously well predicted. Another concern is the completeness of the reaction mechanism: if reactions that are significant for the profiles at hand are absent, the parameter optimization will lead to false values even if the discrepancies have been considerably reduced by the minimization of the distance $d(p)$.

A good parameter estimation/optimization must therefore always include all relevant reactions for the experiment set. The complete set of experiments should ideally include all existing experiments where the parameters of interest play a role. Often, all experiments owing to the computational time cannot be included. Frequently, identifying groups of similar experiments is sufficient, enabling the selection of just one representing the whole group for the estimation. The optimized mechanism is then often capable of well predicting the experiments not considered during the minimization. The purpose of the present work is to evaluate how relevant optimization methods are for the systematic improvement of reaction mechanisms in simplified combustion systems. A particular application field is the formation of PAH and soot.

In chapter 2, the fundamental elements of combustion kinetics necessary to understand this work are provided. The mathematical formulation of such problems is also shown.

In chapter 3, the mathematical formulation of parameter optimization problems in chemical kinetics is described in detail, and the optimization program Kinefit, developed during the course of this thesis in C++, is presented. In chapter 4, the four different optimization methods present in Kinefit are validated by building up artificial optimization problems. Pseudo-experimental profiles are first produced using the exact parameter values of a reaction mechanism. Afterward, huge variations of sensitive parameters are introduced, in order to lead to great discrepancies with the experimental profiles. The abilities of the optimization approaches to retrieve the initial perfect agreement are then compared.

In chapter 5, the consistency of the GRI-mechanism 3.0 (a reaction mechanism aiming at describing the combustion of methane [54]) with a set of experiments is evaluated. Considerable discrepancies exist for the initial parameter values. The following question is then asked: are there reasonable ranges of parameter values consistent with the mechanism, or in other words, is the model refuted by the experimental profiles or not ?

Since reaction mechanism reduction/simplification methods are widely used in the combustion community, also for the optimization of parameters (see [14], [46], and [54]), the reliability of the results obtained through such techniques has been evaluated in chapter 6.

Due to their tremendous impact on human health, environment, and economy, a better understanding of the chemistry pertaining to soot and its precursors is vital. Thus, in chapter 7, the optimization of a semi-detailed reaction mechanism relevant for soot formation against real experimental data is carried out.

Chapter 2

Basics of chemical kinetics applied to combustion problems

2.1 Chemical Kinetics

2.1.1 Thermochemistry

The most obvious and fundamental feature of combustion consists of the release of energy. The chemical reactions taking place in combustion systems are accompanied by the release or consumption of energy, thereby determining the temporal evolution of the temperature which exerts itself a strong influence on many reaction rates. The enthalpy change provoked by the reaction $v_A A + v_B B \rightarrow v_C C + v_D D$ is given by $\Delta H = v_C H_C + v_D H_D - v_A H_A - v_B H_B$. More generally for a reaction

$$\sum_{i=1}^{n_{Sp}} v_i S p_i = 0$$
$$\Delta H = \sum_{i=1}^{n_{Sp}} v_i H_i, \quad (2.1)$$

that is the sum of the enthalpy of each species $S p_i$ multiplied by the stoichiometric coefficient v_i which is positive for products and negative for reactants. Similarly, the entropy change is

$$\Delta S = \sum_{i=1}^{n_{Sp}} v_i S_i. \quad (2.2)$$

For each species $S p_i$ the free enthalpy is defined as

$$G_i = H_i - T S_i, \quad (2.3)$$

T being the temperature of the system. The free enthalpy change corresponding to the reaction is then

$$\Delta G = \sum_{i=1}^{n_{Sp}} v_i G_i. \quad (2.4)$$

The heat capacity C_p at constant pressure describes the temperature change dT of a system receiving an heat quantity δQ :

$$C_p = \frac{\delta Q}{dT}. \quad (2.5)$$

If the reaction rate (see subsection 2.1.2) of the forward reaction $\sum_{i=1}^{n_{Sp}} v_i S_i = 0$ is known, then the reaction rate of the backward (or reverse) reaction $\sum_{i=1}^{n_{Sp}} -v_i S_i = 0$ is given by:

$$k_r(T) = \frac{k(T)}{K(T)}, \quad (2.6)$$

whereby $K(T)$, the equilibrium constant of the reaction, can be deduced from the thermodynamic data. In effect,

$$K(T) = K_p(T) \left(\frac{p^0}{RT} \right)^{\sum_{i=1}^{n_{Sp}} v_i} \quad \text{with } K_p(T) = e^{\frac{-\Delta G^0}{RT}}, \quad (2.7)$$

where K_p is the equilibrium constant in pressure units, p_0 the standard pressure which is equal to 1.013 bar, R the ideal gas constant, T the temperature, and ΔG^0 is the molar free enthalpy of the reaction under standard conditions as defined above. To express the standard free enthalpy G_i^0 and heat capacity $C_{p,i}^0$ of a species as a function of the temperature T of the system, interpolations have been carried out and series of coefficients have been determined and regrouped within thermodynamic tables such as those of Stull and Prophet [57], Kee et al. [21], Burcat [8] and so on. For a given species, the three thermodynamic variables are then given in the form of so-called NASA polynomials, according to the formula below.

$$\frac{C_p^0}{R} = a_1 + a_2 T + a_3 T^2 + a_4 T^3 + a_5 T^4 \quad (2.8)$$

$$\frac{H^0}{RT} = a_1 + a_2 \frac{T}{2} + a_3 \frac{T^2}{3} + a_4 \frac{T^3}{4} + a_5 \frac{T^4}{5} + \frac{a_6}{T} \quad (2.9)$$

$$\frac{S^0}{RT} = a_1 \ln T + a_2 T + a_3 \frac{T^2}{2} + a_4 \frac{T^3}{3} + a_5 \frac{T^4}{4} + a_7, \quad (2.10)$$

where $a_1, a_2, a_3, a_4, a_5, a_6, a_7$ are the numerical coefficients stored in NASA thermodynamic files. The values of the three thermodynamic functions used for the interpolations stem from experiments or theoretical and semi-empirical calculations based on quantum chemistry. For the atom oxygen in the GRI-mechanism 3.0 (a reaction mechanism aiming at describing the combustion of methane [54]), they are given in the following form in a thermodynamic file

```

O          L 1/900  1          G  200.000  3500.000  1000.000  1
2.56942078E+00 -8.59741137E-05 4.19484589E-08 -1.00177799E-11 1.22833691E-15  2
2.92175791E+04 4.78433864E+00 3.16826710E+00 -3.27931884E-03 6.64306396E-06  3
-6.12806624E-09 2.11265971E-12 2.91222592E+04 2.05193346E+00  4

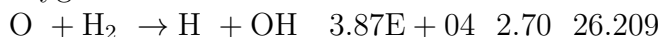
```

Figure 2.1: Thermodynamic data of oxygen

The seven first coefficients are valid on the interval [1000, 3500 K] whereas the seven last coefficients are valid on the interval [200, 1000 K]. This separation in two temperature intervals applies to all species present in such thermodynamic tables. It allows a more accurate interpolation of the three thermodynamic functions.

2.1.2 Elementary reactions

An elementary reaction describes the reactive encounter between molecules or atoms and its outcomes as it really takes place at the molecular level. For example, an important reaction of the $\text{H}_2 - \text{O}_2$ system as found in the GRI-mechanism 3.0 [54] is the H-abstraction of an hydrogen molecule by an oxygen radical



where the three values after the reaction are respectively the pre-exponential factor A (in mol/cm^3), the temperature coefficient n and the activation energy E_a (in kJ/mol). The reaction rate of the reaction is then given by

$$r = -\frac{d[\text{O}]}{dt} = -\frac{d[\text{H}_2]}{dt} = \frac{d[\text{H}]}{dt} = \frac{d[\text{OH}]}{dt} = k_r [\text{O}] [\text{H}_2] \quad (2.11)$$

with k_r being the reaction rate coefficient. Generally, the number of reactants and the number of products of an elementary reaction never exceed three since it is extremely unlikely that a greater number of molecules or radicals would meet simultaneously and react during one single physical collision. The rate of an elementary reaction is always equal to the product of the reaction rate coefficient with the concentrations of all reactants participating in the

reaction. The reaction rate coefficient itself is given by

$$k_r = A T^n e^{-\frac{E_a}{RT}}. \quad (2.12)$$

The so-called collision theory of bi-molecular reactions [3] gives a simplistic explanation of this law. The extended pre-exponential factor AT^n accounts for the frequency of the collision between molecules which meet each other in the appropriate orientation. For a bi molecular reaction $A + B \rightarrow C + D$ the number of collisions per time and volume units can be approximated as

$$Z = \sigma \left(\frac{8kT}{\pi\mu} \right)^{\frac{1}{2}} N_A^2 [A] [B]. \quad (2.13)$$

N_A is the Avogadro's constant, the number of species in one mole, equal to $6.022 \cdot 10^{23} \text{mole}^{-1}$.

σ is the collision diameter $\sigma = \pi d^2$ with $d = \frac{1}{2}(d_A + d_B)$, d_A and d_B being the diameters of A and B respectively. $\mu = \frac{m_A m_B}{m_A + m_B}$ is the reduced mass of A and B. A sterical factor P is introduced in order to account for the fact that collisions between two molecules must satisfy geometrical constraints in order to allow a reaction to occur. The pre-exponential factor in mole per volume units is therefore

$$A = P\sigma \left(\frac{8kT}{\pi\mu} \right)^{\frac{1}{2}} N_A. \quad (2.14)$$

The molecules must then have enough energy in order to react. The activation energy E_a corresponds to the threshold of bond energies that the molecules must overcome in order to react and form the product. The frequency of molecules overcoming this barrier is then given by $e^{-\frac{E_a}{RT}}$. The reaction rate in moles per volume units is thus

$$k_r = P\sigma \left(\frac{8kT}{\pi\mu} \right)^{\frac{1}{2}} N_A e^{-\frac{E_a}{RT}}. \quad (2.15)$$

The temperature coefficient n describes the temperature influence on the collision frequency and would always be 0.5 if the collision theory were correct. Due to some shortcomings, this theory is only useful to get an intuitive representation of what is really happening during an elementary reaction. In many respects, the Transition State Theory (TST) [3] provides a much better description of the processes taking place here. The TST postulates that there exists a continuous trajectory between the reactants and the products marked by a transition state which corresponds to a saddle point of the hyperspace

representing the potential energy of the molecular system. Let us visualize this with the bi-molecular reaction $A + B \rightarrow C + D$. According to the TST, the reaction can be divided into $A + B \rightarrow AB^\ddagger$ and $AB^\ddagger \rightarrow C + D$, that is the reactants first come together to form the so-called activated complex AB^\ddagger which will itself decomposes into the products. The energetic aspect of the process can be visualized in figure 2.2.

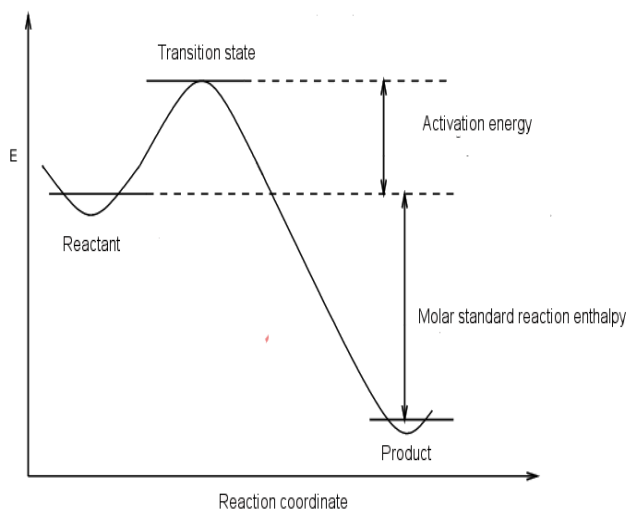


Figure 2.2: Energy profile of an elementary reaction

In a figurative sense, E_a is the energy necessary to climb up the mount before getting into the slope towards the valley. It is assumed that the rate coefficient of decomposition of the activated complex k_d is proportional to the frequency of oscillations along the reaction coordinate ν :

$$k_d = \kappa\nu, \quad (2.16)$$

where κ is the so-called transmission coefficient which is close to unity in many cases. The reaction rate k_r is then given by the Eyring-equation [3]:

$$k_r = \kappa \frac{kT}{h} K. \quad (2.17)$$

k designates the Boltzmann's constant, h the Planck's constant whereas K is akin to an equilibrium constant of the reaction $A + B \rightarrow AB^\ddagger$ and is given by the formula

$$K = \frac{RT}{p^-} \frac{N_A q_{AB}}{q_A q_B} e^{-\frac{E_a}{RT}}, \quad (2.18)$$

where q_A , q_B and q_{AB} are the partition functions of A, B and the activated complex $AB^\#$ respectively. p^- designates the standard pressure equal to 1 bar. Through methods from quantum chemistry like ab-initio and DFT calculations, the configuration and geometry of the activated complex $AB^\#$ must be determined. The partition functions can then be calculated according to the laws and principles of statistical thermodynamics. At the same time, the theoretical calculations also allow to evaluate the activation energy E_a which is the difference between the potential energy of the activated complex and the sum of the potential energies of the reactants.

2.1.3 Pressure dependent reactions

Many reactions taking place in the gas phase are strongly dependent on pressure. This is the case because they need a third body (or collision partner) M, which can be an arbitrary species, in order to either bring up the energy for a molecule dissociation or to receive the energy produced by the formation of a molecule (recombination). As an example, four recombination reactions from the GRI-mechanism 3.0 [54] are given in table 2.1.

Reaction	A	n	E_a
$O + O + M(2) \rightarrow O_2 + M(2)$	1.20E+17	-1.00	0.00
$H + H + M(6) \rightarrow H_2 + M(6)$	1.00E+18	-1.00	0.00
$H + OH + M(9) \rightarrow H_2O + M(9)$	2.20E+22	-2.00	0.00
$H + O_2 + M(5) \rightarrow HO_2 + M(5)$	2.80E+18	-0.86	0.00

Table 2.1: Recombination reactions

A third body is needed in the forward direction because otherwise the activated molecule (e.g. O_2^*) would very quickly decompose into the initial reactants. A third body is also required in the backward direction in order to transmit the energy necessary for breaking the compound. Obviously, the efficiency of this energy transfer depends on the nature and geometrical shape of the collision partner. This fact is taken into account through the introduction of collision efficiency coefficients η_i for each species S_i . The effective concentration of the third body is then

$$[M] = \sum_{i=1}^{n_T} \eta_i [S_i], \quad (2.19)$$

with $[S_i]$ as the concentration of the species S_i , n_T being the number of species participating in the definition of the third body. For instance, the third bodies of the first reaction in table 2.1 with collision efficiencies not equal to 1 are H_2 with $n_{H_2} = 2.40$, H_2O with $n_{H_2O} = 15.4$, CH_4 with $n_{CH_4} = 2.00$, CO with $n_{CO} = 1.75$, CO_2 with $n_{CO_2} = 3.60$, C_2H_6 with $n_{C_2H_6} = 3.00$, and Ar

with $n_{Ar} = 0.83$. According to Lindemann (1922), a unimolecular reaction $A + M \rightarrow B + M$, whereby bonds of A are broken through the collision, can be understood as two elementary steps: $A + M \rightleftharpoons A^* + M$ and $A^* \rightarrow B$. Let us call k_1 the rate coefficient of the reaction $A + M \rightarrow A^* + M$, k_{-1} the rate coefficient of the reverse reaction and k_2 the rate coefficient of $A^* \rightarrow B$. The rate of the product formation is then

$$\frac{d[B]}{dt} = k_2[A^*]. \quad (2.20)$$

Since the activated molecule A^* is extremely unstable, its concentration will always remain very low. The steady state approximation can therefore be assumed. Thus

$$\frac{d[A^*]}{dt} = k_1[A][M] - k_{-1}[A^*][M] - k_2[A^*] = 0, \quad (2.21)$$

which allows to express $[A^*]$ as follows:

$$[A^*] = \frac{k_1[A][M]}{k_2 + k_{-1}[M]}. \quad (2.22)$$

As a consequence, the rate of the reaction may be expressed as a function of the kinetic parameters and reactant concentrations:

$$\frac{d[B]}{dt} = \frac{k_2 k_1 [A][M]}{k_2 + k_{-1}[M]}. \quad (2.23)$$

For very high pressures, the decomposition of A^* becomes the rate-limiting step.

$k_{-1}[M] \gg k_2$, hence one gets approximately

$$\frac{d[B]}{dt} = \frac{k_2 k_1 [A]}{k_{-1}}. \quad (2.24)$$

For very high pressures, the reaction is first order in A and the rate coefficient is thus

$$k_\infty = \frac{k_2 k_1}{k_{-1}}. \quad (2.25)$$

Now, for very low pressures, the activation of A by the third body becomes the rate limiting step. The reaction is second order in A and M and the reaction rate coefficient becomes

$$k_0 = k_1 \quad (2.26)$$

and

$$\frac{d[B]}{dt} = k_1[A][M]. \quad (2.27)$$

Generally, the reaction parameters of Lindemann's three elementary steps are difficult to evaluate experimentally or theoretically. It is usually much easier to estimate the high-pressure and low-pressure rate constants k_∞ and k_0 . Consequently, these are the parameters which are given in every reaction mechanism containing pressure dependent reactions. The rate coefficient is then given by the following equation:

$$k = \frac{k_\infty k_0}{k_\infty + k_0[M]}. \quad (2.28)$$

While Lindemann's model is useful and provides accurate predictions for the extreme cases, it cannot capture well the domain located in between, the so-called "fall-off" domain. The formalism developed by Troe ([62], [63] and [16]) is an extension of Lindemann's model which allows precise predictions of the reaction rate for all pressures in the transition domain. According to this formulation, the rate coefficient can be expressed as follows:

$$k = \frac{k_\infty k_0}{k_\infty + k_0[M]} F. \quad (2.29)$$

F is the broadening factor, which can be calculated according to the expression

$$\log F = \frac{F_{cent}}{1 + \left(\frac{\log P_r + c}{n - d(\log P_r + c)} \right)^2}, \quad (2.30)$$

whereby

$$c = -0.4 - 0.67 \log F_{cent} \quad (2.31)$$

$$n = 0.75 - 1.27 \log F_{cent} \quad (2.32)$$

$$d = 0.14 \quad (2.33)$$

and

$$F_{cent} = (1 - \alpha) \exp\left(-\frac{T}{T^{***}}\right) + \alpha \exp\left(-\frac{T}{T^*}\right) + \exp\left(-\frac{T^{**}}{T}\right). \quad (2.34)$$

In the format of the chemical kinetic simulation software Homrea used in this work, a Troe-reaction must be written as in the following example from the GRI-mechanism.

Reaction	A (mol, cm, s)	n	E_a (kJ mol ⁻¹)	
H + CH2 + M = CH3 + M	6.00E+14	0.00	0.00	
LOW	1.04E+26	-2.76	6.70	
TROE	α 0.562	T^{***} 91.00	T^* 5836.0	T^{**} 8552.0

Table 2.2: Recombination reaction

The Arrhenius parameters of the first line correspond to the high-pressure coefficient whereas the parameters of the second line correspond to the low pressure coefficient.

2.2 Simplified Combustion systems

2.2.1 General characteristics

Practical combustion systems hinge on a very large number of overlapping phenomena, which not only make realistic predictions hard to attain, but also hinders researchers from deducing the values of parameters out of a class of similar experiments. In effect, the behavior of these systems is extremely overdetermined in that many (if not an endless number of) combinations of physical and chemical parameters can lead to the same simulation results (see [71] for an example concerning chemical kinetics alone). This stems from the fact that models typically contain much more parameters than the quantity estimable through experimental information [15]. To reduce the sources of uncertainty and keeping focused on the chemistry, it is thus necessary to decouple the different processes occurring by devising experiments where only a small part of them is active. Homogeneous systems have turned out to be extremely useful for kinetic studies of combustion problems.

Homogeneous systems are constrained in such a way that all variables (including concentrations, temperature, pressure, and sometimes volume) are only time-dependent. This means that the physical phenomena may either be neglected or happen so fast that the evolution of the system is only driven by its chemistry. In this case, a system of ordinary differential equations (see next section) must be solved and the simulations can be carried out with less resources than for other, more complex types of systems.

Ignition delay times are often measured during experiments carried out in either shock tubes or rapid compression machines. They are defined as the period between the beginning of the reactions in the system and the sharp increase in the concentration of free radicals resulting from the onset of chain

reactions. [18]

In every of the three cases described below, output profiles only hinge on initial conditions, kinetic parameters and thermodynamic data.

2.2.2 Shock tubes

Shock tubes have been shown to be appropriate for the investigation of high temperature chemistry (usually for temperatures greater than 1200 K) [30], [17]. They consist of tubes made up of two sections: a driver section at high pressures and a driven section (containing the experimental mixture) at low pressures separated by a membrane. At the beginning of an experiment, the aluminum membrane is burst provoking a strong shock wave which after having been reflected will heat up the mixture very quickly (in less than $1 \mu s$). Close to the end flange of the tube, the temperature and pressure remain constant for several milliseconds during which the experimental measurements are made. The concentration values are estimated through several techniques based on the emission/absorption properties of molecules like mass spectrometry, gas chromatography, and laser absorption [65].

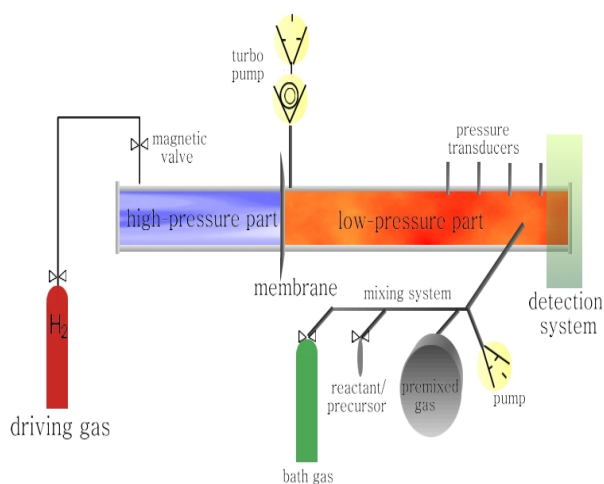


Figure 2.3: Scheme of a typical shock tube, Karlsruhe institute for technology, <http://www.ipc.uni-karlsruhe.de/mol/84.php>

2.2.3 Rapid Compression Machines

Rapid compression machines are currently used by many researchers all over the world for the study of combustion reactions at lower temperatures (500 K - 950 K) [9], [17]. The gaseous mixture containing the reactants and possibly the inert gas is compressed homogeneously and rapidly so as to reach predetermined reaction conditions (pressure and temperature). Afterward, the temporal evolution of the system is followed with the same diagnostic techniques as those utilized for shock tube studies.

2.2.4 Plug Flow reactors

A third kind of systems consists of plug flow reactors [53], [17] for the investigation of intermediate temperature regimes (900 K - 1300 K). According to given temperature and possibly pressure profiles the reacting flow is steadily going through the system which is assumed to be homogeneous in the plane perpendicular to the flow direction. In such a way, the variables only depend on the distance from the inlet point, which can be easily converted into the reaction time. The analyses of the mixture can be done at several points of the flow using the methods evoked above.

2.3 Mathematical handling and analysis of the problem

2.3.1 Formulation of the underlying ODE system

A reaction mechanism consists of an ensemble of elementary reactions aiming at quantitatively describing the combustion chemistry for a given set of conditions. In order to formulate a homogeneous combustion problem, the following elements are required:

1. a reaction mechanism
2. thermodynamic data for all involved species
3. initial conditions in terms of reactant and diluent concentrations, temperature and pressure
4. duration of the experiment

5. possibly, additional conditions like constant volume, pressure, or temperature.

If the system is considered to be homogeneous, all variables only depend on the reaction time t and chemistry is the only origin of the concentration changes.

Their derivatives are therefore given by the formula:

$$\frac{dc_i}{dt} = \sum_{R=1}^n v_{i,R} k_R \prod_{j=1}^{j=N_{Rrea}} c_j \quad (2.35)$$

that is the sum of all stoichiometric coefficients multiplied by the reaction rates, obtained by multiplying the rate coefficients with the concentrations of all reactants. In this formula, n designates the number of reactions whereas N_{Rrea} is the number of reactants which take part in the R -th reaction. It is assumed here that the reaction mechanism contains only elementary reactions whereby the rate is obtained by multiplying k by the products of all present reactants. Let C be the vector regrouping the concentrations of all species. All these reactions form a set of coupled ordinary differential equations which can be written as:

$$\frac{dc_i}{dt} = f_i(t, C, k) \quad \text{and} \quad C(t=0) = C_0, \quad t \in [0, t_e], \quad i = 1, 2, \dots, N_{sp} \quad (2.36)$$

or

$$\frac{dC}{dt} = f(t, C, k) \quad \text{and} \quad C(t=0) = C_0, \quad t \in [0, t_e] \quad (2.37)$$

where k represents the rate constants of all reactions. For solving the system, it is necessary to introduce initial conditions for each species, for the temperature and for the pressure. One equation characterizing the evolution of the temperature T alongside another one concerning the volume and/or pressure must also be added to uniquely characterize the system. In the case of adiabatic systems (like those considered in this work), the differential equation characterizing the evolution of the temperature is:

$$\frac{dT}{dt} = -\frac{1}{C_p(T)} \sum_{i=1}^{N_{Sp}} \frac{dc_i}{dt} h_i(T). \quad (2.38)$$

$C_p(T)$ is the heat capacity of the entire system, defined as:

$$C_p(T) = \sum_{i=1}^{N_{Sp}} c_i c_{p,i}(T). \quad (2.39)$$

$h_i(T)$ and $c_{p,i}(T)$ are respectively the molar enthalpy and the heat capacity of the i -th species (see 2.1.1).

Owing to the different orders of magnitudes of the reaction rates involved, stiffness has long been a major stumbling block for solving such systems. This means that time steps of classical numerical techniques are obliged to be very small for correctly accounting for the fast rates whereas the total computational time is determined by the slow rates [15]. Allowing both cost-efficient and realistic simulations implies the use of implicit methods of numerical integrations like DASAC[27], the Cash-Karp Runge-Kutta, or Bader-Deuffhard integrators [20]. After having solved the system of differential equations for a fixed set of k values, one gets more or less a good approximation of the species temporal evolution, provided of course that the rate constants are correct from the very beginning. As we will see in the following chapters, this is often not the case, so that the values of parameters must be adapted to the experimental measurements by some fitting procedure.

2.3.2 Sensitivity analyses

The ultimate goal of detailed reaction kinetics is to give an accurate and complete description of all that can take place at the molecular level. To describe the pyrolysis and rich oxidation of simple fuels such as methane (CH_4), acetylene (C_2H_2) or ethylene (C_2H_4) or the lean oxidation of greater alkanes like iso-octane (i- C_8H_{18}) under all possible pressure, temperature and concentration conditions, several hundreds of species and thousands of reactions are necessary. However, in almost every case, only a smaller number of them will play an important role for the species concentrations or variables (like temperature or ignition delay time) of interest. Identifying the most important reactions is highly desirable since they are the ones underlying the whole chemical behavior of the system under given conditions.

Sensitivity analyses are a common way to measure the influential strength of parameters on a particular variable which could be either a concentration, the temperature or possibly the ignition delay time. In most cases, sensitivity coefficients of first order are computed according to an OAT (One-At-a-Time) framework whereby the influence of one parameter on the output is evaluated while all other parameters are fixed (see for example [18], [37], [70]). The definition of the sensitivity coefficients s_i is then straightforward and is based upon the derivative of the interesting variable A with respect to the parameters p_i :

$$s_i = \frac{\delta A}{\delta p_i} . \quad (2.40)$$

Usually, relative sensitivities are considered in chemistry. These are defined as follows:

$$s_i = \frac{p_i}{A} \frac{\delta A}{\delta p_i} = \frac{\delta \ln A}{\delta \ln p_i} . \quad (2.41)$$

Sensitivity coefficients for concentrations c_i^{cal} as a function of time can generally be computed simultaneously along the solution of the differential equation system with some additional computational cost [68] according to the formula:

$$\frac{\delta}{\delta t} \left(\frac{\delta c_i^{cal}}{\delta k_j} \right) = \frac{\delta}{\delta k_j} \left(\frac{\delta c_i^{cal}}{\delta t} \right) = \frac{\delta}{\delta k_j} (f_i(C^{cal}, k_j)) \quad (2.42)$$

and if one further develops :

$$\frac{\delta}{\delta t} \left(\frac{\delta c_i^{cal}}{\delta k_j} \right) = \sum_{s=1}^{N_{spe}} \frac{\delta f_i}{\delta c_s^{cal}} \left(\frac{\delta c_s^{cal}}{\delta k_j} \right) + \frac{\delta f_i}{\delta k_j} \quad (2.43)$$

where f is the right hand-side function characterizing the system of differential equations described in the previous section. The $\frac{\delta f_i}{\delta c_s^{cal}}$ form the Jacobian, defined as the matrix of partial derivatives of f with respect to the concentrations. $\frac{\delta c_s^{cal}}{\delta k_j}$ is the sensitivity coefficient of the concentration c_s^{cal} at time t with respect to the j -th kinetic coefficient and $\frac{\delta f_i}{\delta k_j}$ is the derivative of the right hand-side term with respect to the j -th coefficient. It is noteworthy that the differential equation system obtained in this way is always linear, regardless of the non-linearities characterizing the concentrations. The reliance upon first derivatives can however be too simple in that the correlated effects of parameter variations is not at all considered although such non-linear effects can often occur for complex reaction mechanisms such as those encountered in combustion systems. To overcome this limitation, methods considering the correlations between the parameters can be employed. Among them, the FAST (Fourier Amplitude Sensitivity Test) [48] has shown promising successes in other fields of chemical kinetics and could be successfully applied to combustion problems in the near future.

In any case, sensitivity analyses allow for a particular situation to make a distinction between the parameters which must be determined accurately (because having a tremendous impact on the simulated variables due to high sensitivities) and those whose knowledge may be less precise. It is nonetheless not sufficient to trust sensitivity analyses alone for the identification of unimportant reactions because it can often occur that fast reactions with low sensitivity coefficients play a critical role. To see how this can happen, one has just to consider the simple (imaginary) chain $C_2H_6 \rightarrow C_2H_5 + H$ and

$\text{C}_2\text{H}_5 \rightarrow \text{C}_2\text{H}_4 + \text{H}$ with rate coefficients k_1 and k_2 , if k_1 is much greater than k_2 , then the second reaction will be the limiting one whereas the first one will be nearly infinitely fast from this perspective. Thus, to modify the pre-exponential factor of the first reaction slightly (say $0.9 k_{1,0}$ or $1.1 k_{1,0}$ instead of $k_{1,0}$) would have very limited impact on the formation of the product so that the sensitivity would be rather small. To exclude it from the reaction mechanism on the ground of this criterion alone would however lead to the rather undesired result that no more C_2H_4 would be produced at all! This shows the importance of also considering the flow followed by the element C and H between C_2H_6 and C_2H_4 .

2.3.3 Reaction flow analyses

Generally, for the atom sort a and the reactants i and j , the two following normed flow parameters [55] are introduced: f_{ij}^a , the flow of the atom a during the formation of species i from species j relative to the global formation of i , whereas c_{ij}^a is the flow of the atom a during the consumption of species i for forming species j relative to the global consumption of i :

$$f_{ij}^a = \frac{\sum_{k=1}^n r_k v'_{jk} v''_{ik} \frac{n_i^a}{\Delta n_k^a}}{\sum_{k=1}^{k=n} v''_{ik} r_k} \quad (2.44)$$

$$c_{ij}^a = \frac{\sum_{k=1}^n r_k v'_{jk} v''_{ik} \frac{n_i^a}{\Delta n_k^a}}{\sum_{k=1}^{k=n} v'_{ik} r_k} . \quad (2.45)$$

n is the number of uni-directional reactions over which it is summed, r_k is the reaction rate of the k -th reaction, n_i^a is the number of atom a in the species i whereas v''_{ik} and v'_{jk} are the stoichiometric coefficients of the species i and j in the k -th reaction. The number of atoms n_i^a are normalized to the total number of atoms transported in the k -th reaction: $\Delta n_k^a = \sum_{l=1}^{l=N_{Rspe}} v'_{lk} n_l^a$. Both normed flows take on values between 0 and 1 which correspond to the flux part from, respectively, towards species i with respect to species j . In such a way, flow diagrams showing the relative importance of all formation/consumption pathways for an set of species can be generated. They can be defined either for particular points in time or the flows may be integrated over a defined time interval. If a reaction has small sensitivities according to all variables of interest and if its role in the reaction flow is negligible, then there are good grounds for believing it can be excluded from the mechanism without consequences. The thresholds for f_{ij}^a and c_{ij}^a to be respected depend however on the particular context and have often to be chosen arbitrarily.

Chapter 3

Optimization and estimation of kinetic parameters

3.1 Theoretical bases

3.1.1 Motivation

Several possibilities exist for the determination of kinetic parameters. Due to an increased theoretical as well practical knowledge in quantum chemistry, methods like ab-initio [23] or DFT [66] coupled by TST (Transition State Theory) (see section 2.1.2) calculations are now currently employed for estimating the activation energies, temperature coefficients and pre-exponential factors of reactions. These techniques cannot however always guarantee a good precision of the values obtained in this way, especially for big molecules such as polyaromatic compounds. The estimation of parameters through experimental data remains therefore extremely relevant. Generally, experiments are designed in such a way that the evolution of one or several measured species only depends on one reaction. For example, while investigating the pyrolysis of propargyl C_3H_3 , Scherer [50] remarked that the initial rate of decomposition $\frac{d[C_3H_3]}{dt}$ depended linearly on C_3H_3 concentration. He concluded therefore that the recombination of propargyl towards benzene



can be neglected and that only the reaction



played a significant role at the beginning of the experiment, where the initial

reaction rate was measured. By varying the temperature and the initial concentration it was then possible to deduce the Arrhenius parameters of this reaction through the use of simple least squares regression, since the initial decay rates $\frac{d[C_3H_3]}{dt}$ can be expressed analytically as a function of the Arrhenius parameters according to the basic formula

$$\frac{d[C_3H_3]}{dt} = -AT^n e^{\frac{-E_a}{RT}} [C_3H_3]. \quad (3.3)$$

Similarly, other reactions are investigated in the literature in such a way that the measured species concentrations can be expressed as analytical functions of the parameters to be estimated. Unfortunately, many reactions cannot be handled in such a trivial manner because it is not possible to isolate them. As a consequence, their rate coefficients come up in complex systems of differential equations involving a great number of reactions which can only be solved through numerical methods. The kinetic coefficients of such reactions have been mainly estimated by analogy with known reactions or through the use of methods from quantum chemistry evoked above which often leave their values with significantly large uncertainty value intervals. There is however a way to more precisely estimate such parameters by using appropriate experimental data and extending the least squares regression method as described earlier.

Let a detailed reaction mechanism with reactions having parameters characterized by given uncertainty intervals be considered.

First, a set of experimental data must be constructed in such a way that every possible reaction not included in the mechanism only plays a negligible role for every profile.

Second, a set of uncertain reaction parameters must be identified and realistic lower and upper limits must be assigned to each of them.

Third, the distance $d(p)$ between the model and the experiments as a function of all adjustable parameters must be defined and minimized. For given values of the parameters p , the evaluation of $d(p)$ then involves solving the ODE systems underlying the set of experiments.

Fourth, all combinations of parameters able to predict the experimental measurements within their uncertainty intervals have to be determined. It may then be possible to discriminate between them by using additional data not included in the optimization or information originating from computational chemistry.

As Frenklach pointed out [14], this approach is a natural and legitimate extension of the methods used by chemical kineticists over the past century to estimate parameters. It allows however to systematically employ a signifi-

cantly greater amount of information, including the majority of experimental data which cannot be expressed analytically as functions of the parameters to be determined. As emphasized by Singer et al [52], since kinetic parameters are frequently only known within considerable uncertainty intervals, considerable disagreement between a reaction mechanism using the initial parameter values and experimental data is not enough to dismiss the model as being erroneous. The reaction mechanism may actually be the correct one, the discrepancies stemming from inaccurate values of certain parameters. Only a rigorous optimization of the model parameters within realistic bounds may ensure the conclusion that it does not correspond to reality by identifying the best minimum. On the other hand, the optimizability of a reaction mechanism does not guarantee that it is true, but it may increase the accuracy of its predictions under similar circumstances. This aspect is particularly relevant for reaction mechanisms aiming at describing the formation of pollutants such as soot, since a more accurate model may allow industrial users to spare a significant amount of the costs related to reducing pollution.

It is also worth noting that a rigorous optimization in the above sense is not the same thing as what is commonly referred to in the literature as parameter adjustment to a given profile. Most of the time, parameters are successively adjusted so as to produce a better agreement with a given isolated experiment as e.g. in [38] for the adjustment of the pre-exponential factor of the reaction



among others. The whole goal of a parameter estimation problem is however to obtain a good agreement *with the set of all known experimental data*, thereby finding realistic parameter values valid in the ideal case under every possible circumstance.

3.1.2 Choice of the norm

Now, an appropriate norm must be chosen as it is essential for every optimization process. It must allow the simultaneous consideration of variables with very different orders of magnitude without favoring one over the other. Let N be the number of measured profiles, n_i the number of measurements for the i -th profile with $i \in \{1 \dots N\}$ whereas $m_{i,j}$ and $e_{i,j}$ designate respectively the model and experimental concentrations of the i -th species profile at the j -th time point.

Intuitive approach

The problem can first be approached from an intuitive standpoint. While being commonly used for parameter estimation problem, the least squares and least absolute values norms, defined respectively by

$$d = \sum_{i=1}^N \sum_{j=1}^{n_i} (m_{i,j} - e_{i,j})^2 \quad (3.5)$$

and

$$d = \sum_{i=1}^N \sum_{j=1}^{n_i} |m_{i,j} - e_{i,j}| \quad (3.6)$$

are not apt to the task at hand, for their use would lead some variables (like the temperature $T \geq 1000$ K) to completely overwhelm other variables (like a concentration $c \leq 1e-08$ mol/cm³), thereby wholly erasing a great deal of the experimental information available for the parameter optimization. To overcome this hurdle, modified forms of the two norms, the so-called relative least squares and least absolute values norms have revealed themselves to be adequate. They are defined like the norms above except that the terms within the sum are divided by the experimental values of the variable. In Kinefit, a modified form of the relative least squares norm was used

$$d = \sum_{i=1}^N \sum_{j=1}^{n_i} d_{i,j}^2 . \quad (3.7)$$

For the i -th profile, let us call $e_{max,i}$ the greatest value of the experimental variable. Usually, the very small values of e_i (less than $\epsilon e_{max,i}$, where $0 < \epsilon < 1$ is a constant determining the threshold under which the experimental values are taken to be negligible) are going to have huge uncertainties. This also stems from the practical fact that they often must be extracted from experimental plots in logarithmic scale and lie then very close to the time-axis, which makes their values extremely low and imprecise. Consequently they will be ignored by the optimization (offsets). Let us call $\epsilon e_{max,i}$ the zero-limit of the i -th profile. The terms of the double sum are defined in the following manner:

i) for $e_{i,j} > \epsilon e_{i,max}$ $d_{i,j} = \frac{m_{i,j} - e_{i,j}}{e_{i,j}}$

ii) for $e_{i,j} < \epsilon e_{i,max}$ $d_{i,j} = 0$,

These rules also keep numerical and measurement instabilities for very low concentrations from influencing the optimization procedure.

Mathematical and pragmatic justification

Let $\sigma_{i,j}$ denote the standard deviations corresponding to the experimental values. From statistical theories [43] it is known that the ideal parameters are found by minimizing the so-called Chi-squared norm:

$$X^2 = \sum_{i=1}^N \sum_{j=1}^{n_i} \left(\frac{m_{i,j} - e_{i,j}}{\sigma_{i,j}} \right)^2 . \quad (3.8)$$

Generally, the standard deviations are not measured directly and must be approximated. If one assumes that they are proportional to the measurements for a given profile (i.e. $\sigma_{i,j} = v_{dev,i} e_{i,j}$), the formula becomes:

$$X^2 = \sum_{i=1}^N \frac{1}{v_{dev,i}^2} \sum_{j=1}^{n_i} \left(\frac{m_{i,j} - e_{i,j}}{e_{i,j}} \right)^2 . \quad (3.9)$$

If one further supposes that the proportionality constant is the same for all profiles, one gets the expression:

$$X^2 = \frac{1}{v_{dev}^2} \sum_{i=1}^N \sum_{j=1}^{n_i} \left(\frac{m_{i,j} - e_{i,j}}{e_{i,j}} \right)^2 . \quad (3.10)$$

As explained in the last subsection, owing to both numerical and experimental high imprecision for the lowest values, the experimental data below the threshold $\epsilon e_{i,max}$ are ignored (offset) in the previous formula. Minimizing this expression is akin to minimizing the relative least squares norm evoked above. The problem can thus be expressed as follows:

$$d = \sum_{i=1}^N \sum_{j=1}^{n_i} \left(\frac{m_{i,j} - e_{i,j}}{e_{i,j}} \right)^2 \quad (3.11)$$

and

$$X^2 = \frac{1}{v_{dev}^2} d . \quad (3.12)$$

in which the experimental points with the lowest values are ignored. This norm, nevertheless, does not suit all the purposes of optimizing/ estimating kinetic parameters because it automatically gives more importance to the experiments having a greater number of points. As an illustration, let us consider the following situation: for optimizing seven parameters, three experimental profiles are taken at three different conditions:

1. $[\text{CH}_4] = 2\%$, $[\text{Ar}] = 98\%$, $p = 3.2$ bar, $T = 1400$ K with 120 time points

2. $[\text{C}_2\text{H}_6] = 5\%$, $[\text{Ar}] = 95\%$, $p = 20$ bar, $T = 1200$ K with 15 time points
3. $[\text{C}_2\text{H}_4] = 0.3\%$, $[\text{Ar}] = 99.7\%$, $p = 120$ bar, $T = 1600$ K with 15 time points.

Clearly, a good model would be one capable of correctly describing the trends for these three very different conditions. However, the norm defined above would privilege the first experiment: a model which captures perfectly well the first profile but poorly performs for the two other ones would be considered as being better than a model giving a good agreement for all three. To overcome this hurdle, it is necessary to impose weights on the contributions of each experiment in such a way that they receive the same importance regardless of the number of points. Generally, let there be N experimental profiles containing $m = \sum_{i=1}^N n_i$ experimental points. The average number of points per profile is then $n_{mean} = \frac{m}{N}$. The weighted norm is then defined as

$$d = \sum_{i=1}^N \frac{n_{mean}}{n_i} \sum_{j=1}^{n_i} \left(\frac{m_{i,j} - e_{i,j}}{e_{i,j}} \right)^2 \quad (3.13)$$

$$X^2 = \frac{1}{v_{dev}^2} d \quad (3.14)$$

under the assumption that all standard deviations are proportional to the experimental concentrations and that the very small experimental values are ignored. If this is not the case, the norm to be minimized can be generally written as:

$$X^2 = \sum_{i=1}^N \frac{n_{mean}}{n_i} \sum_{j=1}^{n_i} \left(\frac{m_{i,j} - e_{i,j}}{\sigma_{i,j}} \right)^2. \quad (3.15)$$

The problem at hand now consists of determining a set of parameters p minimizing the distance $X^2(p)$ or $d(p)$ in the favorable case. This is a non-linear optimization problem which has been handled in this work by four optimization methods described in section 3.2. Before going into this practical aspect, it is necessary to turn our attention to the mathematical formulation of the optimization problem and then to the statistical meaning and ways of interpreting an optimized set of parameters.

3.1.3 Mathematical formulation of a kinetic parameter optimization problem

Let us consider the general formulation of a kinetic parameter optimization/estimation problem consisting in a complete reaction mechanism . Some parameters q (q_1, q_2, \dots, q_f) are accurately known and will thus be fixed as such. Other parameters p (p_1, p_2, \dots, p_u) are only known within uncertainty intervals of varying widths and should therefore be adjusted to experimental measurements between the constraint box $[low, up]$ such that

$$low_i \leq p_i \leq up_i \text{ with } i \in \{1 \dots u\} \quad (3.16)$$

hold. Vectorially, the inequality

$$low \leq p \leq up \quad (3.17)$$

holds component-wise.

Likewise, the parameters may also be subject to a certain number of non-linear constraints which are summed up here in vectorial form as:

$$g(p) \geq 0. \quad (3.18)$$

In subsection 3.2.3 the frequent case of constraints on the whole reaction rate k_j will be addressed. Let there be data from N profiles from N_e experiments which stand at disposal. These may be temporal or temperature-dependent concentration profiles or ignition delay times or any other variable which may be deduced from the concentration trajectories (like peak concentrations).

Let n_i be the number of points of the i -th profile. Let E be defined as $E = \{e_{i,j}, i \in \{1 \dots N\} \text{ and } j \in \{1 \dots n_i\}\}$, $e_{i,j}$ being the variable measured at the j -th point for the i -th profile. The goal is to find a set of parameters p_{opt} which minimizes the distance between the results of the model and those of the experiment, where

$$d_{min} = \min \{d(Y(C(p)), E), \text{ with } low \leq p \leq up \text{ and } g(p) \geq 0 \} \quad (3.19)$$

The variable $C(p)$ consists of the concentration trajectories (C_1, C_2, \dots, C_{N_e}) for all simulated experiments. For the k -th experiment, C_k must fulfill the ensemble of differential equations mentioned in the last chapter:

$$\frac{dC_k}{dt} = f(t, C_k, p, q) \text{ and } C_k(t=0) = C_{k,0}, t \in [0, t_e] \quad (3.20)$$

along other equations concerning the evolution of the pressure, temperature and volume. $Y(C(p))$ are the variables corresponding to the experimental measurements, which are deducible from the concentration set.

3.1.4 Statistical interpretation of an optimization problem

Basic functions

For a model with n_p optimizable parameters and n_e experimental points, the degree of freedom of the system is defined as

$$v = n_e - n_p. \quad (3.21)$$

The following function allows to evaluate the consistency between an optimized model and a series of experiments: [52]:

$$Pr(X^2) = \frac{\Gamma(\frac{v}{2}, \frac{X^2}{2})}{\Gamma(\frac{v}{2})}. \quad (3.22)$$

where Γ is the so-called incomplete Gamma function [43]. It is defined as

$$\Gamma(a, x) = \int_x^\infty t^{a-1} e^{-t} dt. \quad (3.23)$$

Formally, Pr represents the probability that the observed chi-square would exceed the value X^2 by chance if the optimized model is correct, provided that the number of experimental points considerably exceeds the number of parameters. Singer et al. [52] state that values superior to 0.75 indicate that the model is in good agreement with the experiment, values inferior to 0.25 indicate that the model is refuted by the experiments, whereas values between 0.25 and 0.75 are ambiguous and show the need for additional experimental information or the consideration of other parameters. However this indicator is only reliable if the errors are normally distributed and if the standard deviations are at least approximately known. If this is not the case, values as low as 0.001 may be acceptable. [43].

If n_e is considerably greater than n_p , low values of $Pr(X^2)$ indicate that the model could not be satisfactorily optimized with the active parameters taken into consideration. If $n_p \approx n_e$ the problem is over-determined, low values of $Pr(X^2)$ do not mean that the optimized model is inconsistent with the experiment but rather that more experimental data are needed for the unambiguous optimization of the parameters.

To simply estimate the agreement of a **fixed** model with experiments, formula 3.1.4 can be applied with the number of fitted parameters equal to zero:

$$Pr_0(X^2) = \frac{\Gamma(\frac{n_e}{2}, \frac{X^2}{2})}{\Gamma(\frac{n_e}{2})}. \quad (3.24)$$

The interpretation and the recommended values are the same as those of $Pr(X^2)$.

Application to the evaluation of kinetic models

Let a given reaction mechanism lead to important discrepancies with given experiments. While trying to fit a model to a set of experimental data, the first question arising can be formulated as follows:

Is the reaction mechanism consistent with the ensemble of experimental data available? In other words, is there a set of reasonable parameter values (i.e. contained within their uncertainty intervals), for which the model agrees with the experiments [52] ?

To answer this question, three steps are necessary:

- identifying all parameters having a significant influence on the experiments
- optimizing them within reasonable ranges of values and identify the global minimum
- calculating $Pr_0(X^2)$ and evaluating the agreement with the experiments according to the recommendations given above.

It is worth noting that $Pr_0(X^2)$ rather than $Pr(X^2)$ must be employed here. If the number of significant parameters is relatively small, $Pr(X^2)$ will be close to $Pr_0(X^2)$.

If however the number of significant parameters is relatively large, small values of $Pr(X^2)$ will mean that more data are needed for fitting the parameter, but not necessarily that the considered experimental data refute the model. If $Pr(X^2)$ is low whereas $Pr_0(X^2)$ is high, the model is consistent with the data, but additional experiments are to be brought up in order to fit the parameters in a statistically meaningful way.

If $Pr_0(X^2)$ and $Pr(X^2)$ have high values, indicating that the fit allowed the determination of new parameter values consistent with the experiment, the second question is how to estimate the uncertainties of the optimized parameter values. A current method used for determining the standard deviations of the parameters is described in what follows.

Let m_i be the simulated variable corresponding to the i -th measurement. The matrix J is defined as:

$$J = \begin{pmatrix} \frac{1}{\sigma_1} \frac{\delta m_1}{\delta p_1} & \frac{1}{\sigma_1} \frac{\delta m_1}{\delta p_2} & \cdots & \frac{1}{\sigma_1} \frac{\delta m_1}{\delta p_{n_p}} \\ \frac{1}{\sigma_2} \frac{\delta m_2}{\delta p_1} & \frac{1}{\sigma_2} \frac{\delta m_2}{\delta p_2} & \cdots & \frac{1}{\sigma_2} \frac{\delta m_2}{\delta p_{n_p}} \\ \cdots & \cdots & \cdots & \cdots \\ \frac{1}{\sigma_{n_e}} \frac{\delta m_{n_e}}{\delta p_1} & \frac{1}{\sigma_{n_e}} \frac{\delta m_{n_e}}{\delta p_2} & \cdots & \frac{1}{\sigma_{n_e}} \frac{\delta m_{n_e}}{\delta p_{n_p}} \end{pmatrix}.$$

The information matrix H (see [24]) is then formed as :

$$H = J^T J. \quad (3.25)$$

If J rank is the same as the number of parameters, C the inverse of H , is then the covariance matrix. The diagonal of C contains the squared standard deviations of the parameters, according to:

$$\sigma_{p_i} = \sqrt{C_{ii}}. \quad (3.26)$$

The parameter covariances are then given by:

$$\sigma_{p_i,l} = \sqrt{C_{il}}. \quad (3.27)$$

3.2 The optimization program library Kinefit

For the optimization and evaluation of kinetic parameters, a C++ set of programs called Kinefit has been created.

3.2.1 General characteristics of the optimization interface

As input, Kinefit must receive the following information:

1. the reaction mechanism alongside the parameters to be optimized and the uncertainty intervals in which they may vary. Bounds for the global rate coefficient k of each reaction must also be provided,
2. the set of all experiments to be simulated with the target variables which may be time or temperature-dependent,
3. the choice of the optimization method along its intrinsic parameters,
4. the choice of the norm for the distance $d(p)$.

As output, Kinefit returns:

1. the optimal set of parameter values minimizing $d(p)$,
2. the distance between optimized model and experiment,
3. the derivatives of the variables as functions of the parameters.

From this information, it is then possible to obtain (using software like Matlab or Octave) :

4. the likelihood that the optimized model is consistent with the measurements,
5. the uncertainties of the final parameter values deducible from the experimental errors (provided the problem is well defined)

It is not possible to force Homrea to compute the concentrations at exactly the time points of the measurements. Consequently, the values from the model are systematically interpolated to the experimental time points or temperature points by using a monotone cubic interpolation.

3.2.2 Optimization methods used by Kinefit

In this subsection, n_p denotes the number of optimizable parameters.

Adaptive Random Search method (RS)

The Adaptive Random Search (referred to as RS) is an intuitive optimization method allowing convergence to a local minimum of the objective function $d(p)$. Four parameters max_{fail} , $step_{beg}$, $factor$ and N_{steps} are to be given by the user. They determine the behavior of the minimization technique. Starting from an initial set of parameters p_0 , a series of point leading to a local minimum is generated according to the following recurrence formula, which is valid for $j \in \{1 \dots n_p\}$:

$$p_{j,i+1} = p_{j,i} + r_{j,i+1} w_{step_{i+1}} (up_j - low_j) \quad (3.28)$$

where $r_{j,i+1}$ is a random real number belonging to the interval $[-1, 1]$ and w_{step_i} is the width of the current search interval. Up and low designate the upper and lower bounds. The series w_{step_i} is defined according to the formula:

$$w_{step_i} = \frac{1}{factor^{step_i}} \cdot \quad (3.29)$$

$factor$ is a real number greater than one determining the widths of the search region during the optimization.

$step_{beg} = step_0$ is a integer greater than or equal to zero. It is an index designating the step number. The greater it becomes, the smaller becomes the width w_{step_i} .

Let us define d_i as the distance corresponding to the i -th set of parameters. An iteration $i > 0$ is considered as a success if $d_i < d_{i-1}$, otherwise it is viewed as being a failure.

If the number of **successive** failures becomes greater than the threshold max_{fail} , the width of the search region is reduced by increasing the index $step_i$ with one unity (which is akin to dividing the width by *factor*).

In this way, as the method approaches a local minimum, large steps can no longer bring any improvement and the diameter of the search becomes smaller, thereby allowing a greater precision. N_{steps} is the maximum number for the step index $step_i$ before the local search converges. Since the first local minimum identified can be insufficient for the problem at hand, the search has been globalized. This is done by resetting the index $step_i$ to its initial value $step_{beg}$ and starting an other local search with a new set of initial parameters p_0 , chosen completely randomly between the lower and upper limits.

As stopping criterion of the global search, the user can either give a number of iterations or a threshold the distance between model and experiment must reach. Contrarily to the three other optimization methods which are going to be described, the RS has been written in C++ as an integral part of Kinefit, allowing it to work as a stand-alone program for the estimation of kinetic parameters.

Genetic algorithm Galib (GA)

A genetic algorithm is a method used to minimize or maximize non-linear functions which are not necessarily differentiable or even continuous. It is based on the Darwinian principles of natural selection and survival of the fittest. Each set of parameters is coded as a genome and is associated to a fitness value which must be maximized. A population of genomes containing N_{pop} individuals is then generated and evolves until a criterion (i.e. sufficient reduction of the distance) has been reached. The working of the kind of genetic algorithms used in this work is characterized by the following steps:

1. Initialization: a sufficient quantity of genomes or individuals N_{pop} is generated so as to form a population. In this work, all individuals of the first generation are generated randomly with the Adaptive Random Search. The step $step_{beg}$ defining the width of the search must be given. If $step_{beg} = 0$, the initial individuals making up the population are chosen completely randomly in the feasible region. This is appropriate

if no good point is known at the beginning. If however a set of parameter values corresponding to a small distance is known, it may be interesting to start the genetic algorithm at this point with a smaller width for the generation of the population. In this way, the information already available can immediately be exploited by the genetic algorithm.

2. Evaluation: a fitness value $f(p)$ related to the quantity to be optimized is assigned to each genome, and the GA will try to maximize it. Here, since the goal consists of minimizing the distance $d(p)$ between model and experiment, the fitness value may either be defined as $-d(p)$ or as $\frac{1}{K+d(p)}$, where K is a constant like $1e - 06$ preventing the appearance of numerical instabilities as the distance $d(p)$ tends towards zero. The last option has been chosen during the entirety of the present work.
3. If a completion criterion is fulfilled, the search stops here.
4. Selection: random choice of the parents of the next generation. The individuals with the greatest fitness values are more likely to get selected.
5. Recombination: the genomes of the selected individuals are mixed up to produce the next generation of offsprings.
6. Mutation: random modifications of the new individuals, allowing thus a diversification, that is an exploration of the unknown regions of the search space.
7. Forming the new generation: the members of the new generation are selected out of the offspring generations as well as out of the previous generation.
8. Return to step 2.

For each step, many options exist which lead to a great diversity of genetic algorithms. During the present work, *Galib*, a C++ library of genetic algorithm objects was considered, coupled with and adapted to Kinefit.

Quadratic model based minimization: CONDOR and Bobyqa

The function $d(p)$ to be minimized is often characterized by a regular mathematical structure, which may mean for example that it is twice differentiable. Global heuristics like genetic algorithms do not exploit this underlying structure. On the one hand it is one of their main strengths since it allows to solve minimization problems with extremely complex functions presenting many local minima and irregularities. On the other hand, it considerably reduces the

convergence rate for problems with smooth functions as well as the precision of the obtained solutions. On the contrary, derivative based techniques like the quasi-Newton and the conjugate gradient methods systematically utilize the information contained in the derivatives, thereby ensuring a faster convergence to the next local minimum than the Adaptive Random Search which only use function values to get information about the function structure.

In what follows, $\langle A, B \rangle$ denotes the multiplication of the matrix or vector A with the matrix or vector B . Within a trust-region framework, Newton and quasi-Newton methods approximate the function $d(p)$ in the neighborhood of p with a quadratic function $m(s)$ defined in the following manner:

$$m(p + s) = d(p) + \langle g, s \rangle + 0.5 \langle s, H, s \rangle \text{ for } -s \leq \Delta. \quad (3.30)$$

g is the gradient of $d(p)$ and H is its hessian matrix, which may be either directly computed (Newton methods) or indirectly evaluated through algebraic techniques (Quasi-Newton Methods). The model $m(s)$ is then minimized, leading to a new point $p + s_{min}$, where the function $d(p)$ is evaluated. The width of the trust region Δ is then either decreased or increased according to the extent of the improvement or worsening. With Homrea however, only the derivatives of the pre-exponential coefficients may be determined through the use of sensitivity analyses. Since the temperature coefficients and the activation energies may also be taken as parameters to be optimized, an alternative approach had to be employed. The optimization softwares CONDOR and Bobyqa works with the same principles as the quasi-Newton methods, but they only need function values. The quadratic model evoked above is then formed through a judicious interpolation of a sufficient number of points chosen appropriately. These optimization techniques evaluate thus indirectly the derivatives and Hessian of the function to be minimized through the formation of local quadratic models, by-passing the numerical instabilities which may be generated by the use of automatic differentiation techniques.

3.2.3 Consideration of non-linear constraints

The mere consideration of box constraints on each kinetic parameter is often-times not satisfying if several parameters of the same reaction are optimized simultaneously. If for instance the realistic bounds

$$\begin{aligned} \frac{A_0}{10} &\leq A \leq A_0 * 10 \text{ (mol, cm, s),} \\ n_0 - 0.6 &\leq n \leq n_0 + 0.6, \\ E_{a,0} - 5 &\leq E_a \leq E_{a,0} + 5 \text{ (kJ mol}^{-1}\text{)} \end{aligned}$$

are imposed, each coefficient will be coerced to only accept realistic values, but it may well be the case that the rate coefficient

$$k = AT^n e^{\frac{-E_a}{RT}} \quad (3.31)$$

will significantly diverge from its original value by a factor of 100 or even more. Often, such a change is too great to be physically meaningful. It is thus necessary to establish global constraints on the rate such that for every temperature $T \in [T_{inf}, T_{sup}]$ the inequality system

$$k_0(T) * q_i \leq k(T) \leq k_0(T) * q_s \quad (3.32)$$

holds. q_i and q_s are constants taking on values like 0.1 and 10 in such a manner that $k(T)$ will only vary within a realistic range. Since the inequalities must be true for every temperature, they imply non-linear constraints which cannot be expressed analytically at the beginning of a minimization process. Penalty functions are particularly apt to tackle the task at hand. They work through the systematic addition of terms penalizing the non-consideration of constraints which rapidly increase the more the constraints are violated.

Let us define

$$Q(T) = \frac{k(T)}{k_0(T)} \quad (3.33)$$

this function must satisfy :

$$q_i \leq Q(T) \leq q_s. \quad (3.34)$$

Due to the mathematical nature of the function, there always exists two temperatures T_{min} and T_{max} such that for each temperature $T \in [T_{inf}, T_{sup}]$

$$Q_{min} = Q(T_{min}) \leq Q(T) \leq Q_{max} = Q(T_{max}) \quad (3.35)$$

is true, hence if the inequalities $q_i \leq Q_{min}$ and $Q_{max} \leq q_s$ hold, one can be certain that for every temperature T between T_{inf} and T_{sup} the inequalities $q_i \leq Q(T) \leq q_s$ are satisfied.

The temperatures T_{min} and T_{max} however depend on the combination of the reaction parameters (A, n, E_a) and must be determined for each new values, thus prohibiting the declaration of constraints generally valid at the beginning of the optimization procedure. Given (A, n, E_a) , it is now necessary to determine the inflexion point T_i of the function $Q(T)$, that is the point where the derivative of $Q(T)$ $\frac{dQ(T)}{dT}$ changes its signs. This is the same inflexion point as for the function $f(T) = \log(Q(T))$, where $\frac{df(T)}{dT} = 0$. If one develops

$$f(T) = \log \left(\frac{AT^n e^{\frac{-E_a}{RT}}}{A_0 T_0^n e^{\frac{-E_{a0}}{RT}}} \right) \quad (3.36)$$

$$f(T) = \log\left(\frac{A}{A_0}\right) + (n - n_0)\log(T) - \frac{E_a - E_{a0}}{RT} \quad (3.37)$$

As a consequence

$$\frac{df(T)}{dT} = \frac{n - n_0}{T} + \frac{E_a - E_{a0}}{RT^2} \quad (3.38)$$

and

$$\frac{df(T_i)}{dT} = 0 \quad (3.39)$$

thus

$$\frac{(n - n_0)}{T_i} + \frac{(E_a - E_{a0})}{(RT_i^2)} = 0 \quad (3.40)$$

which leads to the expression:

$$T_i = \frac{(E_{a0} - E_a)}{(R(n - n_0))} \quad (3.41)$$

considering that $n \neq n_0$, otherwise the function $Q(T)$ is monotone on the interval $[T_{inf}, T_{sup}]$ which leads to a straightforward determination of Q_{min} and Q_{max} .

Now, if

$$T_{inf} \leq T_i \leq T_{sup} \quad (3.42)$$

Q_{min} and Q_{max} are given by:

$$Q_{min} = \min\{Q(T_{inf}), Q(T_i), Q(T_{sup})\} \text{ and } Q_{max} = \max\{Q(T_{inf}), Q(T_i), Q(T_{sup})\}. \quad (3.43)$$

If T_i is outside of the temperature range or $n = n_0$ or $E_a = E_{a0}$, then $Q_{min} = \min\{Q(T_{inf}), Q(T_{sup})\}$ and $Q_{max} = \max\{Q(T_{inf}), Q(T_{sup})\}$.

All what is required are the values Q_{min} and Q_{max} which must fulfill $q_i \leq Q_{min}$ and $Q_{max} \leq q_s$. Whatever the values are, a penalty term

$$pen = \left(\frac{q_i}{Q_{min}}\right)^{2n_p} + \left(\frac{Q_{max}}{q_s}\right)^{2n_p} \quad (3.44)$$

is added to the distance $d(p)$ between model and experiment, whereby n_p must be chosen in such a way to quickly penalize faulty points as well as to keep the objective function continuous. In this work, $n_p = 10$, except if specified otherwise.

Above, the case where all three parameters of a reaction are optimizable was considered. If only some of the parameters are considered, like for example just A and E_a , then n in the equation only takes on the value n_0 . This penalty method was successful during the course of this work for keeping the rates between their bounds, as shown in 4.2.2.

3.2.4 Analyses of reaction significances

The sensitivity analyses defined in the second chapter are a useful tool for identifying the most significant reactions at given time points. For the purpose of optimizing parameters, they present however one drawback: they are limited at one species, whereas one is typically interested in the global impact of a parameter on the distance $d(p)$ between experiment and model. This is why a new method called "Analyses of Reaction Significances" (ARS) has been introduced in the present work.

Let the following general situation be considered: the distance d between experiment and model for an arbitrary quantity of experimental points must be minimized. The reaction mechanism contains N reactions $r_i, i = 1..N$, some are much more significant for d than others. Each pre-exponential factor A_i must be bound between a lower Al_i and an higher values Au_i and has the initial value $A_{0,i}$. While A_i varies separately, the significance of the i -th reaction for the distance d is defined as

$$S_i = \max\{d(A_i), Al_i \leq A_i \leq Au_i\} - \min\{d(A_i), Al_i \leq A_i \leq Au_i\} . \quad (3.45)$$

Usually, A_i is discretely varied between its bounds according to

$$A_{i,j} = \{Al_i + j \frac{Au_i - Al_i}{M} \quad j = 1..M \} \quad (3.46)$$

so that if M is great enough, the following approximation holds:

$$S_i \approx \max\{d(A_{i,j}), j = 1..M\} - \min\{d(A_{i,j}), j = 1..M\} . \quad (3.47)$$

The reactions are then sorted according to their significances S_i in a decreasing order, and the most significant reactions are considered for the optimization. It may however be the case that certain reactions significantly increase the distance $d(A_i)$ with respect to $d(A_{i,0})$ but fail to decrease it, which may indicate that this parameter has already reached its optimal value. To exclude it from the optimization process on that ground alone is however not advisable because the modification of other parameters could lead to a new minimum for it. As a rule, it is desirable to include all parameters having a significant influence on the distance.

Chapter 4

Numerical tests

To evaluate the capacities and performance of Kinefit, the $\text{H}_2 - \text{O}_2$ sub-system from the GRI-mechanism 3.0 [54] was considered. The GRI-mechanism 3.0 [54] is a compilation of elementary reactions along with reaction rate coefficient values and thermodynamic parameters which aims at describing the oxidation of methane (CH_4). Without the chemistry involving nitrogen N_2 , it contains 38 species and 422 (uni-directional) reactions and is valid over a wide range of conditions for fuel lean to stoichiometric flames. For given combustion conditions, artificial experimental data were first generated using the initial values of the parameters p_0 . The most influential parameters were then varied to the values p_{var} in such a way as to produce a significant distance $d(p_{var})$ from the results obtained with the initial parameter values. The "experimental time points" generated are less numerous than the time points considered by the model so as to reflect real situations where there are less experimental measurements than points originating from the simulation. The solution of such a parameter estimation problem $d(p_0) = 0$ is exactly known, thereby enabling the evaluation and comparison of the different minimization techniques employed by Kinefit. By convenience, the pseudo-experimental data will be referred to as experimental data henceforth.

The norm $d(p)$

$$d = \sum_{i=1}^N \frac{n_{mean}}{n_i} \sum_{j=1}^{n_i} \left(\frac{m_{i,j} - e_{i,j}}{e_{i,j}} \right)^2 \quad (4.1)$$

was used. In all simulations, Argon is the diluent. In the first part of this section, a problem often encountered in practice, namely the oscillation of the distance d as a function of separately varied parameters, is presented through a representative example and its causes are analyzed. In the second part, the optimization methods are compared for a problem where such oscillations do

not appear. In the third part, the behavior of the minimization techniques is visualized for an example where oscillations do play a significant role. In the fourth part, an example showing the link between experimental information and parameter accuracies is presented.

4.1 Oscillation of the distance

While in many cases the distance $d(p_i)$ as function of a parameter p_i has a smooth shape with one unique local minimum, oscillations of its values sometimes occur. An example (whose conditions are given below) has been constructed to identify the causes of this behavior.

Experiment	[H ₂] (%)	[O ₂] (%)	T (K)	p (bar)	t (s)	Target-species
1	5	5	1000	300.08	0.0011	H ₂ O ₂

Table 4.1: Initial conditions

The great pressure chosen here have proven suitable for generating oscillations. The target variables from which the distance between experiment and model d was calculated were the mole fractions of H₂O₂. The experimental data contained 70 time points to which the results of the model were compared. Originally, six Arrhenius factors were modified as reported in table 4.2, while the other parameters of the rate coefficients were unchanged.

N	Reaction	A	A_{mod}	n	E_a
1	O + H ₂ = H + OH	3.87E+04	1.00E+05	2.70	26.198
2	H + O ₂ + AR = HO ₂ + AR	7.00E+17	1.00E+17	-0.80	0.00
3	H + O ₂ = O + OH	2.65E+16	8.00E+17	-0.67	71.32
4	H + HO ₂ = O ₂ + H ₂	4.48E+13	1.00E+15	0.00	4.47
5	H + HO ₂ = OH + OH	8.40E+13	1.00E+13	0.00	2.66
6	OH + OH + M = H ₂ O ₂ + M	7.40E+13	1.00E+12	-0.37	0.00

Table 4.2: Modified reactions for the example which causes oscillations

While the five last parameters were maintained at their fixed modified values, the variation of the distance as a function of the first parameter $d(p_1)$ between 3.01E+04 and 1.97E+05 was computed and is given in figure 4.1.

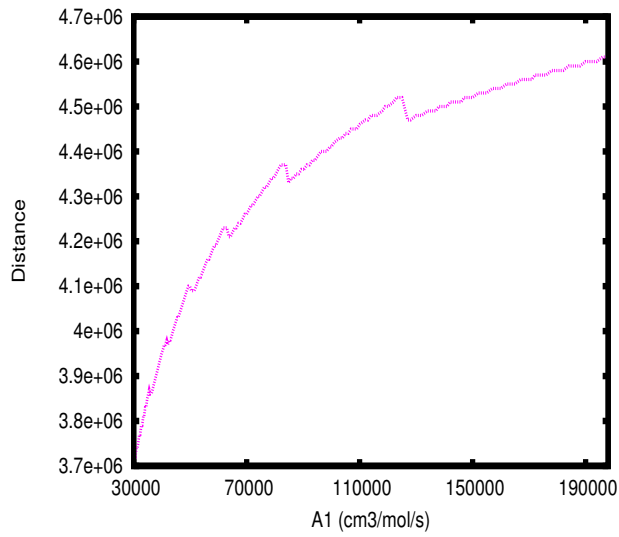


Figure 4.1: Distance between the modified model and the experiment as function of the first parameter

As can be seen in fig. 4.1 several oscillations appear in the curve, thereby creating diverse local minima. To identify the cause of this behavior, the evolutions of the H_2O_2 -concentrations $[\text{H}_2\text{O}_2]_i, i = 1, \dots, 70$ for the 70 time points as function of the first parameter were computed. The concentrations as function of A_1 have a smooth form at the first sixty-two time points, as is well illustrated in figures 4.2 and 4.3 representing two time points.

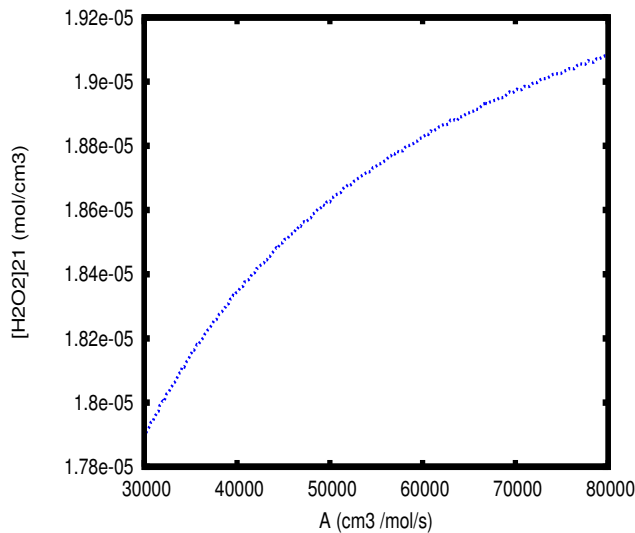


Figure 4.2: $[\text{H}_2\text{O}_2](A_1)$ at the 21-th time point

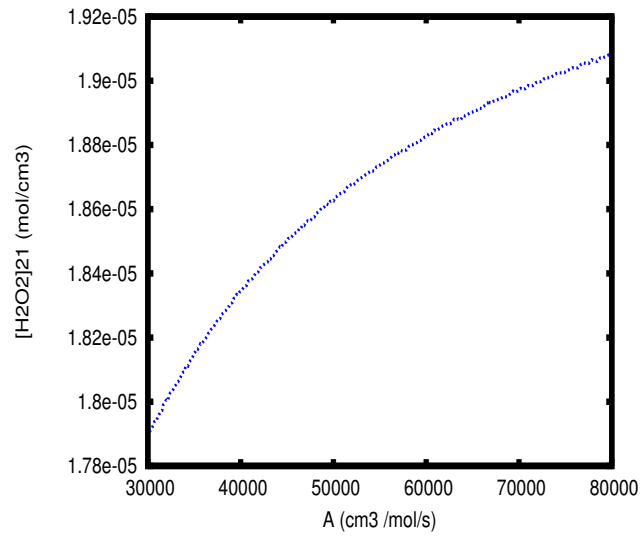


Figure 4.3: $[\text{H}_2\text{O}_2](A1)$ at the 38-th time point

However, the concentration at at the 63-th and 65-th time points has an almost discontinuous form as is reported in figure 4.4 and 4.5.

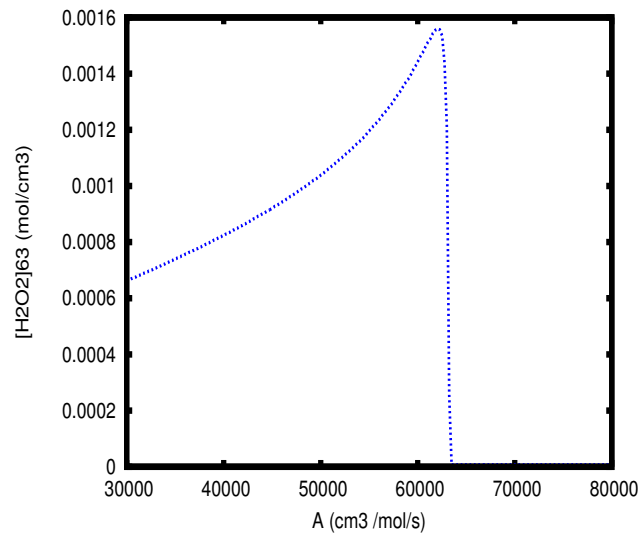


Figure 4.4: $[\text{H}_2\text{O}_2](A1)$ at the 63-th time point

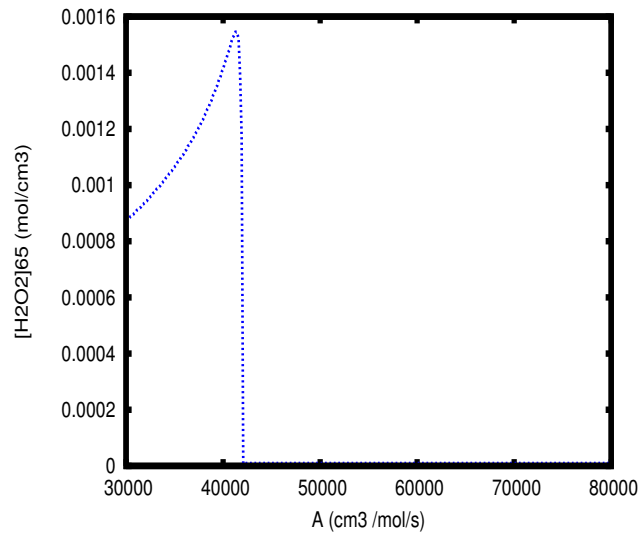


Figure 4.5: $[\text{H}_2\text{O}_2](A_1)$ at the 65-th time point

These sharp decreases of the concentrations while the parameter A_1 takes on greater values are due to the exponential decrease of the concentration $[\text{H}_2\text{O}_2]$ as a function of time, as will be explained below. Let us consider to that end the evolution of the 63-th concentration as a function of A_1 . In figures 4.6 - 4.8, temporal profiles of H_2O_2 are given for different values of A_1 whereas the 63-th time point is highlighted in pink. The value of the first parameter is progressively increased so as to visualize the corresponding evolution of the concentration at the 63-th time point.

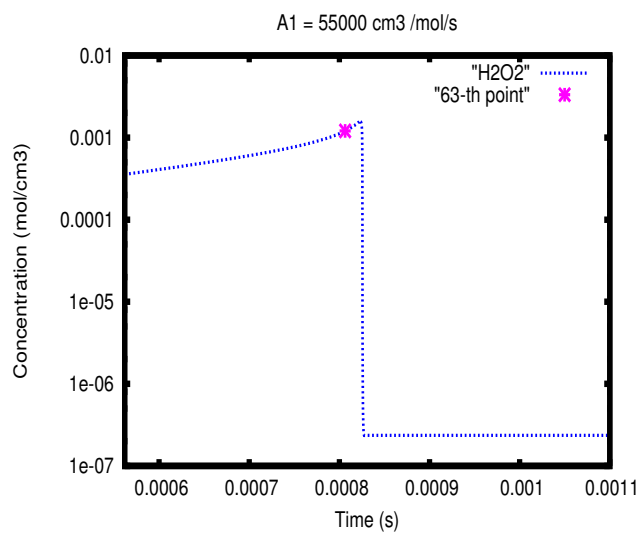


Figure 4.6: $[H_2O_2](t)$

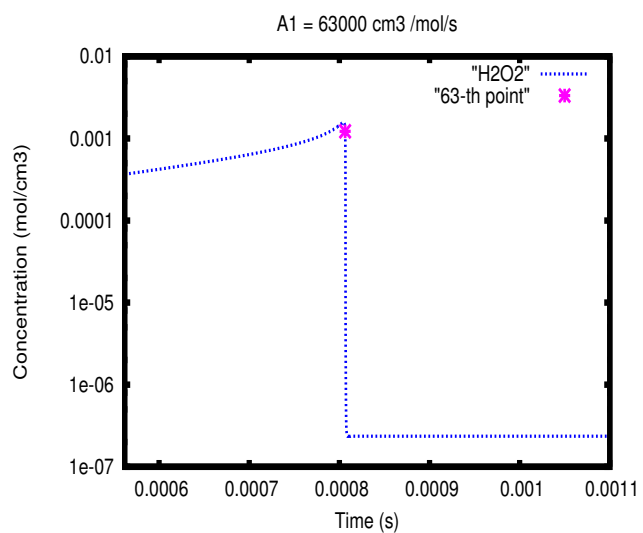


Figure 4.7: $[H_2O_2](t)$

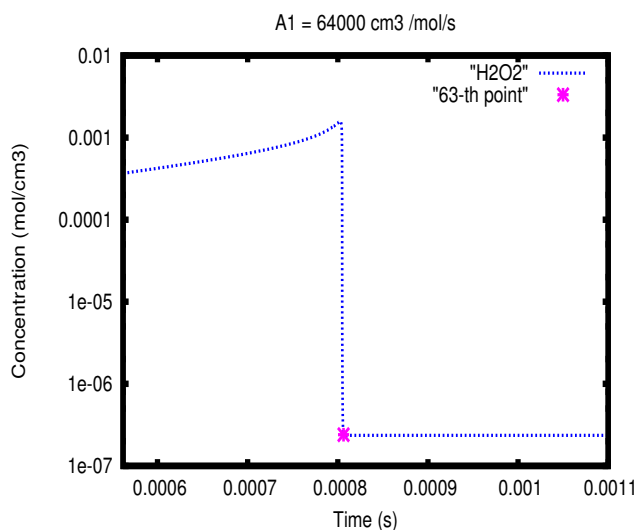


Figure 4.8: $[\text{H}_2\text{O}_2](t)$

As can be seen, the exponential decrease of H_2O_2 concentration occurs earlier if the parameter is increased. For the parameter values considered here, the fast decrease always occurs after the sixty-two first time points, this is why their curves remain smooth and regular. For the 63,64,65, and 66-th points however, the transition occurs after a certain threshold of the parameter value has been reached. This is the cause of the strong decrease in the four curves and thus also of the oscillations of the distance d as function of A_1 . This suggests the possibility that systems without self-ignition and exponential changes will produce few local minima whereas systems undergoing a self-ignition process may be characterized by an extremely complex optimization landscape. This rule however only indicates the likely features of chemical kinetic optimization problem. Due to the complex interaction of parameters which may have contradictory effects on different measured profiles, local minima may also show up in the case without self-ignition. It is therefore necessary to be cautious before choosing and configuring the appropriate optimization method.

4.2 Optimization when no oscillations happen

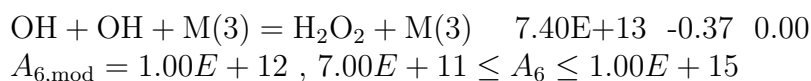
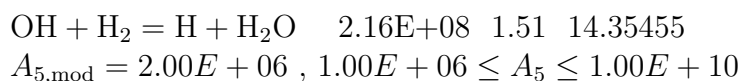
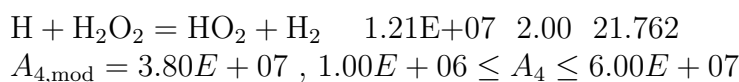
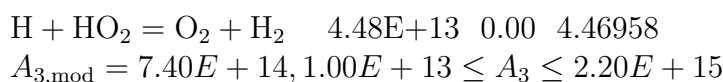
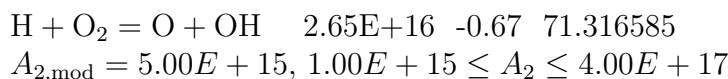
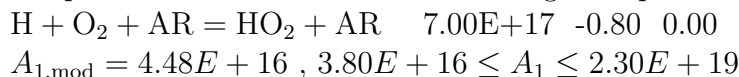
4.2.1 Optimization of six pre-exponential factors

A parameter estimation problem was constructed in such a way that no ignition and no exponential decrease or increase of any concentration took place. It is thus expected that only a few local minima will be present. The conditions of six artificial experiments are given in table 4.3.

Experiment	[H ₂] (ppm)	[O ₂] (ppm)	<i>T</i> (K)	<i>p</i> (bar)	<i>t</i> (s)	Target-species
1	500	500	1000	300.08	0.0081	OH, H ₂ O and H ₂ O ₂
2	100	1000	1000	200.00	0.0081	OH, H ₂ O and H ₂ O ₂
3	1000	4000	1000	100.90	0.0081	OH, H ₂ O and H ₂ O ₂
4	4000	1000	1020	100.90	0.0081	OH, H ₂ O and H ₂ O ₂
5	400	100	1020	100.90	0.0081	OH, H ₂ O and H ₂ O ₂
6	200	200	1000	70.9	0.0081	OH, H ₂ O and H ₂ O ₂

Table 4.3: Initial conditions

The high dilution of the compounds and the low temperatures prevent an ignition to occur. The reactions considered here are reported in the following lines. They are written in the following form: $A + B + C = D + E + F$ A (mol/cm³/s), n , E_a (kJ/mol). The modified value of the pre-exponential factor is then given along the bound constraints between which all values of the parameters must be included during the optimization.



The distance d as function of separately varied parameters (see figures 4.9 - 4.14, the units of the parameters being mol, cm, and s) has always a smooth shape without fluctuations, thus considerably reducing the number of local optima while all parameters are varied simultaneously.

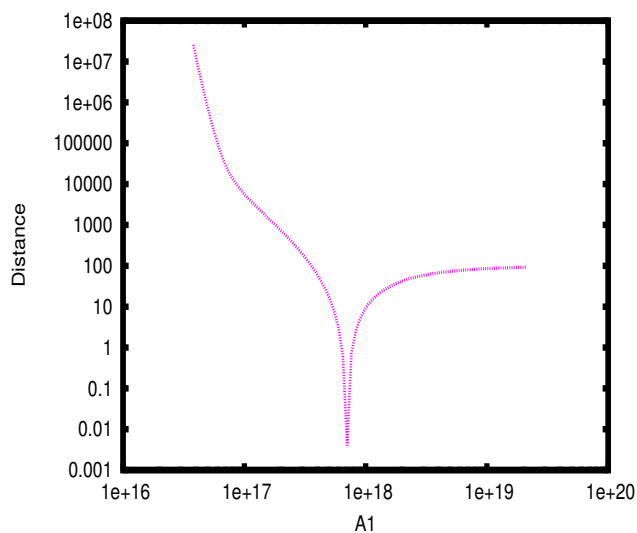


Figure 4.9: $d(A_1)$

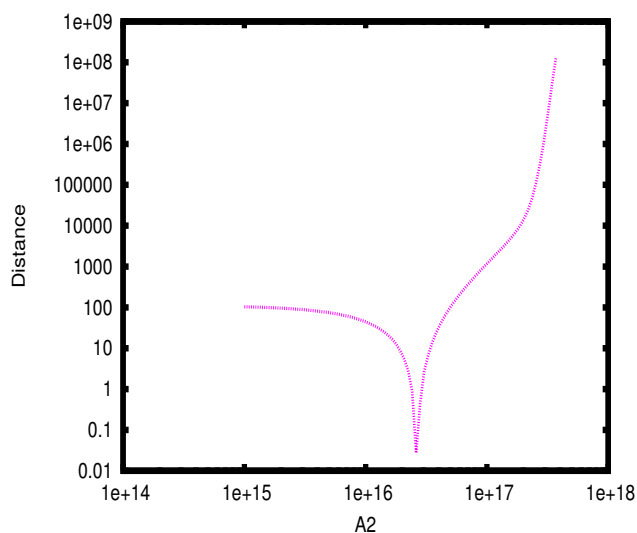


Figure 4.10: $d(A_2)$

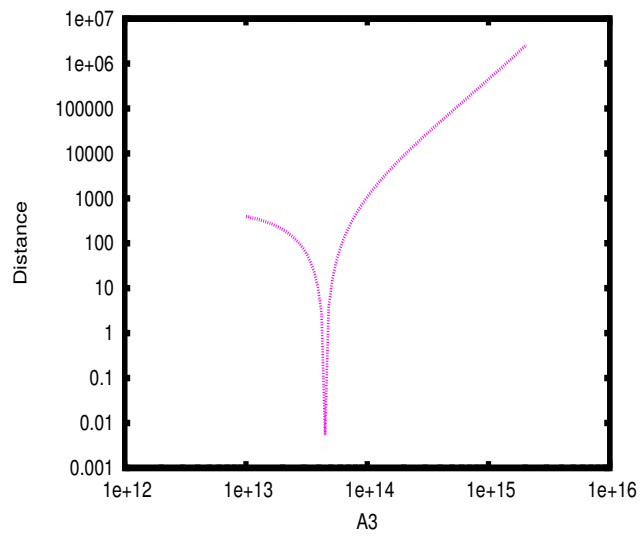


Figure 4.11: $d(A_3)$

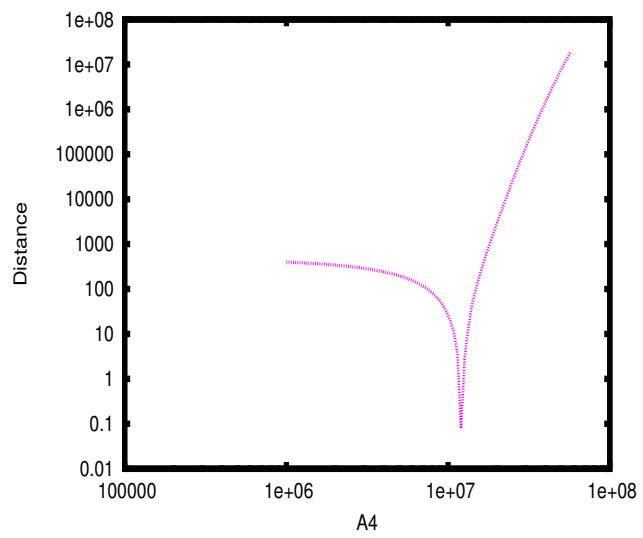


Figure 4.12: $d(A_4)$

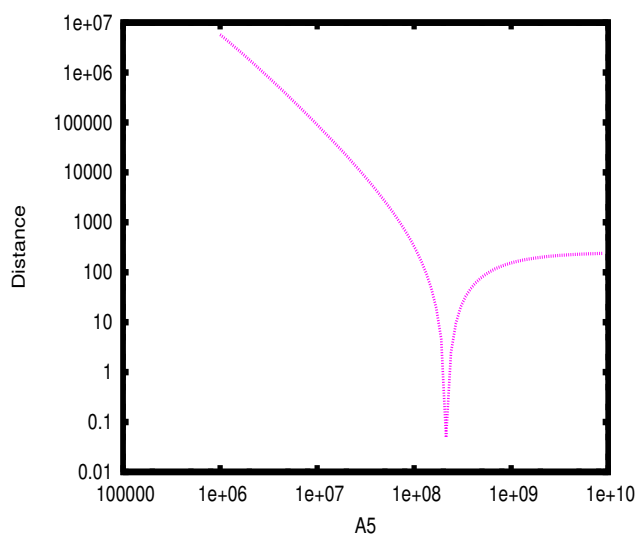


Figure 4.13: $d(A_5)$

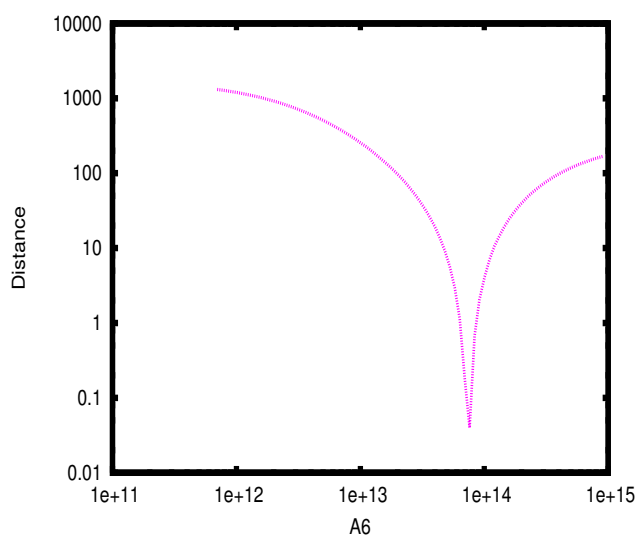


Figure 4.14: $d(A_6)$

Given enough time, all four methods converged towards a satisfying minimum, where no difference is visible with the "experiment", as illustrated in figures 4.15, 4.16 and 4.17 showing the profiles of OH for the first experiment, H_2O_2 for the fourth experiment and H_2O for the sixth experiment. The agreement for the other profiles is similar and well represented by these three profiles. The points denoted by "exp" correspond to the pseudo-experimental

data generated with the "true" values of the GRI-mechanism. The curves referred to as "modified" are the new profiles after modification of the initial values. The curves referred to as "best" correspond to the best fit found by the current optimization method. They were brought about by the Random Search (RS) method.

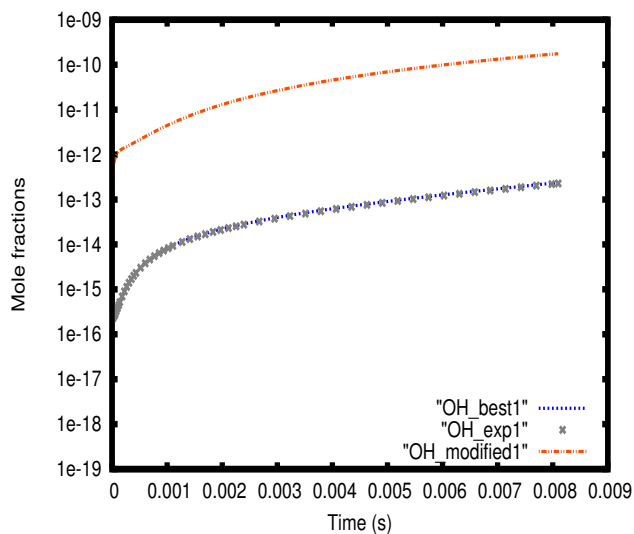


Figure 4.15: OH, 1-st experiment

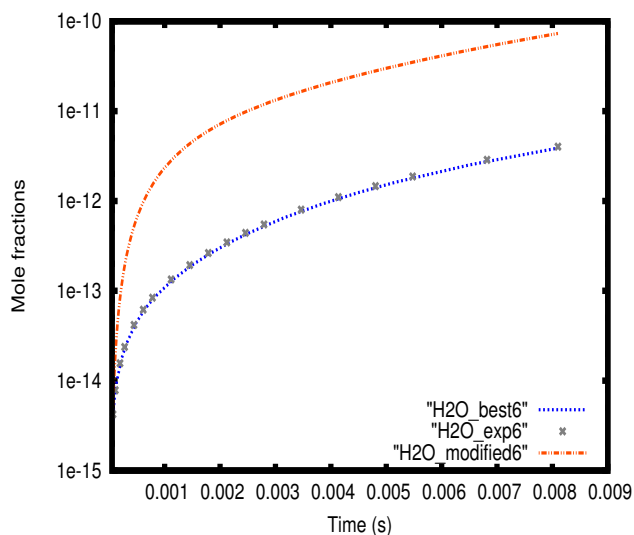


Figure 4.16: H₂O₂, 4-th experiment

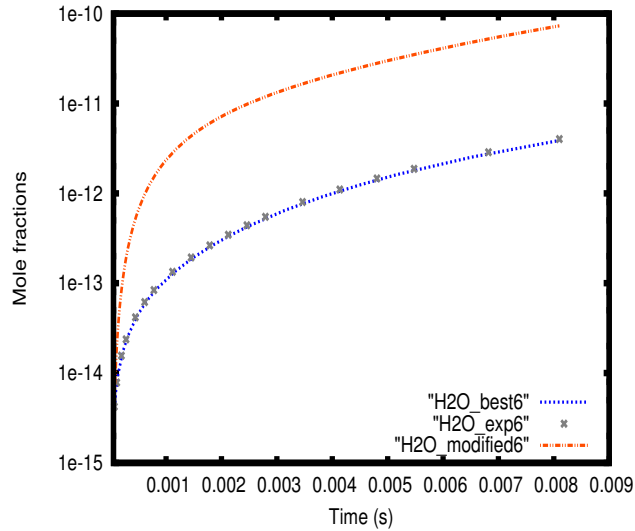


Figure 4.17: H₂O, 6-th experiment

The values of the optimized parameters are given in table 4.4. $r_i = \frac{A_{i,ini} - A_i}{A_{i,ini}}$ is the relative difference of the parameter A_i with respect to its initial (optimal) value.

Method	RS	CONDOR	BOBYQA	GA	Initial	Modified
A_1	6.70E+17	6.94E+17	7.69E+17	9.72E+17	7.00E+17	4.48E+016
r_1	0.043	0.008	-0.098	-0.389	0	0.936
A_2	2.51E+16	2.62E+16	2.91E+16	3.52E+16	2.65E+16	5.00E+015
r_2	0.0539	0.0111	-0.0991	-0.328	0	0.811
A_3	4.35E+13	4.49E+13	4.46E+13	4.56E+13	4.48E+13	7.40E+014
r_3	0.0285	-0.003	0.005	-0.0175	0	-15.518
A_4	1.22E+07	1.21E+07	1.21E+07	1.20E+07	1.21E+07	3.80E+007
r_4	-0.009	0.003	0.000	0.005	0	-2.140
A_5	2.02E+08	2.16E+08	2.15E+08	2.19E+08	2.16E+08	2.00E+006
r_5	0.066	0.001	0.007	-0.016	0	0.991
A_6	7.02E+13	7.41E+13	7.33E+13	7.60E+13	7.40E+13	1.00E+012
r_6	0.052	-0.001	0.009	-0.027	0	0.986
d	0.525	0.003	0.015	0.498	0	6.12E+08

Table 4.4: Optimized parameters

All methods converged towards the original parameter values. The local optimization methods were capable of retrieving them with greater accuracy than the GA. The performance of the four optimization techniques is illustrated in fig. 4.18 which represents the evolution of the smallest distance found as a function of the iteration number.

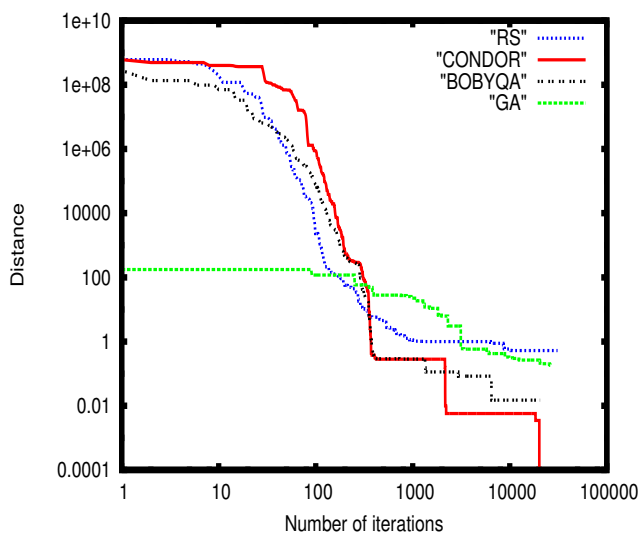


Figure 4.18: Compared performances of the optimization techniques

The solution found by Condor was more accurate than the one found by Bobbyba which itself fared better than the two other methods. The genetic algorithm and the random search reached approximately the same solution. The genetic algorithm was however less performing than the RS in that the distance reduction from the starting point was less considerable.

4.2.2 Optimization of six pre-exponential factors located on bounds

To check the reliability of the penalty-term method allowing the consideration of non-linear constraints in subsection 3.2.3, the same example as in 4.2.1 was considered in such a way that the optimal values were located on bounds defined by the penalty functions. The reactions considered here as well as the initial values of the pre-exponential factors (used to generate the experimental profiles) are the same as in 4.2.1. The new modified parameter values are given in table 4.5.

Parameter	Initial	Modified	Lower bound	Upper bound
A_1	7.00E+17	7.00E+16	3.80E+16	2.30E+19
A_2	2.65E+16	2.65E+17	1.00E+15	4.00E+17
A_3	4.48E+13	4.48E+14	1.00E+13	2.20E+15
A_4	1.21E+07	1.21E+06	1.00E+06	6.00E+07
A_5	2.16E+08	2.61E+07	1.00E+06	1.00E+10
A_6	7.40E+13	7.40E+14	7.00E+11	1.00E+15

Table 4.5: Chosen parameters

In addition to the lower and upper bounds, which are box constraints naturally taken into account by each of the four optimization approaches, constraints handled through penalty functions as explained in subsection 3.2.3 were imposed, with $q_i = 0.1$ and $q_s = 10$. At the beginning of the optimization, the initial parameter values A_0 are the modified values of table 4.5, and the additional bounds defined by the penalty terms are reported in table 4.6. The initial values of the $H_2 - O_2$ system are also the optimal values for the minimization of the distance $d(A)$.

Parameter	Initial	Modified	Lower penalty bound	Upper penalty bound
A_1	7.00E+17	7.00E+16	7.00E+15	7.00E+17
A_2	2.65E+16	2.65E+17	2.65E+16	2.65E+18
A_3	4.48E+13	4.48E+14	4.48E+13	4.48E+15
A_4	1.21E+07	1.21E+06	1.21E+05	1.21E+07
A_5	2.16E+08	2.61E+07	2.61E+06	2.61E+08
A_6	7.40E+13	7.40E+14	7.40E+13	7.40E+15

Table 4.6: Chosen parameters

A factor ten was used for the definitions of the bounds in such a way to produce a relatively simple optimization problem whereby attention can be focused on the validity of the penalty terms. As can be seen in table 4.6, all optimal values are located on a bound defined by a penalty function.

Method	RS	CONDOR	BOBYQA	GA	Initial	Modified
A_1	7.00E+17	7.00E+17	6.91E+17	6.91E+17	7.00E+17	7.00E+16
r_1	0.000	0.000	0.013	0.013	0.000	0.900
A_2	2.65E+16	2.65E+16	2.62E+16	2.66E+16	2.65E+16	2.65E+17
r_2	0.000	0.000	0.011	-0.004	0.000	-9.000
A_3	4.48E+13	4.48E+13	4.48E+13	4.60E+13	4.48E+13	4.48E+14
r_3	0.000	0.000	0.000	-0.027	0.000	-9.000
A_4	1.21E+07	1.21E+07	1.21E+07	1.20E+07	1.21E+07	1.21E+06
r_4	0.000	0.000	0.000	0.008	0.000	0.900
A_5	2.16E+08	2.16E+08	2.16E+08	2.25E+08	2.16E+08	2.61E+07
r_5	0.000	0.000	0.000	-0.042	0.000	0.879
A_6	7.40E+13	7.39E+13	7.46E+13	7.63E+13	7.40E+13	7.40E+14
r_6	0.000	0.001	-0.008	-0.031	0.000	-9.000
d	0	0.000	0.006	0.262	0	6.12E+08

Table 4.7: Optimized parameters

$r_i = \frac{A_{i,ini} - A_i}{A_{i,ini}}$ is the relative difference of the parameter A_i with respect to its initial (optimal) value. Each of the four optimization method could identify the global minimum of the problem, showing thus that the introduction of penalty terms does not hinder the convergence to solutions located at the boundaries. As in 4.2.1, the optimal and optimized curves could not be visually distinguished despite the fact that the original values were not retrieved. The performance of the optimization methods is shown in figure 4.19.

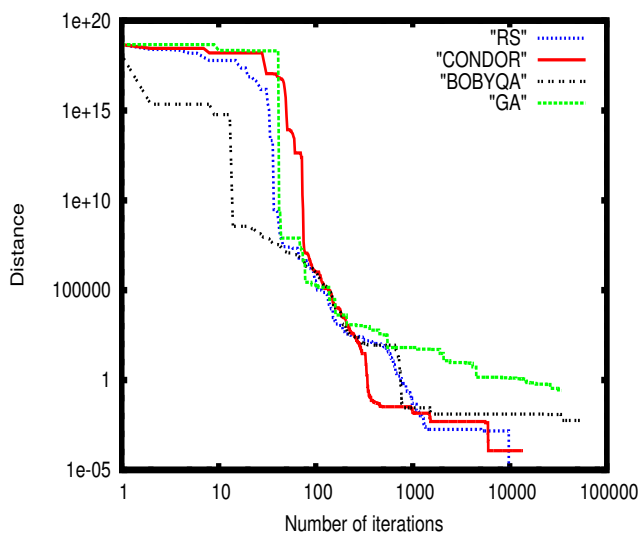


Figure 4.19: Compared performances of the optimization techniques

This time the GA brought the poorest fit whereas the RS led to the best solution and the performances of CONDOR and BOBYQA were in between.

4.2.3 Optimization of six pre-exponential factors, temperature coefficients and activation energies

The same problem (experimental conditions, target species and reactions) was considered, but this time the temperature coefficients and activation energies were modified and optimized alongside the pre-exponential factors, thereby resulting in a minimization problem of 18 variables. The modification of the eighteen coefficients reported in table 4.8 led to important changes of the concentration profile but not to irregularities/fluctuations of the distance d as a function of separately varied parameters. Nevertheless, the existence of more local minima is expected here. In effect, the three parameters of one reaction are highly correlated, and several combinations of their values will correspond to local optima if they lead to reaction rates $k(T)$ with similar values within the prescribed bounds.

Parameter	Initial value	Modified values	Lower bound	Upper bound
A_1	7.00E+17	8.00E+16	5.00E+16	1.00E+19
n_1	-0.80	-0.30	-1.2	-0.2
$E_{a,1}$	0.00	15.00	-10	15
A_2	2.65E+16	4.00E+17	1E+14	5E+17
n_2	-0.67	-1.40	-1.5	-0.25
$E_{a,2}$	71.32	60.00	55	80
A_3	4.48E+13	1.00E+15	1.0E+12	5E+15
n_3	0.00	0.80	-0.4	1.0
$E_{a,3}$	4.47	-7.00	-10	20
A_4	1.21E+07	8.00E+07	1.00E+06	1.00E+08
n_4	2.00	2.30	1.6	2.4
$E_{a,4}$	21.76	15.00	10.00	30.00
A_5	2.16E+08	5.00E+06	1.00E+06	5.00E+09
n_5	1.51	1.80	0.6	2.0
$E_{a,5}$	14.35	22.00	0	25
A_6	7.40E+13	2.00E+12	1.00E+12	1.00E+16
n_6	-0.37	-1.00	-1.5	0.5
$E_{a,6}$	0.00	13.00	-15	15

Table 4.8: Chosen parameters

The optimized parameters are reported in table 4.9.

Method	RS	CONDOR	BOBYQA	GA	Initial	Modified
A_1	2.79E+18	3.02E+17	9.50E+16	1.49E+17	7.00E+17	8.00E+16
n_1	-0.831	-0.827	-0.535	-0.304	-0.80	-0.30
$E_{a,1}$	10.177	-6.763	-5.983	13.913	0.00	15.00
A_2	9.15E+16	4.67E+15	3.66E+17	1.80E+17	2.65E+16	4.00E+17
n_2	-0.885	-0.483	-0.972	-0.891	-0.67	-1.40
$E_{a,2}$	69.134	69.937	71.773	71.506		60.00
A_3	1.84E+13	1.10E+13	1.43E+13	2.91E+12	4.48E+13	1.00E+15
n_3	0.224	0.280	0.179	0.520	0.00	0.80
$E_{a,3}$	9.905	8.661	5.861	12.241	4.47	-7.00
A_4	5.04E+07	2.63E+07	8.70E+07	1.10E+06	1.21E+07	8.00E+07
n_4	1.728	1.843	1.787	2.199	2.00	2.30
$E_{a,4}$	17.958	19.0971	26.1091	12.967	21.76	15.00
A_5	2.00E+07	4.14E+09	2.84E+06	1.23E+07	2.16E+08	5.00E+06
n_5	1.934	0.993	1.999	1.953	1.51	1.80
$E_{a,5}$	18.722	8.923	7.735	15.352	14.35	22.00
A_6	1.50E+14	7.38E+12	3.12E+12	2.88E+12	7.40E+13	2.00E+12
n_6	-0.428	-0.202	0.255	0.178	-0.37	-1.00
$E_{a,6}$	2.397	-9.813	11.227	4.889	0.00	13.00
d	0.041	0.152	3.060	0.935	0	2.01E+13

Table 4.9: Optimized parameters

As in 4.2.1, the optimal and optimized curves could not be visually distinguished. However, the optimized parameters are often very different from one another. To avoid self-ignition and the appearance of oscillations (see 4.1), initial temperatures equal or close to 1000 K had to be chosen. Since the temperature remained almost constant during all six experiments, the six reaction rate coefficients always kept the same values, thereby preventing a discrimination between pre-exponential factors, temperature coefficients and activation energies. This stems from the fact that several combinations of the three parameters of one reaction will lead to the same value of the reaction rate coefficient. The reaction rates at 1000 K had close values, as can be seen in table 4.10. $r_i = \frac{A_{i,ini} - A_i}{A_{i,ini}}$ is the relative difference of the parameter A_i with respect to its initial (optimal) value.

Method	RS	CONDOR	BOBYQA	GA	Initial	Modified
k_1	2.64E+15	2.26E+15	4.86E+15	3.43E+15	2.79E+15	1.66E+15
r_1	0.054	0.190	-0.742	-0.229	0.000	4.050E-01
k_2	4.95E+10	3.70E+10	7.91E+10	7.00E+10	1.90E+11	2.52E+13
r_2	0.739	0.805	0.584	0.632	0.000	-1.316E+02
k_3	2.62E+13	2.70E+13	2.44E+13	2.42E+13	2.62E+13	5.83E+17
r_3	0.000	-0.031	0.069	0.076	0.000	-2.225E+04
k_4	8.90E+11	8.92E+11	8.62E+11	9.16E+11	8.83E+11	1.05E+14
r_4	-0.008	-0.010	0.024	-0.037	0.000	-1.179E+02
k_5	1.34E+12	1.35E+12	1.11E+12	1.40E+12	1.30E+12	8.91E+10
r_5	-0.031	-0.038	0.146	-0.077	0.000	9.315E-01
k_6	5.84E+12	5.94E+12	4.72E+12	5.47E+12	5.74E+12	4.19E+08
r_6	-0.017	-0.035	0.178	0.047	0.000	9.999E-01
d	0.041	0.152	3.060	0.935	0	2.02E+13

Table 4.10: Optimized rate coefficients at 1000 K

Most rate coefficient values are close from one another but some differences exist, as example for k_1 and k_2 , reflecting the presence of several local minima. The performances of the optimization methods are depicted in figure 4.20.

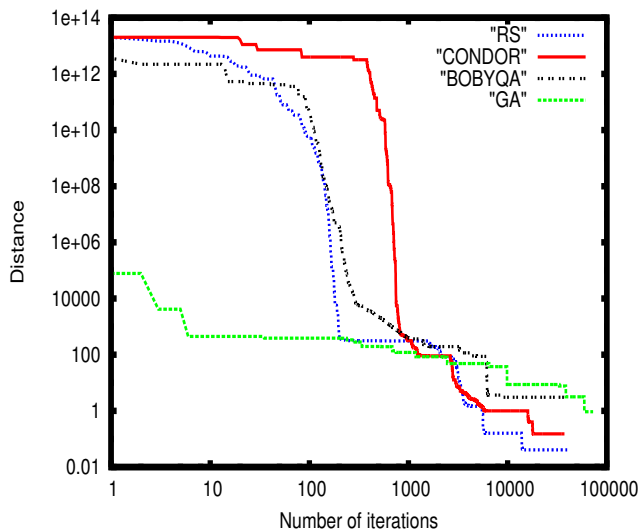


Figure 4.20: Compared performances of the optimization techniques

The efficiencies of the methods were relatively close to one another, the Random Search bringing in the end the best results.

4.3 Optimization when fluctuations take place

4.3.1 Optimization of seven pre-exponential factors

Six experimental conditions were chosen in such a way that the systems underwent ignition with exponential increases and decreases of the species concentrations, thereby creating fluctuations of the distance $d(p)$ and thus many

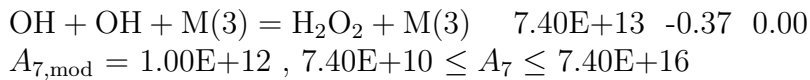
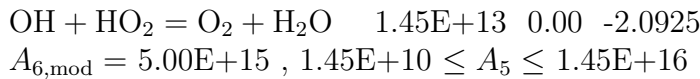
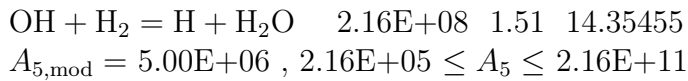
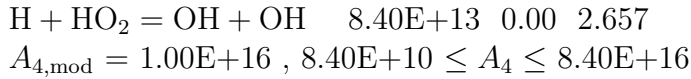
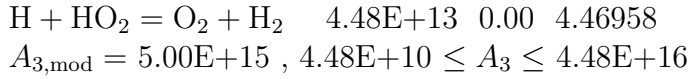
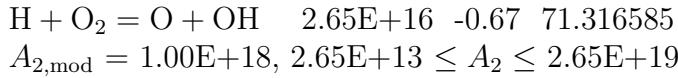
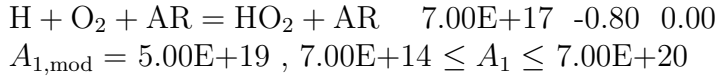
local minima. The conditions of the six artificial experiments are given in table 4.11.

Experiment	[H ₂] (ppm)	[O ₂] (ppm)	T (K)	p (bar)	t (s)	Target-species
1	50000	50000	1200	3.08	6.00E-04	OH, H ₂ O and H ₂ O ₂
2	5000	5000	1300	100.08	2.0E-03	OH, H ₂ O and H ₂ O ₂
3	9000	1000	1600	5.08	2.0E-03	OH, H ₂ O and H ₂ O ₂
4	700	300	1500	60.00	2.0E-03	OH, H ₂ O and H ₂ O ₂
5	500	500	1700	300.00	2.0E-03	OH, H ₂ O and H ₂ O ₂
6	3000	2000	1450	51.0	2.0E-03	OH, H ₂ O and H ₂ O ₂

Table 4.11: Initial conditions

Artificial experimental profiles for OH, H₂O, and H₂O₂ were generated with the initial reaction mechanism. The sensitive reactions considered here are reported in the following lines. Like previously, they are written in the following form:

$A + B + C = D + E + F$ A (mol, cm, s), n , E_a (kJ/mol). The modified value of the pre-exponential factor is then given along the bound constraints.



The evolution of the distance between model and experiment as a function of separately varied parameters is given in figures. 4.21 - 4.27. The units of the pre-exponential factors are mol, s, cm.

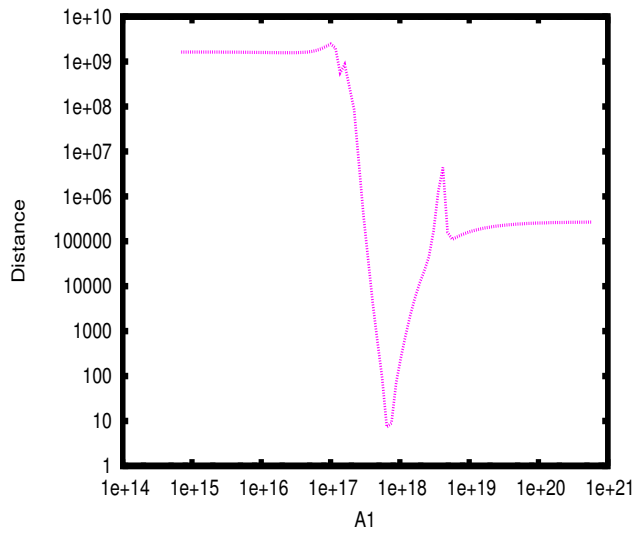


Figure 4.21: $d(A_1)$

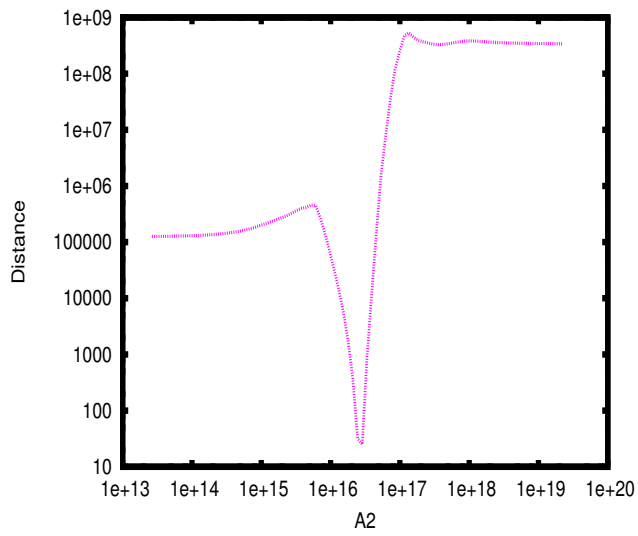


Figure 4.22: $d(A_2)$

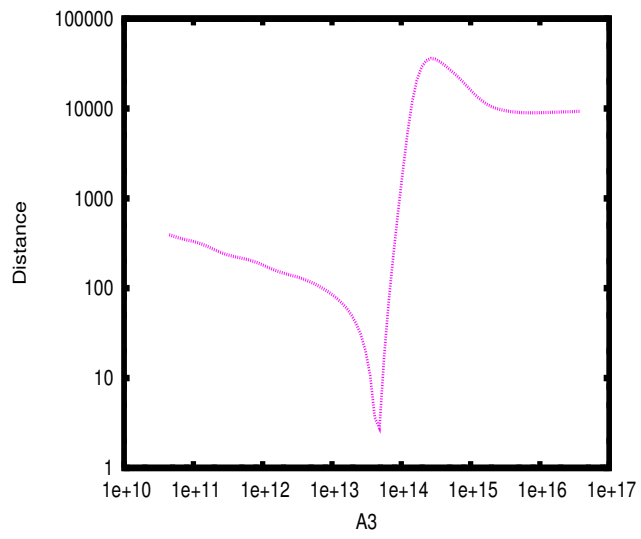


Figure 4.23: $d(A_3)$

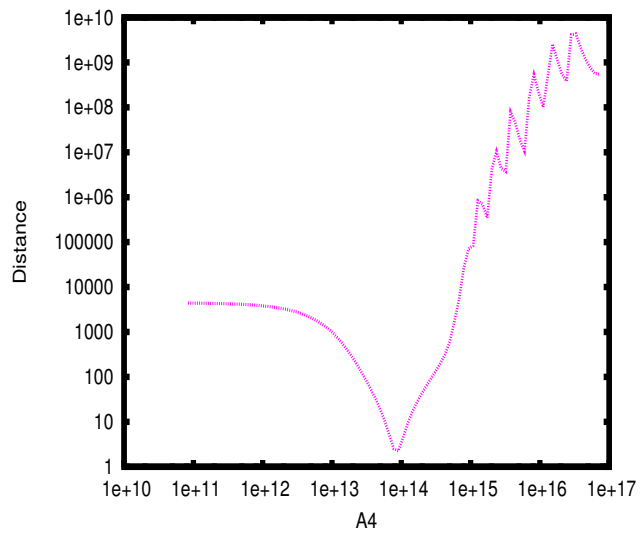


Figure 4.24: $d(A_4)$

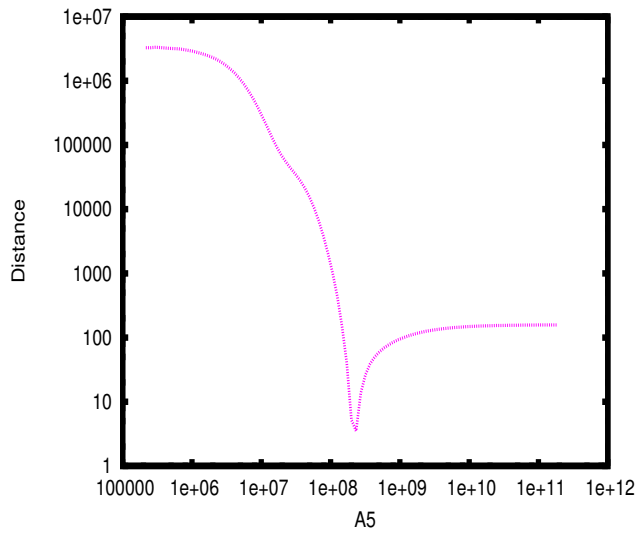


Figure 4.25: $d(A_5)$

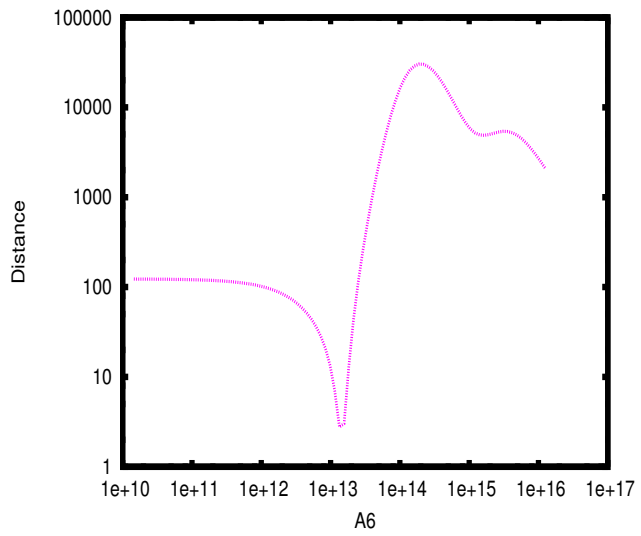


Figure 4.26: $d(A_6)$

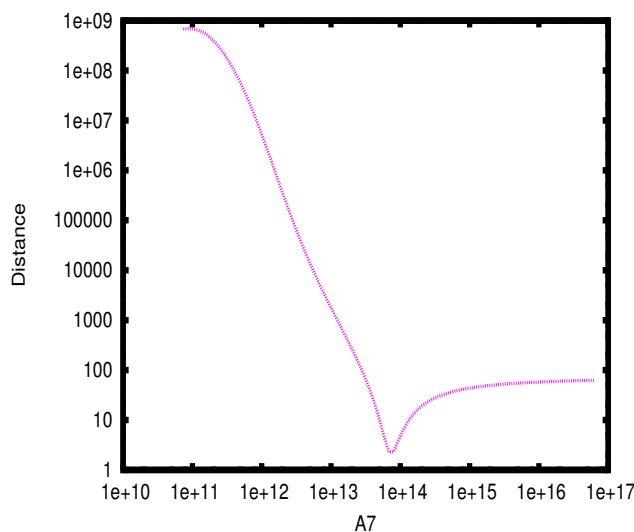


Figure 4.27: $d(A_7)$

Due to the fluctuations coming up in most of the curves, the distance $d(p)$ encompasses numerous local minima. The genetic algorithm, CONDOR and the random search converged to a satisfying solution indistinguishable from the optimum with respect to the target concentrations. The optimized values are given in table 4.12. $r_i = \frac{A_{i,ini} - A_i}{A_{i,ini}}$ is the relative difference of the parameter A_i with respect to its initial (optimal) value.

Method	RS	CONDOR	BOBYQA	GA	Initial	Modified
A_1	7.41E+17	7.23E+17	9.39E+17	6.78E+17	7.00E+17	5.00E+19
r_1	-0.059	-0.033	-0.341	0.031	0	-70.429
A_2	2.64E+16	2.73E+16	2.45E+16	2.65E+16	2.65E+16	1.00E+18
r_2	0.004	-0.03	0.075	0	0	-36.736
A_3	5.31E+13	4.50E+13	9.02E+13	4.46E+13	4.48E+13	5.00E+15
r_3	-0.185	-0.004	-1.013	0.004	0	-110.607
A_4	1.17E+14	7.82E+13	1.87E+14	8.58E+13	8.40E+13	1.00E+16
r_4	-0.393	0.069	-1.226	-0.021	0	-118.048
A_5	2.21E+08	2.19E+08	2.37E+08	2.21E+08	2.16E+08	5.00E+06
r_5	-0.023	-0.014	-0.097	-0.023	0	0.977
A_6	1.19E+13	1.53E+13	1.71E+11	1.46E+13	1.45E+13	5.00E+15
r_6	0.179	-0.055	0.988	-0.007	0	-343.828
A_7	6.69E+13	7.87E+13	1.30E+14	5.96E+13	7.40E+13	1.00E+12
r_7	0.096	-0.064	-0.757	0.195	0	0.986
d	3.235	1.084	63.740	2.162	0	83.637

Table 4.12: Optimized parameters

It is worth noting that in almost every case each method converged to the optimal value although the optimization landscape was very complex. Small discrepancies were present for some of the profiles optimized with Bobyqa as illustrated in figures 4.28- 4.30. For all other minimization methods, no differences between the experimental and optimized profiles are visible.

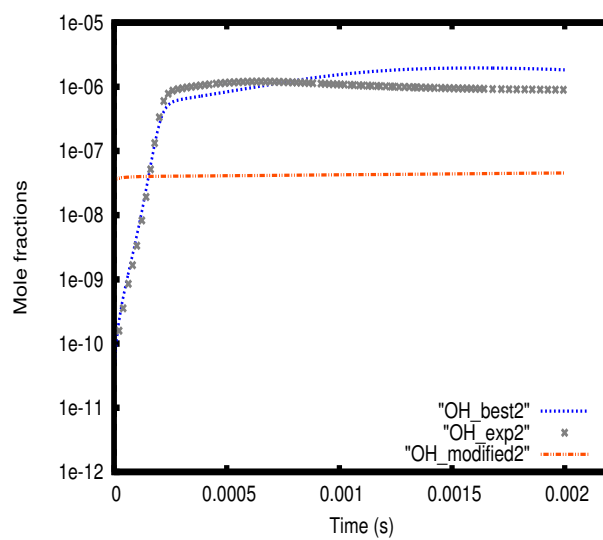


Figure 4.28: OH-profile for the second experiment

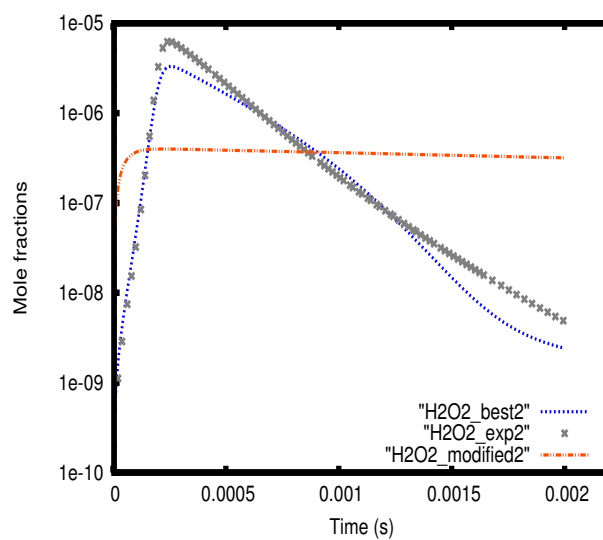


Figure 4.29: H₂O₂ -profile for the second experiment

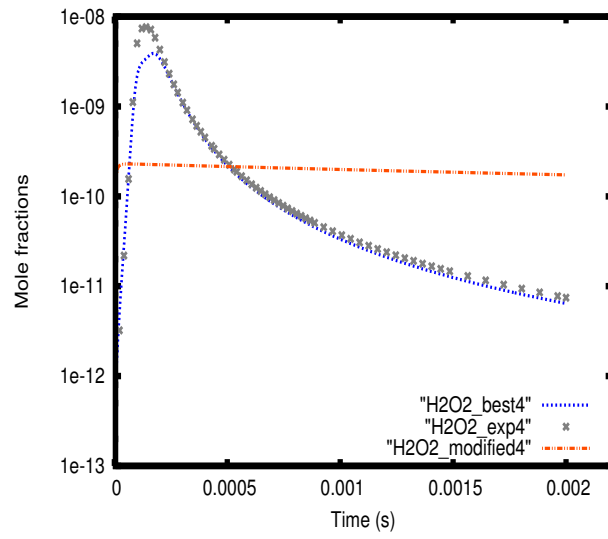


Figure 4.30: H₂O₂-profile for the fourth experiment

The different performances of the optimization methods are plotted in figure 4.31 .

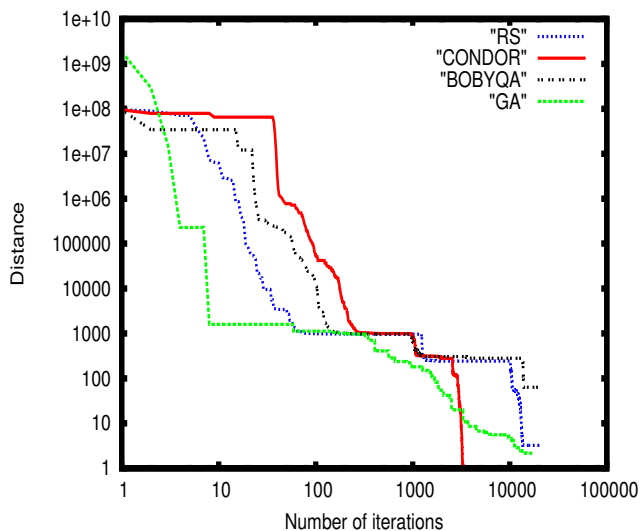


Figure 4.31: Compared performances of the optimization techniques

Ga and Condor led to the best solution whereas the Random Search was approaching it. Bobyqa performed the most poorly but found a solution consistent with the experimental data.

4.3.2 Optimization of seven temperature coefficients and seven activation energies

To test the flexibility and performance of Kinefit, the same experiments and reactions were considered, but this time the temperature coefficients and activation energies were modified and then optimized as reported in table 4.13.

Parameter	Initial value	Modified values	Lower bound	Upper bound
n_1	-0.80	-1.50	-2.0	0.0
$E_{a,1}$	0.00	15.0	-20	20
n_2	-0.67	-1.00	-1.5	0
$E_{a,2}$	71.32	89.0	55.00	90.00
n_3	0.00	0.50	-0.5	1.0
$E_{a,3}$	4.46	-3.00	-5.00	0.0
n_4	0.00	1.00	-0.5	1.50
$E_{a,4}$	2.66	10.00	-10.00	15.00
n_5	1.51	0.40	0.30	2.00
$E_{a,5}$	14.35	30.00	0	35.00
n_6	0.00	0.75	-0.5	1.5
$E_{a,6}$	-2.09	-15.00	-20.00	15.00
n_7	-0.37	-1.50	-2.0	0.5
$E_{a,7}$	0.00	17.00	-10	20

Table 4.13: Chosen parameters

The optimized values are given in table 4.14.

Method	RS	CONDOR	BOBYQA	GA	Initial	Modified
n_1	-0.625	-0.786	-0.456	-0.864	-0.800	-1.500
$E_{a,1}$	15.03	-9.721	-0.456	-7.553	0.00	15.0
n_2	-0.596	-0.829	-0.558	-0.757	-0.67	-1.00
$E_{a,2}$	77.621	57.226	81.158	63.771	71.32	89.0
n_3	-0.082	-0.040	-0.2300	-0.0457	0.00	0.50
$E_{a,3}$	-3.974	-4.117	-4.362	-0.896	4.46	-3.00
n_4	0.074	0.423	0.591	0.161	0.00	1.00
$E_{a,4}$	6.353	14.448	-4.864	7.648	2.66	10.00
n_5	1.405	1.398	1.520	1.625	1.51	0.40
$E_{a,5}$	3.811	6.337	9.846	25.237	14.35	30.00
n_6	-0.118	0.027	0.083	-0.174	0.00	0.75
$E_{a,6}$	-11.0593	11.915	6.459	-8.903	-2.09	-15.00
n_7	-0.262	-0.383	-0.839	-0.218	-0.37	-1.50
$E_{a,7}$	10.214	2.713	-8.536	15.061	0.00	17.00
d	8.874	37.326	299.854	15.867	0	2.37E+06

Table 4.14: Optimized parameters

The final optimum identified by Bobyqa is characterized by great discrepancies with the perfect solution for the OH and H₂O₂-profiles as illustrated by figures 4.32- 4.34.

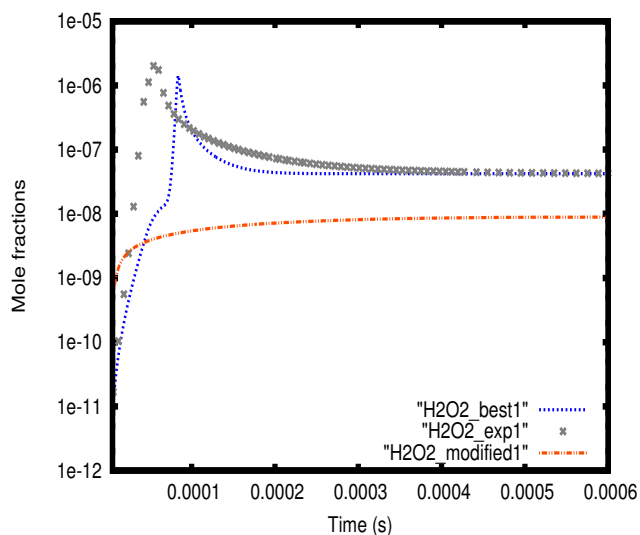


Figure 4.32: Bobyqa, H₂O₂-profiles, 1-st experiment

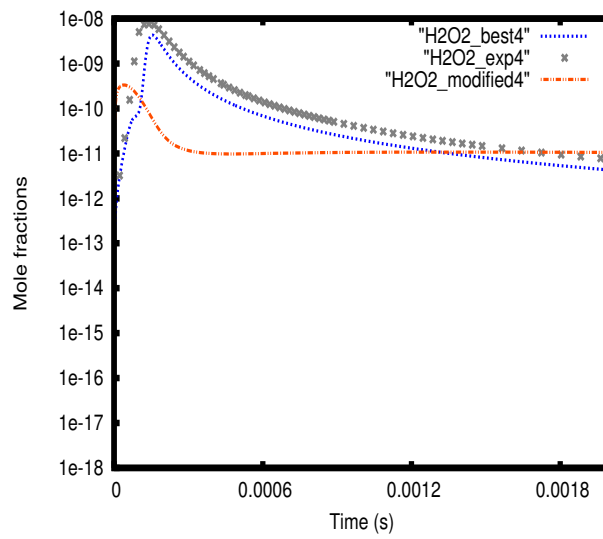


Figure 4.33: Bobyqa, H₂O₂-profiles, 4-st experiment

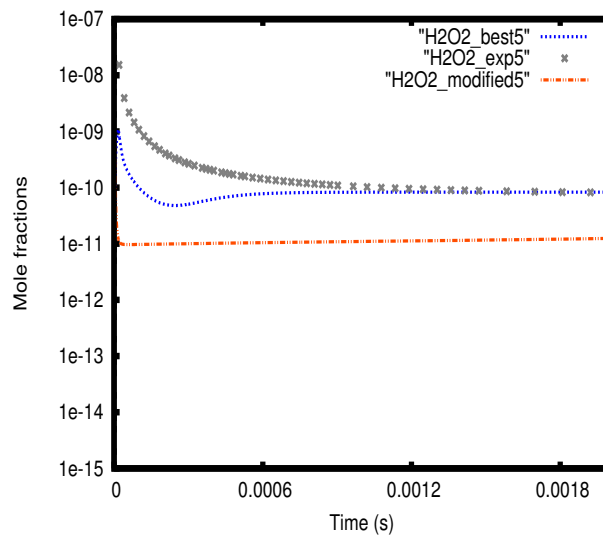


Figure 4.34: Bobyqa, OH-profile, 5-th experiment

Nevertheless, the H₂O-profiles are very well predicted by Bobyqa's optimal solution as can be visualized in figure 4.35.

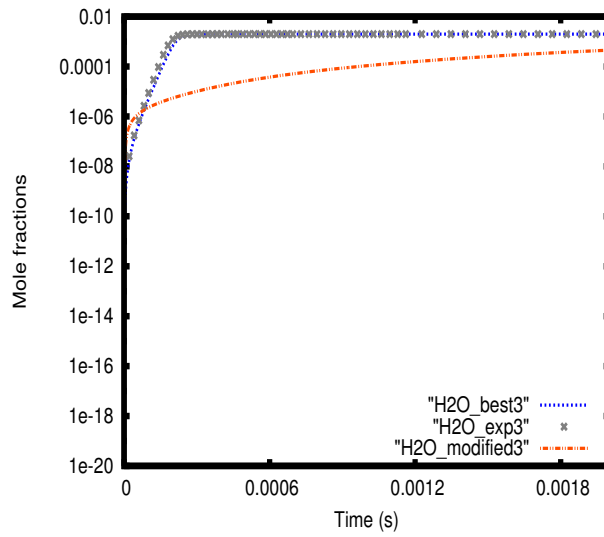


Figure 4.35: Bobbyqa, H₂O-profile, 3-rd experiment

Condor, the Genetic Algorithm and the Random Search brought up a good solution with almost perfect agreements for most profiles and minor discrepancies for some of them. As typical examples, three profiles optimized by Condor are reported in figures 4.36- 4.38.

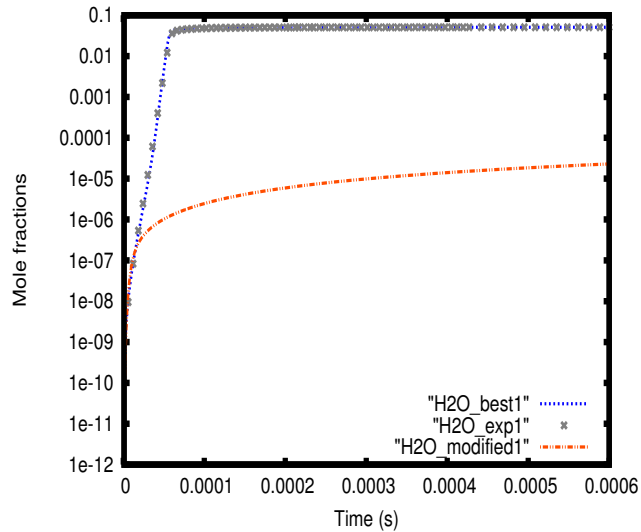


Figure 4.36: Condor, H₂O-profile, 1-st experiment

For this profile, the optimal and optimized curves are completely identical.

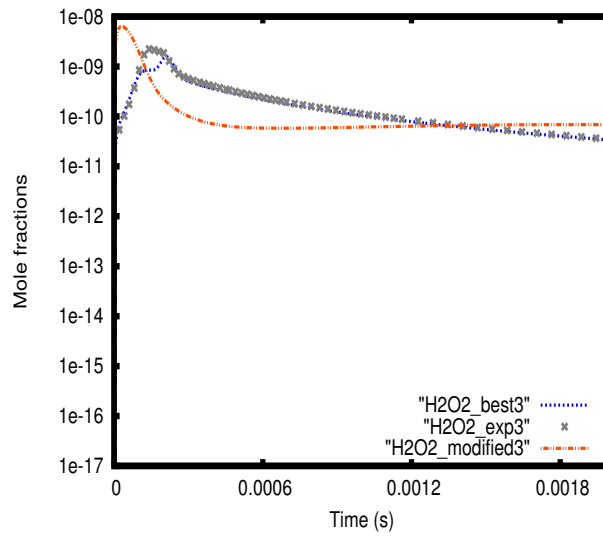


Figure 4.37: Condor, H_2O_2 -profile, 3-rd experiment

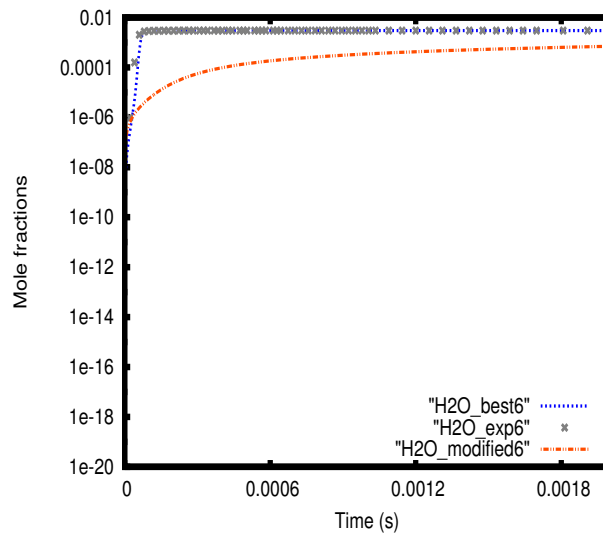


Figure 4.38: Condor, OH-profile, 6-th experiment

The performances of the optimization methods are given in figure 4.39 .

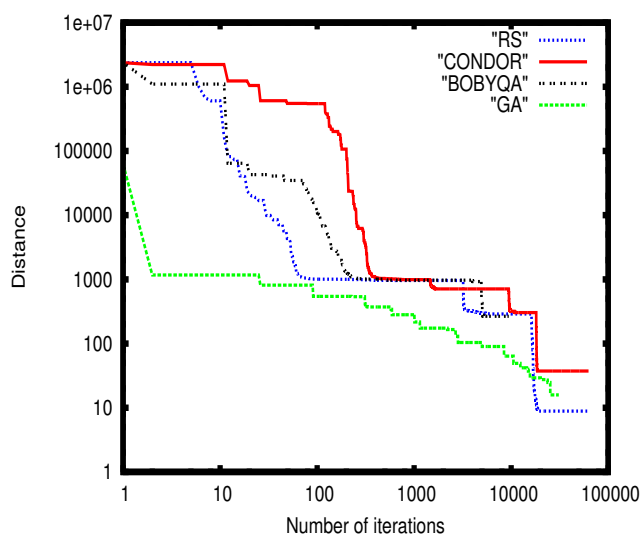


Figure 4.39: Compared performances of the optimization techniques

At the end, the random search brought the best results whereas the genetic algorithm was not far from an optimal solution. Condor and Bobyqa did not converge to a solution of a similar quality.

4.3.3 Optimization of seven pre-exponential factors, temperature coefficients and activation energies

Considering the same six experiments and seven reactions, the pre-exponential factors, temperature coefficients and activation energies of all reactions were modified and then optimized (see 4.15), resulting thus in an extremely complex minimization problem of 21 factors, containing many valleys, ridges and local minima. Due to the huge number of local minima stemming from the natural oscillation of the distance (see chapter 4.1) and the width of the search space, no optimization method was able to converge to an optimum solution, although significant improvements were reached through the random search method and Condor. Condor led to a global improvement, whereby some profiles (see figures 4.40 and 4.41) are perfectly reproduced.

Parameter	Initial	Modified	Lower bound	Upper bound
A_1	7.0E+17	1.0E+17	1.00E+16	1.00E+20
n_1	0.8	-1.5	-2.0	0.0
$E_{a,1}$	0.0	15.0	-20	20
A_2	2.65E+16	1.0E+18	1.00E+15	1.00E+19
n_2	-0.67	-1.0	-1.5	0
$E_{a,2}$	71.32	89.0	55.0	90.0
A_3	4.48E+13	8.0E+15	1.0E+12	1.0E+16
n_3	0.0	0.50	-0.5	1.0
$E_{a,3}$	4.47	-3.0	-5	0.0
A_4	8.4E+13	1.0E+16	1.0E+12	1.0E+17
n_4	0	1	-0.5	1.5
$E_{a,4}$	2.66	10.0	-10	15
A_5	2.16E+08	5.0E+16	1.0E+06	1.0E+10
n_5	1.51	0.4	0.30	2.0
$E_{a,5}$	14.35	30.0	0	35
A_6	1.45E+13	5.0E+15	1.0E+12	1.5E+16
n_6	0	0.75	-0.5	1.5
$E_{a,6}$	-2.0925	-15	-20.0	15.0
A_7	7.40E+13	5.0E+12	1.0E+12	1.0E+15
n_7	-0.37	-1.50	-2.0	0.5
$E_{a,7}$	0.0	17	-10	20

Table 4.15: Modified parameters

The optimized results are reported in table 4.16.

Method	BOBYQA	RS	CONDOR	GA	Initial	Modified
A_1	2.35E+18	6.56E+18	1.36E+18	5.12E+19	7.00E+17	1.00E+17
n_1	-0.396	-1.213	-1.106	-1.683	0.8	-1.5
$E_{a,1}$	19.564	-0.7071	-5.667	-12.440	0.0	15.0
A_2	2.20E+16	5.35E+16	2.37E+15	2.72E+16	2.65E+16	1.0E+18
n_2	-0.742	-0.734	-0.340	-0.598	-0.67	-1.0
$E_{a,2}$	68.202	72.051	71.480	77.938	71.32	89.0
A_3	3.85E+12	1.05E+13	1.38E+15	1.25E+12	4.48E+13	8.0E+15
n_3	0.31	-0.104	-0.490	0.452	0.0	0.50
$E_{a,3}$	-4.510	-0.518	-3.399	-0.556	4.47	-3.0
A_4	3.99E+12	1.98E+16	2.24E+12	2.33E+15	8.40E+13	1.0E+16
n_4	1.198	0.457	0.524	-0.331	0	1
$E_{a,4}$	-0.808	9.742	12.148	14.427	2.66	10.0
A_5	8.16E+08	6.15E+08	4.97E+08	6.96E+09	2.16E+08	5.0E+16
n_5	1.444	1.312	1.571	1.055	1.51	0.4
$E_{a,5}$	4.262	11.290	2.226	7.169	14.35	30.0
A_6	2.11E+13	9.91E+15	3.35E+15	1.41E+15	1.45E+13	5.0E+15
n_6	0.198	0.904	0.576	1.165	0	0.75
$E_{a,6}$	-6.850	4.221	-11.061	12.291	-2.093	-15
A_7	1.20E+13	1.19E+14	2.96E+14	8.80E+12	7.40E+13	5.0E+12
n_7	-0.061	-0.705	-0.831	-0.313	-0.37	-1.50
$E_{a,7}$	5.090	-7.593	-5.605	5.883	0.0	17
d	334.492	265.878	267.508	259.05	0	1.38E+10

Table 4.16: Optimized parameters

Since it is clear that most parameters widely diverge from the optimal values, the relative differences are not reported.

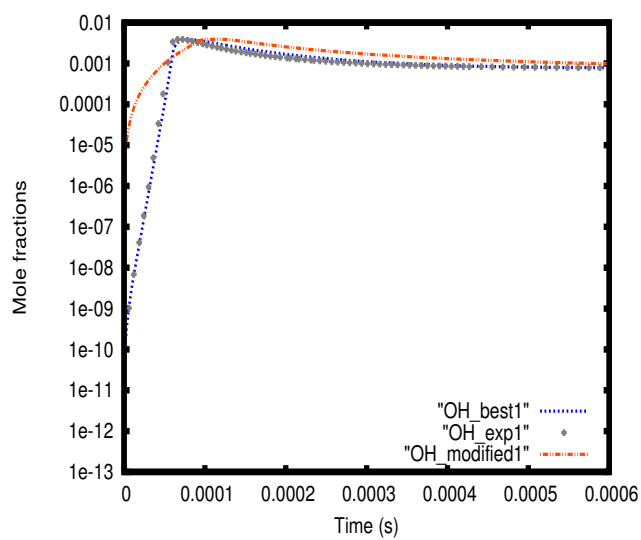


Figure 4.40: Condor, OH-profile, 1-th experiment

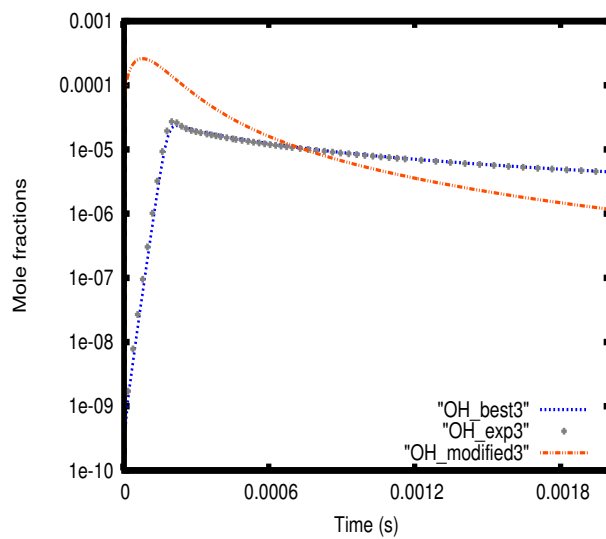


Figure 4.41: Condor, OH-profile, 3-rd experiment

The improvements are more modest for other profiles (fig. 4.42 and 4.43).

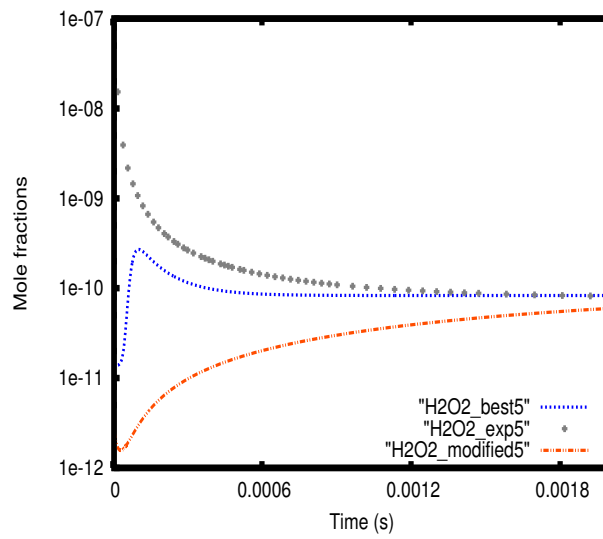


Figure 4.42: Condor, H_2O_2 -profile, 5-th experiment

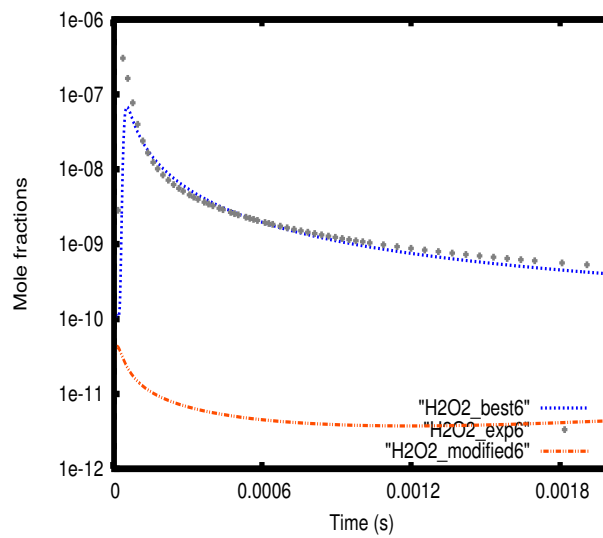


Figure 4.43: Condor, H_2O_2 -profile, 6-th experiment

However the predictions of some profiles, like OH for the second experiment (fig. 4.44), are considerably worse than at the beginning of the minimization.

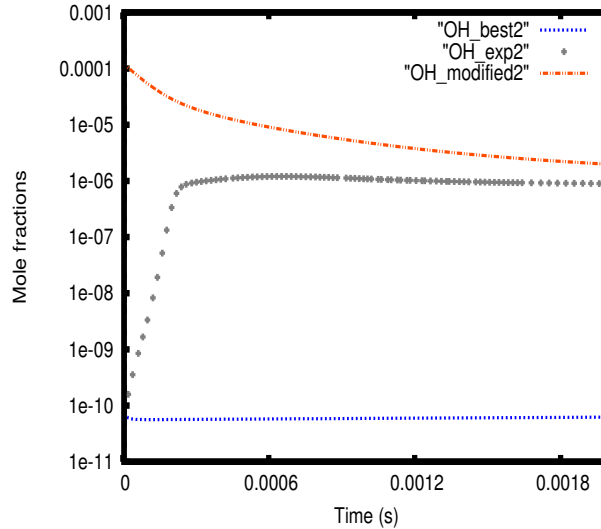


Figure 4.44: Condor, OH-profile, 2-th experiment

Such a situation comes up very often when the parameter optimization landscape contains numerous local minima like in the present case. To further test the optimization methods and to avoid this type of difficulties, the same problem was considered but with more realistic bounds, as reported in table 4.17.

Parameter	Initial	Modified	Lower bound	Upper bound
A_1	7.0E+17	9.00E+16	7.00E+16	7.00E+18
n_1	0.8	-1.10	-1.2	-0.4
$E_{a,1}$	0.0	4.00	-5	5
A_2	2.65E+16	1.60E+17	2.6E+15	2.6E+17
n_2	-0.67	-0.97	-1.1	-0.27
$E_{a,2}$	71.32	74.3166	66.3166	76.3166
A_3	4.48E+13	3.50E+14	4.5E+12	4.5E+14
n_3	0.0	-0.33	-0.53	0.4
$E_{a,3}$	4.47	8.47	-0.53042	9.4696
A_4	8.4E+13	6.40E+12	8.4E+12	8.4E+14
n_4	0	0.20	-0.4	0.4
$E_{a,4}$	2.66	1.34253	-2.34253	7.65747
A_5	2.16E+08	1.2E+07	2.2E+07	2.2E+09
n_5	1.51	1.7	1.1	1.9
$E_{a,5}$	14.35	17.355	9.3545	19.355
A_6	1.45E+13	3.4E+12	1.4E+12	1.4E+14
n_6	0	-0.3	-0.4	0.4
$E_{a,6}$	-2.0925	1.908	-7.092	2.908
A_7	7.40E+13	9.4E+12	7.4E+12	7.4E+14
n_7	-0.37	-0.13	-0.77	0.03
$E_{a,7}$	0.0	-3.00	-5	5

Table 4.17: Modified parameters

Due to the smaller bounds, better solutions could be reached, as reported in table 4.18.

Method	BOBYQA	RS	CONDOR	GA	Initial	Modified
A_1	3.78E+17	1.86E+18	5.93E+17	7.60E+17	7.00E+17	9.00E+16
n_1	-0.744	-0.910	-0.806	-0.745	0.8	-1.10
$E_{a,1}$	-2.949	1.615	-3.523	3.651	0.0	4.00
A_2	3.96E+16	5.91E+16	5.75E+16	5.97E+15	2.65E+16	1.60E+17
n_2	-0.696	-0.769	-0.777	-0.503	-0.67	-0.97
$E_{a,2}$	73.238	71.8151	70.7332	68.1719	71.32	74.3166
A_3	1.60E+13	5.32E+12	1.06E+14	3.48E+14	4.48E+13	3.50E+14
n_3	0.111	0.245	-0.127	-0.235	0.0	-0.33
$E_{a,3}$	2.059	0.091	2.777	6.715	4.47	8.47
A_4	7.62E+13	5.79E+13	9.35E+13	1.42E+14	8.40E+13	6.40E+12
n_4	-0.028	-0.003	-0.0469	-0.105	0	0.20
$E_{a,4}$	5.362	-0.948	-1.097	-1.984	2.66	1.343
A_5	3.44E+08	7.30E+07	2.03E+08	3.17E+08	2.16E+08	1.20E+07
n_5	1.523	1.730	1.478	1.542	1.51	1.7
$E_{a,5}$	15.509	17.728	12.507	18.468	14.35	17.355
A_6	2.98E+13	3.63E+13	7.30E+12	1.24E+14	1.45E+13	3.40E+12
n_6	-0.057	-0.102	0.068	-0.327	0	-0.3
$E_{a,6}$	-6.696	-0.460	-1.139	1.824	-2.093	1.908
A_7	3.74E+14	7.09E+14	4.75E+13	1.28E+14	7.40E+13	9.4E+12
n_7	-0.418	-0.677	-0.316	-0.287	-0.37	-0.13
$E_{a,7}$	-3.793	-0.426	-1.485	1.198	0.0	-3.00
d	24.401	0.857	0.266	9.008	0	4.37E+09

Table 4.18: Optimized parameters

The results from Condor, Bobyqa and the genetic algorithm are almost identical to the experimental values. The optimized profiles from Bobyqa are nearly indistinguishable from the solutions except for the second experiment whereby small discrepancies exist, as reported in figures 4.45 and 4.46.

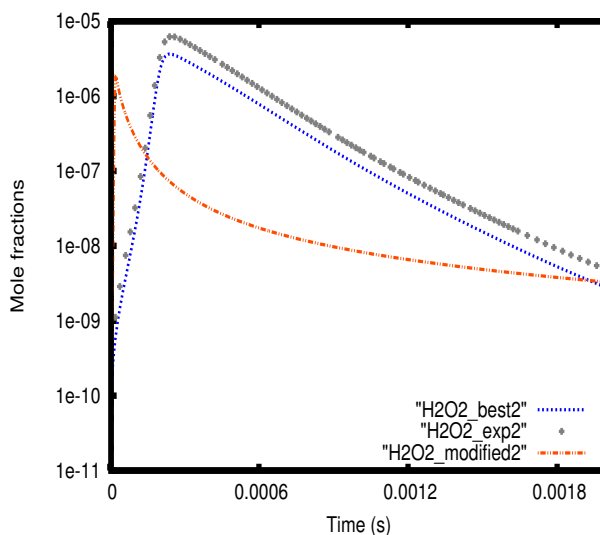


Figure 4.45: Condor, H2O2-profile, 2-nd experiment

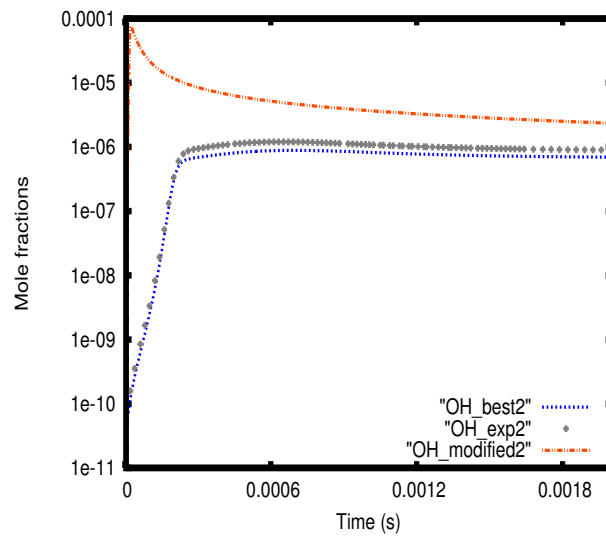


Figure 4.46: Condor, OH-profile, 2-nd experiment

The reaction rate coefficients at $T = 1200$ K and $T = 1700$ K obtained with the different methods were calculated with the units mol, cm, s. $r_i = \frac{A_{i,ini} - A_i}{A_{i,ini}}$ is the relative difference of the parameter A_i with respect to its initial (optimal) value.

Method	BOBYQA	RS	CONDOR	GA	Initial	Modified
$k_1(1200)$	2.60E+15	2.49E+15	2.78E+15	2.68E+15	2.03E+20	2.47E+13
$r_1(1200)$	1.000	1.000	1.000	1.000	0.000	1.000
$k_1(1700)$	1.84E+15	1.90E+15	1.89E+15	2.30E+15	2.69E+20	1.90E+13
$r_1(1700)$	1.000	1.000	1.000	1.000	0.000	1.000
$k_2(1200)$	1.85E+11	1.89E+11	1.94E+11	1.82E+11	1.80E+11	9.60E+10
$r_2(1200)$	-0.028	-0.050	-0.078	-0.011	0.000	0.467
$k_2(1700)$	3.96E+16	5.91E+16	5.75E+16	5.97E+15	2.65E+16	1.60E+17
$r_2(1700)$	-0.494	-1.230	-1.170	0.775	0.000	-5.038
$k_3(1200)$	2.86E+13	2.99E+13	3.26E+13	3.37E+13	2.86E+13	1.44E+13
$r_3(1200)$	0.000	-0.045	-0.140	-0.178	0.000	0.497
$k_3(1700)$	1.60E+13	5.32E+12	1.06E+14	3.48E+14	4.48E+13	3.50E+14
$r_3(1700)$	0.643	0.881	-1.366	-6.768	0.000	-6.813
$k_4(1200)$	3.66E+13	6.23E+13	7.49E+13	8.21E+13	6.43E+13	2.31E+13
$r_4(1200)$	0.431	0.031	-0.165	-0.277	0.000	0.641
$k_4(1700)$	4.24E+13	6.05E+13	7.13E+13	7.46E+13	6.96E+13	2.58E+13
$r_4(1700)$	0.391	0.131	-0.024	-0.072	0.000	0.629
$k_5(1200)$	3.55E+12	2.63E+12	2.06E+12	2.80E+12	2.29E+12	3.62E+11
$r_5(1200)$	-0.550	-0.148	0.100	-0.223	0.000	0.842
$k_5(1700)$	9.53E+12	8.09E+12	4.98E+12	8.26E+12	5.91E+12	1.09E+12
$r_5(1700)$	-0.613	-0.369	0.157	-0.398	0.000	0.816
$k_6(1200)$	3.89E+13	1.84E+13	1.32E+13	1.02E+13	1.79E+13	3.35E+11
$r_6(1200)$	-1.173	-0.028	0.263	0.430	0.000	0.981
$k_6(1700)$	3.13E+13	1.75E+13	1.31E+13	9.59E+12	1.68E+13	3.19E+11
$r_6(1700)$	-0.863	-0.042	0.220	0.429	0.000	0.981
$k_7(1200)$	2.82E+13	6.09E+12	5.87E+12	1.47E+13	5.37E+12	5.05E+12
$r_7(1200)$	-4.251	-0.134	-0.093	-1.737	0.000	0.060
$k_7(1700)$	2.18E+13	4.75E+12	5.03E+12	1.38E+13	4.72E+12	4.42E+12
$r_7(1700)$	-3.619	-0.006	-0.066	-1.924	0.000	0.064
d	24.401	0.857013	0.266179	9.00813	0	4.37E+09

Table 4.19: Optimized reaction rate coefficients

Oddly, the four methods converged towards similar values for the rate coefficients of the first two reactions, which were however very distant from the optimal values. This may be due to the insignificance of these rates at those temperature, or to the insignificance of the temperature coefficients, table 4.18 shows that the pre-exponential factors are relatively close from one another. Although most other rate coefficients are very similar, a comparison between the results from RS and CONDOR for the coefficient k_3 have different values at $T = 1700$ K ($5.31741E+12$ and $1.06145E+14$ respectively) whereas the values $T = 1200$ K are very close ($2.99E+13$ and $3.26E+13$ respectively). The relative differences of reaction rates account for the different distances (0.857013 and 0.266179 respectively) and shows that at $T = 1700$ K, reaction 3 plays only a small role.

It is worth noting however that Bobyqa probably did not converge towards a local minimum. In effect, a local random search with small steps and high precision was started from Bobyqa's best solution ($d = 24.401$) and converged towards a local minimum where d equals 9.40567 . The performances of the optimization methods are given in figure 4.47.

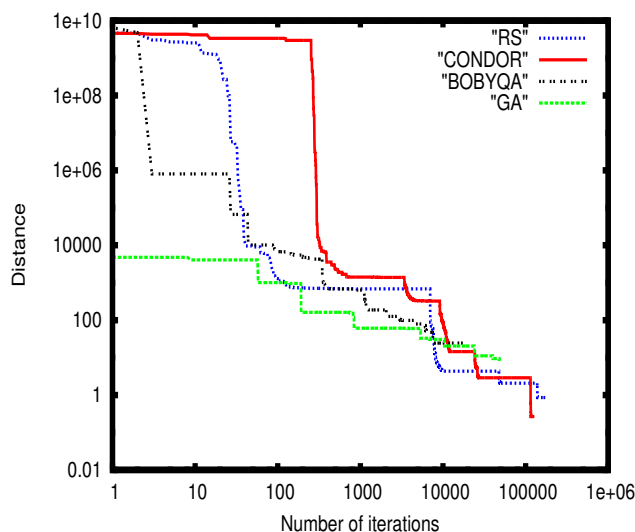


Figure 4.47: Compared performances of the optimization techniques

While in the beginning it was the least effective method, Condor outshined finally all other ones and led to the best results. The random search led to a close distance. The genetic algorithm and Bobyqa had average performances but had a smaller number of iterations as the computations were stopped.

4.4 Experimental information and parameter accuracy

Below, an example illustrating the relationship between the experimental data used for the optimization and the accuracy of the estimated parameter was designed. Considering this time the whole GRI-mechanism 3.0, the initial conditions reported below have been chosen to generate pseudo-experimental data.

$[\text{CH}_4] = 9 \%$, $[\text{O}_2] = 18 \%$, $T = 1300 \text{ K}$, and $p = 1 \text{ bar}$
 Target-species: CO, CH₃, O, OH, H₂O₂, C₂H₄, and H₂.

The reactions considered here are reported in the following lines. They are written in the following form:

$A + B + C = D + E + F$ A (mol, cm, s) n E_a (kJ/mol). The modified value of the pre-exponential factor is then given along the bound constraints between which all values of the parameters must be included during the optimization.

$O + H_2 = H + OH$ 3.87E+04 2.70 26.1981
 $A_{1,mod} = 1.00E + 06$, $1.00E+04 \leq A_1 \leq 1E+10$

$O_2 + CO = O + CO_2$ 2.50E+12 0.00 200.043
 $n_{2,mod} = 0.50$, $-1 \leq n_2 \leq 2$

$H + O_2 = O + OH$ 2.65E+16 -0.67 71.316585
 $n_{3,mod} = -0.40$, $-1.5 \leq n_3 \leq 0.5$

$OH + CH_4 = CH_3 + H_2O$ 1.00E+08 1.60 13.0572
 $A_{4,mod} = 1.00E+07$, $1E+06 \leq A_4 \leq 1E+09$

$HO_2 + CH_3 = O_2 + CH_4$ 1.00E+12 0.00 0.00
 $A_{5,mod} = 9.00E+12$, $1E+11 \leq A_5 \leq 1E+13$

$CH_3 + CH_3 + M(3) = C_2H_6 + M(3)$ 6.77E+16 1.18 2.73699
 $A_{6,mod} = 1.00E+18$, $1E+16 \leq A_5 \leq 1E+20$

The distance d between experimental values and model predictions proved to be particularly sensitive to the previous reactions under the chosen conditions. As in the previous examples, these modifications led to important changes for the profiles of the target species. The four optimization methods converged towards optimal minima indistinguishable from the original solution. The values of the optimized parameters are given in table 4.20. $r_i = \frac{A_{i,ini} - A_i}{A_{i,ini}}$ is the relative difference of the parameter A_i with respect to its initial (optimal) value.

Method	RS	CONDOR	BOBYQA	GA	Initial	Modified
A_1	8.11409E+06	10394.4	726821	107374	3.87E+04	5.00E+09
r_1	-208.666	0.731	-17.781	-1.775	0.000	-129197.966
n_2	0.874523	-0.885409	0.760483	-0.314122	0	1.75
n_3	-0.671	-0.672	-0.672	-0.681	-0.67	0.25
r_3	-0.001	-0.003	-0.003	-0.016	0.000	1.373
A_4	1.00E+08	1.00E+08	1.00E+08	9.28E+07	1.00E+08	4.00E+06
r_4	0.000	0.000	0.000	0.072	0.000	0.960
A_5	1.00E+12	1.00E+12	1.00E+12	9.86E+11	1.00E+12	9.00E+12
r_5	0.000	0.000	0.000	0.014	0.000	-8.000
A_6	6.77E+16	6.77E+16	6.77E+16	6.73E+16	6.77E+16	8.00E+19
r_6	0.000	0.000	0.000	0.006	0.000	-1180.684
d	0.001	1.97E-05	1.26E-04	0.312	0	2.21E+06

Table 4.20: Optimized parameters

The four last parameter could be unequivocally estimated by the optimization methods because their optimal values are located in sharp local minima, as shown in figures ??- ??.

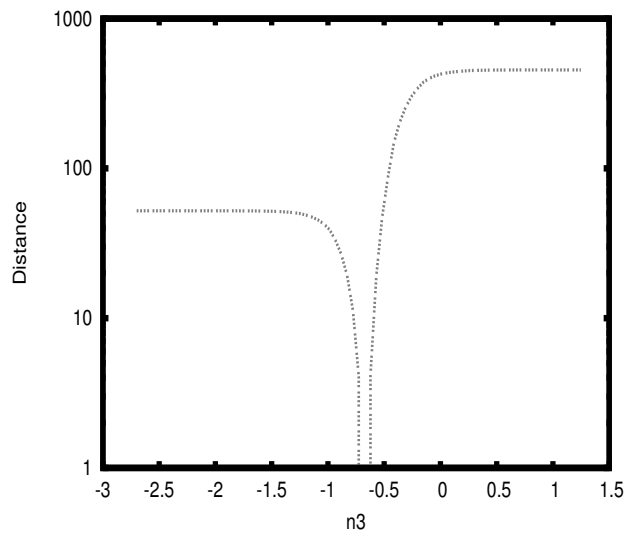


Figure 4.48: Distance as function of n_3

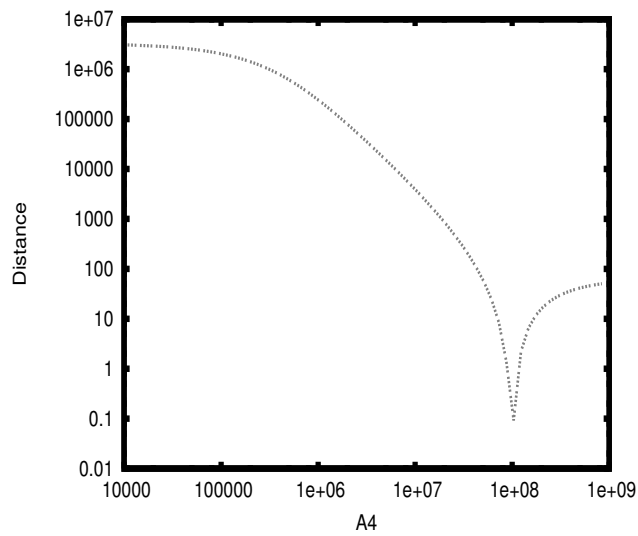


Figure 4.49: Distance as function of A_4

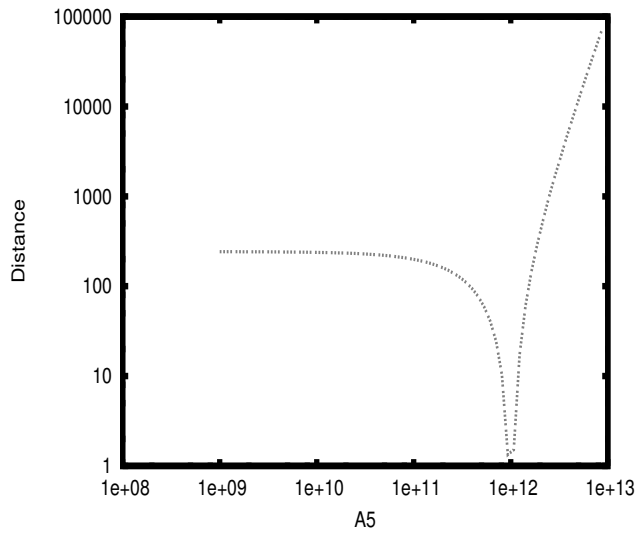


Figure 4.50: Distance as function of A_5

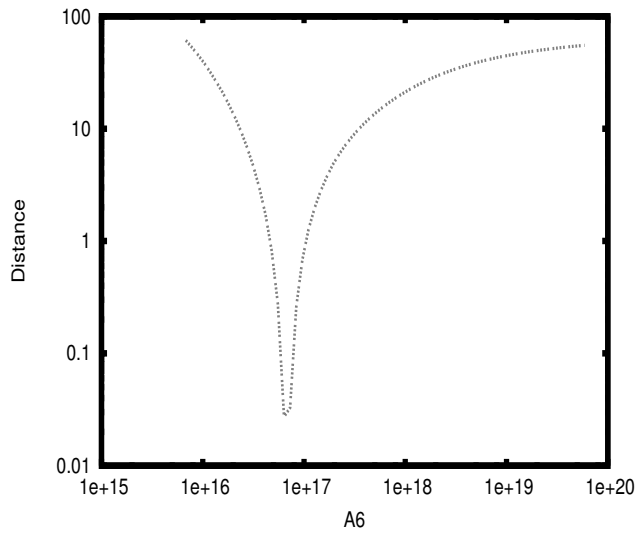


Figure 4.51: Distance as function of A_6

The strong slopes at the optima allowed convergence towards the true values with great accuracy. The two first parameters A_1 and n_2 nevertheless have much weaker slopes, as shown in figures 4.52 and 4.53 .

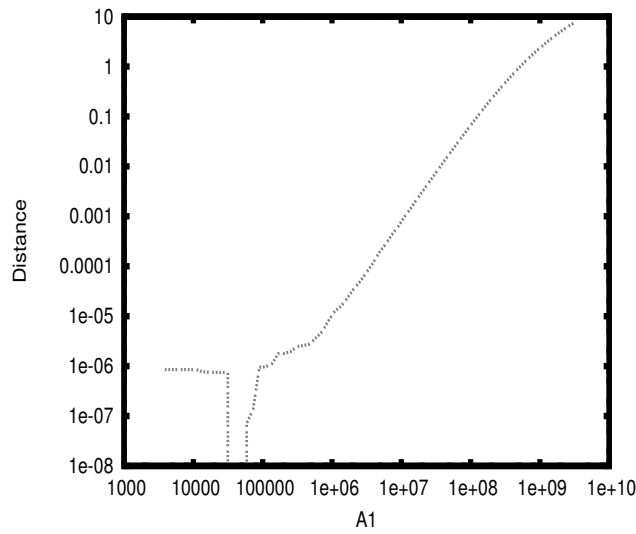


Figure 4.52: Distance as function of A_1

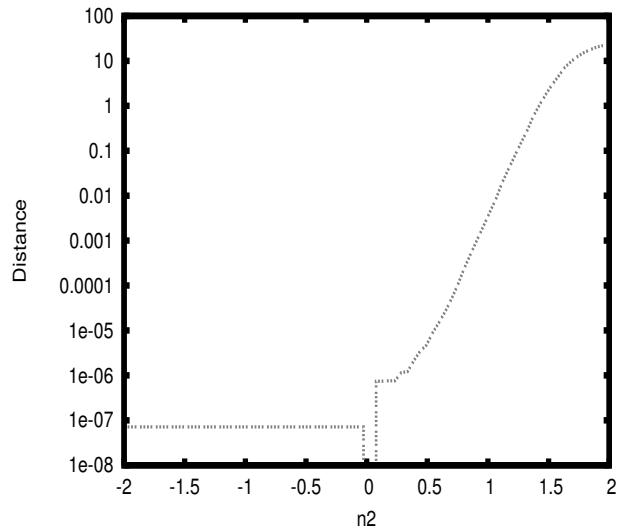


Figure 4.53: Distance as function of n_2

A great part of the variation intervals of A_1 and n_2 lead to a satisfactory agreement with the pseudo-experimental profiles generated with the initial parameter values. In spite of that, the differences are so small that they cannot be visualized, as can be seen from two typical profiles optimized with the Genetic Algorithm (figures 4.54 and 4.54).

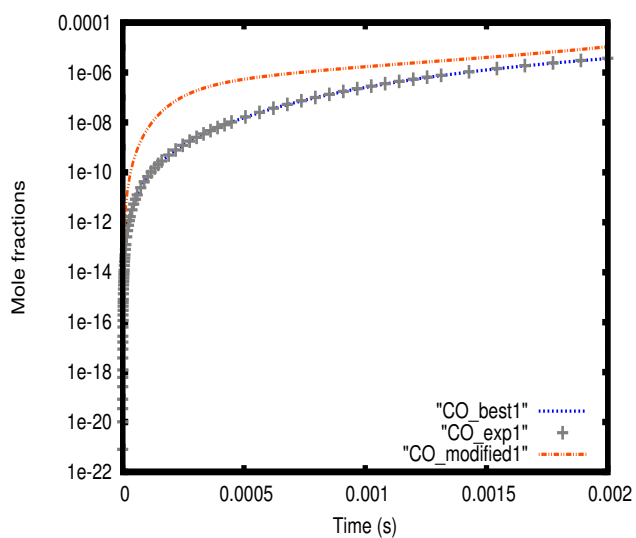


Figure 4.54: CO-profile optimized by the GA

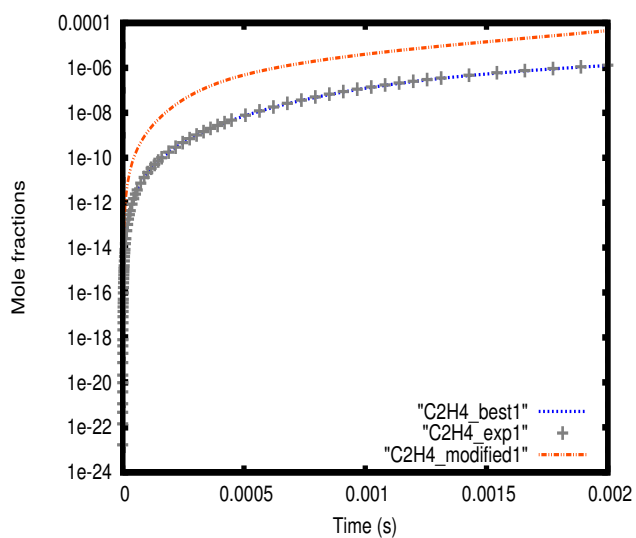


Figure 4.55: C₂H₄-profile optimized by the GA

Such a situation comes up very often in the field of parameter estimation: the experimental information available is insufficient for precisely determining the true values of some parameters. This hurdle can be overcome through the introduction of additional experimental information to which the concerned parameters are more sensitive. Three other experiments with specific profiles

were added, as reported in table 4.21 encompassing all experimental information used for the new estimation.

Experiment	Reactant1(ppm)	Reactant2 (ppm)	T (K)	p (bar)	t (s)
1	[CH ₄] = 90000	[O ₂] = 180000	1300	1.0	2.00E-03
2	[O] = 60	[H ₂] = 400	1400	6.0	2.00E-03
3	[O ₂] = 30000	[H ₂] = 30000	1500	9.0	2.00E-03

Table 4.21: Initial conditions

The target species for the first experiment are CO, CH₃, O, OH, H₂O₂, C₂H₄, and H₂. Those of the second experiment are O, H, and H₂. Those of the third experiment are O and CO₂. This time, the two first parameters were located at a true minimum as illustrated by figures 4.56 and 4.57.

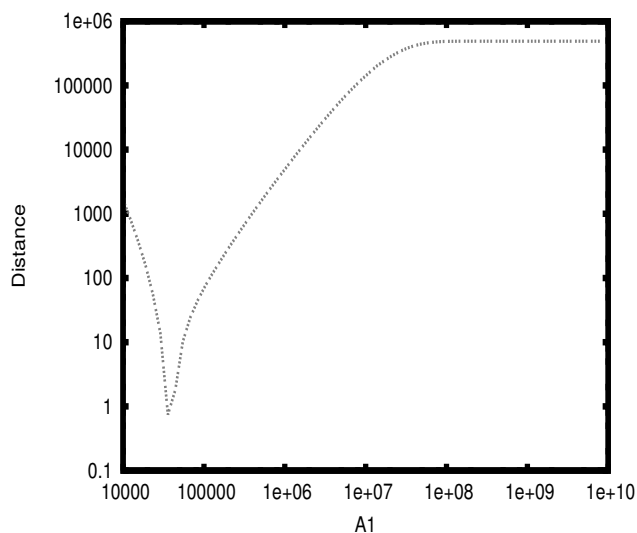


Figure 4.56: Distance as function of A_1

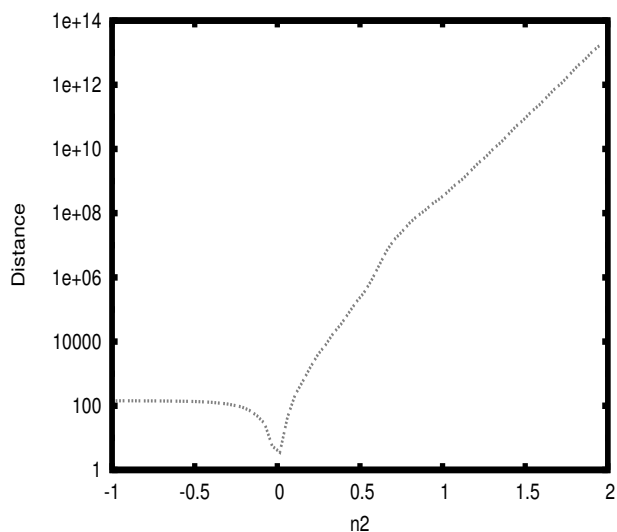


Figure 4.57: Distance as function of n_2

All three local methods converged towards the true original values of the two parameters (see table below).

Method	RS	CONDOR	GA	BOBYQA	Original	Modified
A_1	3.87E+04.4	3.87E+04	3.65E+04	3.82E+04.9	3.87E+04	5.00E+09
n_2	-0.002	0.004	-0.253	-0.005	0.00	1.75

It is worth noting that the GA did not lead to the optimal value of n_2 . This is due to the fact that there is no convergence guarantee to any local minimum for a genetic algorithm given a finite amount of time. An optimal solution for n_2 could nevertheless be achieved by starting a local random search from the best point of the GA. The value of n_2 was -0.00153062, very close to the optimal value 0.

4.5 Conclusion of the validation of the optimization methods

As seen in the previous subsections, the program Kinefit has been successfully validated for what pertains to the determination of kinetic parameters in a combustion context. The three local optimization methods (that is RS, CONDOR and BOBYQA) were superior to the genetic algorithm. Overall, their performance are very close to one another. The initial expectation was

that the genetic algorithm would outperform the other approaches for problems with a huge number of local minima due to its alleged better capacity to converge to the global optima. This could not be confirmed here as the local minimization methods with random restarts considered globally were always at least as good as as the genetic algorithm and tend to converge more rapidly. Most optimizations were carried out for very large parameter spaces which do not generally appear for real problems. It was believed that a good performance for such problems would be a more reliable indicator of good performances for realistic systems. In spite of such lengths, the algorithms were able to retrieve an optimal solution in all but one cases. The methods employed by Kinefit are therefore reliable for parameter estimation problems in combustion kinetics.

Chapter 5

Application of the optimization methods to the GRI-mechanism

As explained in 3.1.4, an important question in combustion kinetics concerns the compatibility of models with experiments, in other words the question whether or not a model is contradicted by given experimental measurements. The GRI-mechanism 3.0 [54] is a reference for the combustion of methane and is employed all over the world for many kinds of applications. With its original values, it is in disagreement with data from Saito et al. [47] who carried out a series of experiments whereby temporal profiles of O and H radicals were measured. It is interesting to determine if the GRI-mechanism is really not able to account for the experimental data under the given conditions or if reasonable changes of parameters can potentially lead to a satisfactory agreement. The experimental conditions are given in table 5.1.

Table 5.1: Initial conditions

Exp	Reactant1 (mol/cm ³)	O ₂ (mol/cm ³)	T (K)
1	[C ₂ H ₆] = 2.00E-05	1.00E-03	1520.0
2	[CH ₃] = 2.00E-05	1.00E-03	1550.0
3	[C ₂ H ₆] = 1.00E-05	2.00E-03	1620.0
4	[C ₂ H ₆] = 1.00E-05	2.00E-03	1660.0
5	[CH ₃] = 1.00E-05	2.00E-03	1700.0
6	[C ₂ H ₆] = 1.00E-05	2.00E-03	1740.0
7	[C ₂ H ₆] = 1.00E-05	2.00E-03	1750.0
8	[CH ₃] = 2.00E-05	1.00E-03	1800.0
9	[CH ₃] = 1.00E-05	2.00E-03	1930.0
10	[CH ₃] = 2.00E-05	1.00E-03	1940.0
11	[CH ₃] = 1.00E-05	2.00E-03	2000.0
12	[CH ₃] = 1.00E-05	2.00E-03	2150.0

Exp	<i>p</i> (bar)	<i>p_{min}</i> (bar)	<i>p_{max}</i> (bar)	Measured species
1	1.620	1.54	1.69	H
2	1.610	1.46	1.77	H
3	1.720	1.64	1.8	H
4	1.770	1.68	1.85	O
5	1.770	1.6	1.94	O
6	1.850	1.77	1.94	H
7	1.860	1.78	1.95	O
8	1.870	1.69	2.05	O
9	2.010	1.81	2.2	H
10	2.020	1.82	2.21	H
11	2.080	1.88	2.28	O
12	2.230	2.02	2.45	O

Only those free radicals were measured during the experiments. The duration of each experiment is 0.6 ms. The authors gave the initial pressures within significant uncertainty interval, thus adding to the measurement uncertainties further uncertainties from the model input. The first step of every optimization process (see 3.1.4) was carried out here: verifying that the model (GRI reaction mechanism 3.0) is consistent with the 12 experimental profiles, that is seeing if there exists a set of reasonable parameter values in good agreement with the experiments. First of all, an analysis of the reaction significances (see 3.2.4) was done. Thirty reactions were identified and are reported in table 5.2.

Table 5.2: Reactions chosen for the optimization

Number	Reaction	A (mol, cm, s)	n	E_a (kJ mol ⁻¹)
1	O + CH ₃ ⇌ H + CH ₂ O	5.06E+13	0.00	0.00
2	O + CH ₂ O ⇌ OH + HCO	3.90E+13	0.00	14.8149
3	O + C ₂ H ₆ ⇌ OH + C ₂ H ₅	8.98E+07	1.92	23.81265
4	O ₂ + CH ₂ O ⇌ HO ₂ + HCO	1.00E+14	0.00	167.4
5	H + CH ₂ O ⇌ HCO + H ₂	5.74E+07	1.90	11.47527
6	H + CH ₂ OH ⇌ OH + CH ₃	1.65E+11	0.65	-1.18854
7	OH + CH ₃ ⇌ CH ₂ + H ₂ O	5.60E+07	1.60	22.6827
8	OH + CH ₃ ⇌ CH ₂ (S) + H ₂ O	6.44E+17	-1.34	5.930145
9	OH + CH ₂ O ⇌ HCO + H ₂ O	3.43E+09	1.18	-1.870695
10	OH + C ₂ H ₆ ⇌ C ₂ H ₅ + H ₂ O	3.54E+06	2.12	3.64095
11	CH ₂ + O ₂ → OH + H + CO	5.00E+12	0.00	6.2775
12	CH ₂ + CH ₄ ⇌ CH ₃ + CH ₃	2.46E+06	2.00	34.60995
13	CH ₂ (S) + O ₂ ⇌ CO + H ₂ O	1.20E+13	0.00	0.00
14	CH ₂ (S) + CH ₄ ⇌ CH ₃ + CH ₃	1.60E+13	0.00	-2.38545
15	CH ₃ + O ₂ ⇌ O + CH ₃ O	3.56E+13	0.00	127.5588
16	CH ₃ + O ₂ ⇌ OH + CH ₂ O	2.31E+12	0.00	85.018275
17	CH ₃ + CH ₃ ⇌ H + C ₂ H ₅	6.84E+12	0.10	44.361
18	CH ₃ + CH ₂ O ⇌ HCO + CH ₄	3.32E+03	2.81	24.5241
19	CH ₃ + C ₂ H ₆ ⇌ C ₂ H ₅ + CH ₄	6.14E+06	1.74	43.73325
20	O + CH ₃ → H + H ₂ + CO	3.37E+13	0.00	0.00
21	OH + CH ₃ → H ₂ + CH ₂ O	8.00E+09	0.50	-7.344675
22	CH ₂ + O ₂ → H + H + CO ₂	5.80E+12	0.00	6.2775
23	CH ₂ + O ₂ ⇌ O + CH ₂ O	2.40E+12	0.00	6.2775
24	H + CH ₂ + M(3) ⇌ CH ₃ + M(3) LOW	1.04E+26	-2.76	6.70
25	H + CH ₃ + M(4) ⇌ CH ₄ + M(4) LOW	2.62E+33	-4.76	10.2114
26	H + HCO + M(3) ⇌ CH ₂ O + M(3) LOW	2.47E+24	-2.57	1.778625
27	H + C ₂ H ₅ + M(3) ⇌ C ₂ H ₆ + M(3) LOW	1.99E+41	-7.08	27.976725
28	CH ₃ + CH ₃ + M(3) ⇌ C ₂ H ₆ + M(3)	6.77E+16	-1.18	2.73699
29	CH ₃ + CH ₃ + M(3) ⇌ C ₂ H ₆ + M(3) LOW	3.40E+41	-7.03	11.55897
30	CH + H ₂ + M(3) ⇌ CH ₃ + M(3) LOW	4.82E+25	-2.8	2.46915

For pressure-dependent reactions with a third body, LOW means the parameters of the reaction for the low-pressure limit as explained in 2.1.3. The absence of LOW in such reaction lines means that the parameters correspond to the high-pressure limit. The pre-exponential factors, temperature coefficients and activation energies of the thirty reactions were optimized between the following bounds:

$$\frac{A_0}{20} \leq A \leq 20A_0,$$

$$n_0 - 0.8 \leq n \leq n_0 + 0.8,$$

$$E_{a,0} - 0.8 \leq E_a \leq E_{a,0} + 0.8, \text{ and}$$

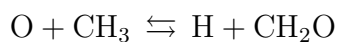
$$\frac{k_0}{20} \leq k \leq 20k_0.$$

The initial pressures (p_1 to p_{12}) were also optimized within their uncertainty limits. The random search method brought up the best optimized values

which are reported in the lines below.

Optimized parameters

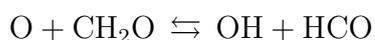
Parameters Original values Optimized values



$$A_1 \quad 5.06058\text{E}+13 \quad 1.84077\text{E}+13$$

$$n_1 \quad 0 \quad -0.08$$

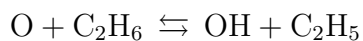
$$E_{a,1} \quad 0 \quad -1.64$$



$$A_2 \quad 3.90032\text{E}+13 \quad 4.0411\text{E}+13$$

$$n_2 \quad 0 \quad 0.18$$

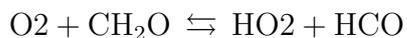
$$E_{a,2} \quad 14.8149 \quad 12.64$$



$$A_3 \quad 8.98008\text{E}+07 \quad 1.51524\text{E}+08$$

$$n_3 \quad 1.92 \quad 2.24$$

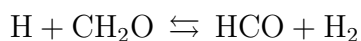
$$E_{a,3} \quad 23.8127 \quad 23.69$$



$$A_4 \quad 1\text{E}+14 \quad 5.62341\text{E}+13$$

$$n_4 \quad 0 \quad 0.05$$

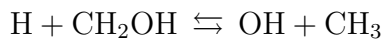
$$E_{a,4} \quad 167.4 \quad 167.28$$



$$A_5 \quad 5.73997\text{E}+07 \quad 6.11209\text{E}+07$$

$$n_5 \quad 1.9 \quad 1.78$$

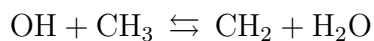
$$E_{a,5} \quad 11.4753 \quad 8.03$$



$$A_6 \quad 1.65006\text{E}+11 \quad 8.72369\text{E}+11$$

$$n_6 \quad 0.65 \quad 0.81$$

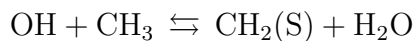
$$E_{a,6} \quad -1.18854 \quad -2.22$$



$$A_7 \quad 5.60003\text{E}+07 \quad 2.79608\text{E}+07$$

$$n_7 \quad 1.6 \quad 1.53$$

$$E_{a,7} \quad 22.6827 \quad 22.94$$



A_8 6.44021E+17 4.39643E+17
 n_8 -1.34 -1.36
 $E_{a,8}$ 5.93015 7.11

OH + CH₂O ⇌ HCO + H₂O
 A_9 3.42997E+09 4.6489E+09
 n_9 1.18 1.14
 $E_{a,9}$ -1.87069 -0.59

OH + C₂H₆ ⇌ C₂H₅ + H₂O
 A_{10} 3.53997E+06 562121
 n_{10} 2.12 2.06
 $E_{a,10}$ 3.64095 4.33

CH₂ + O₂ → OH + H + CO
 A_{11} 5.00035E+12 1.41221E+13
 n_{11} 0 0.09
 $E_{a,11}$ 6.2775 -0.02

CH₂ + CH₄ ⇌ CH₃ + CH₃
 A_{12} 2.46003E+06 757269
 n_{12} 2 2.01
 $E_{a,12}$ 34.6099 33.01

CH₂(S) + O₂ ⇌ CO + H₂O
 A_{13} 1.20005E+13 6.09818E+12
 n_{13} 0 0.01
 $E_{a,13}$ 0 -1.26

CH₂(S) + CH₄ ⇌ CH₃ + CH₃
 A_{14} 1.59993E+13 9.4254E+12
 n_{14} 0 0.11
 $E_{a,14}$ -2.38545 -3.76

CH₃ + O₂ ⇌ O + CH₃O
 A_{15} 3.55959E+13 3.25162E+13
 n_{15} 0 0.09
 $E_{a,15}$ 127559 126.49

CH₃ + O₂ ⇌ OH + CH₂O
 A_{16} 2.30994E+12 8.59409E+11

n_{16} 0 -0.05
 $E_{a,16}$ 85.0183 85.55

$\text{CH}_3 + \text{CH}_3 \rightleftharpoons \text{H} + \text{C}_2\text{H}_5$
 A_{17} 6.84069E+12 2.90135E+12
 n_{17} 0.1 -0.15
 $E_{a,17}$ 44361 45.7

$\text{CH}_3 + \text{CH}_2\text{O} \rightleftharpoons \text{HCO} + \text{CH}_4$
 A_{18} 3320.01 1407.44
 n_{18} 2.81 2.79
 $E_{a,18}$ 24.5241 24.21

$\text{CH}_3 + \text{C}_2\text{H}_6 \rightleftharpoons \text{C}_2\text{H}_5 + \text{CH}_4$
 A_{19} 6.14002E+06 8.34142E+06
 n_{19} 1.74 1.42
 $E_{a,19}$ 43.7332 40.1

$\text{O} + \text{CH}_3 \rightarrow \text{H} + \text{H}_2 + \text{CO}$
 A_{20} 3.36977E+13 3.71108E+13
 n_{20} 0 -0.22
 $E_{a,20}$ 0 1.8

$\text{OH} + \text{CH}_3 \rightarrow \text{H}_2 + \text{CH}_2\text{O}$
 A_{21} 8E+09 8.91148E+09
 n_{21} 0.5 0.19
 $E_{a,21}$ -7.34467 -5.69

$\text{CH}_2 + \text{O}_2 \rightarrow \text{H} + \text{H} + \text{CO}_2$
 A_{22} 5.79963E+12 3.26137E+12
 n_{22} 0 0.42
 $E_{a,22}$ 6.2775 7.69

$\text{CH}_2 + \text{O}_2 \rightleftharpoons \text{O} + \text{CH}_2\text{O}$
 A_{23} 2.39994E+12 5.68198E+11
 n_{23} 0 -0.07
 $E_{a,23}$ 6.2775 3.26

$\text{H} + \text{CH}_2 + \text{M}(3) \rightleftharpoons \text{CH}_3 + \text{M}(3)$ LOW
 A_{24} 1.03992E+26 2.6996E+26
 n_{24} -2.76 -2.51

$E_{a,24}$ 6.7 5.13

$\text{H} + \text{CH}_3 + \text{M}(4) \rightleftharpoons \text{CH}_4 + \text{M}(4)$ LOW

A_{25} 2.61999E+33 1.16038E+33

n_{25} -4.76 -4.87

$E_{a,25}$ 10.2114 10.04

$\text{H} + \text{HCO} + \text{M}(3) \rightleftharpoons \text{CH}_2\text{O} + \text{M}(3)$ LOW

A_{26} 2.47002E+24 7.27612E+23

n_{26} -2.57 -2.23

$E_{a,26}$ 1.77862 0.88

$\text{H} + \text{C}_2\text{H}_5 + \text{M}(3) \rightleftharpoons \text{C}_2\text{H}_6 + \text{M}(3)$ LOW

A_{27} 1.99022E+41 1.19729E+41

n_{27} -7.08 -6.92

$E_{a,27}$ 27.9767 25.38

$\text{CH}_3 + \text{CH}_3 + \text{M}(3) \rightleftharpoons \text{C}_2\text{H}_6 + \text{M}(3)$

A_{28} 6.77018E+16 2.8655E+16

n_{28} -1.18 -1.14

$E_{a,28}$ 2.73699 2.47

LOW $\text{CH}_3 + \text{CH}_3 + \text{M}(3) \rightleftharpoons \text{C}_2\text{H}_6 + \text{M}(3)$

A_{29} 3.40017E+41 4.62914E+41

n_{29} -7.03 -7.05

$E_{a,29}$ 11559 14.5

$\text{CH} + \text{H}_2 + \text{M}(3) \rightleftharpoons \text{CH}_3 + \text{M}(3)$ LOW

A_{30} 4.81948E+25 7.47137E+25

n_{30} -2.8 -2.61

$E_{a,30}$ 2.46915 5.4

$p1$ (bar) 1.62 1.58

$p2$ (bar) 1.61 1.59

$p3$ (bar) 1.72 1.8

$p4$ (bar) 1.77 1.72

$p5$ (bar) 1.77 1.72

$p6$ (bar) 1.85 1.94

$p7$ (bar) 1.86 1.79

$p8$ (bar) 1.87 2.04

p_9 (bar)	2.01	1.81
p_{10} (bar)	2.02	2.19
p_{11} (bar)	2.08	2.08
p_{12} (bar)	2.23	2.44
d	30.7424	3.15

For each reaction, the ratio $Q_i = k_{i,opt}/k_{i,0}$ was always included between 0.05 and 20 for all relevant temperatures, as can be seen in figures 5.1- 5.3 reporting this ratio for the three first optimizable reactions.

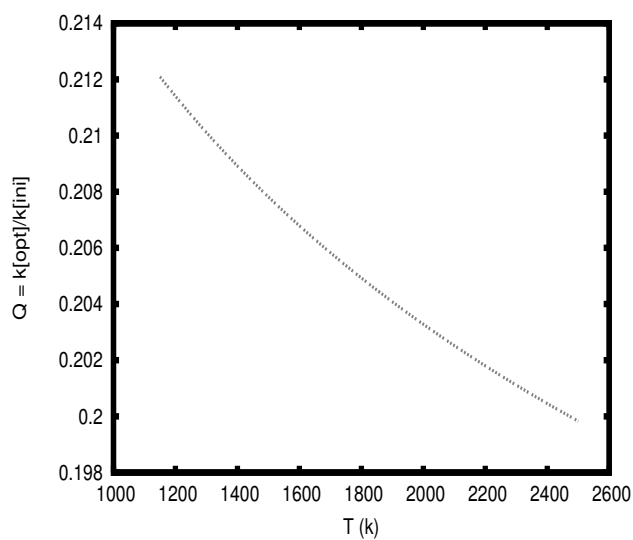


Figure 5.1: Q_1 for $O + CH_3 \rightleftharpoons H + CH_2O$

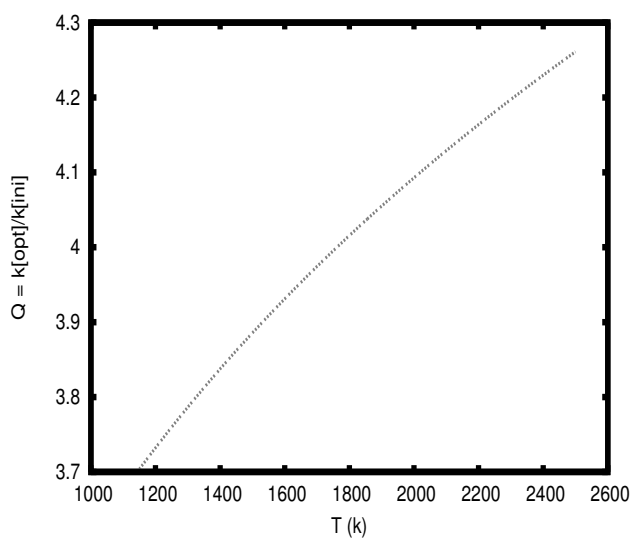


Figure 5.2: Q_2 for $\text{O} + \text{CH}_2\text{O} \rightleftharpoons \text{OH} + \text{HCO}$

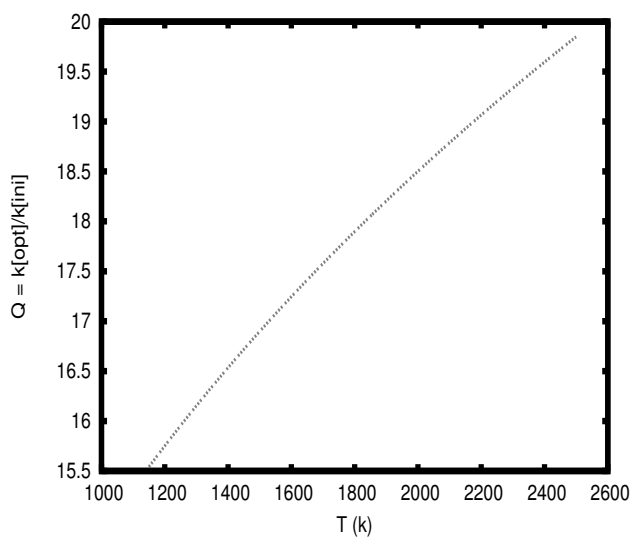


Figure 5.3: Q_3 for $\text{O} + \text{C}_2\text{H}_6 \rightleftharpoons \text{OH} + \text{C}_2\text{H}_5$

For most reactions, the rate changes were rather limited. The optimized curves are reported in figures 5.4 - 5.15 "_exp" denotes the experiment, "_fit" the best fit found during the optimization and "_ini" denotes the results obtained with the initial parameter values.

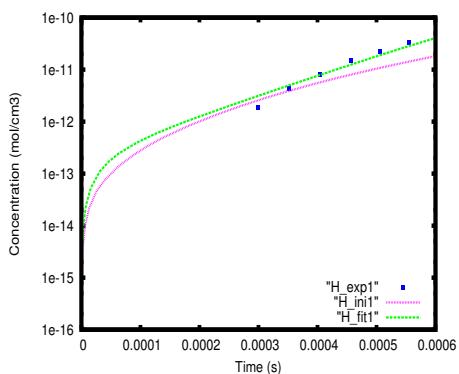


Figure 5.4: First experiment

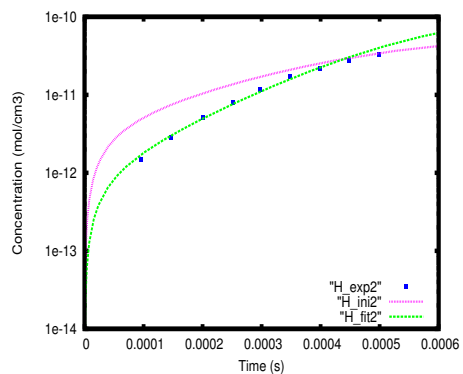


Figure 5.5: Second experiment

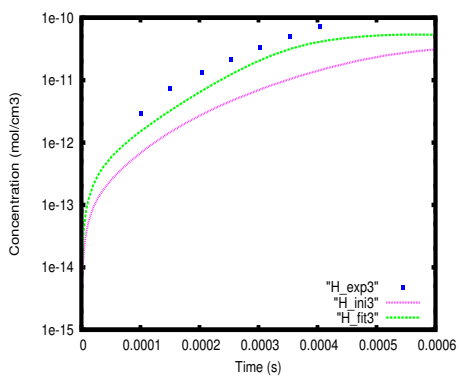


Figure 5.6: Third experiment

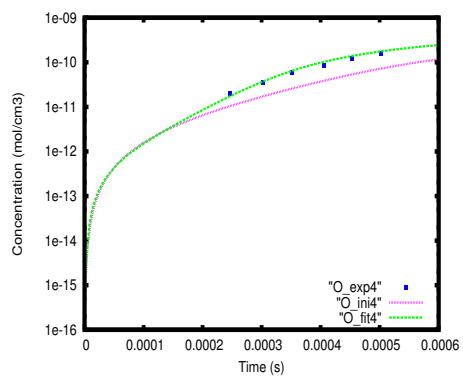


Figure 5.7: Fourth experiment

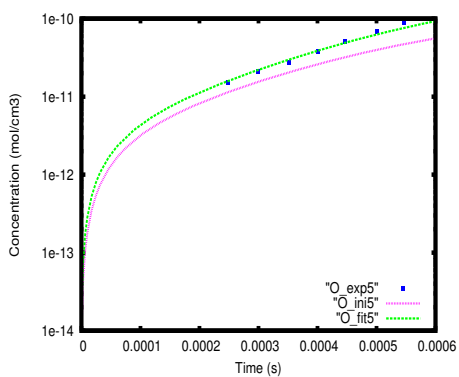


Figure 5.8: Fifth experiment

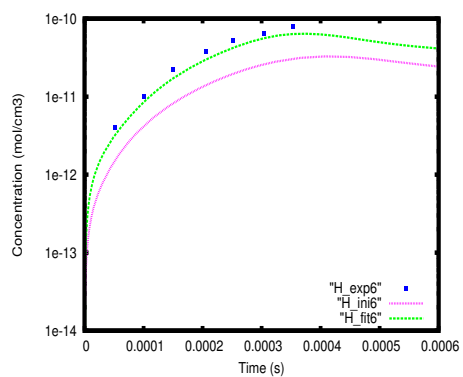


Figure 5.9: Sixth experiment

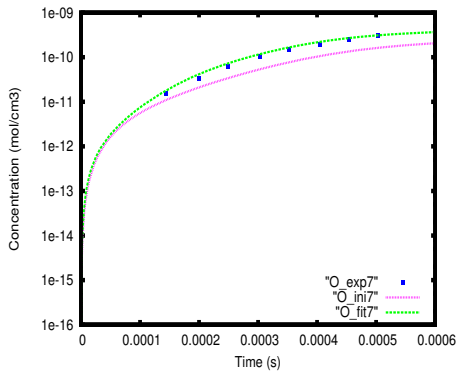


Figure 5.10: Seventh experiment

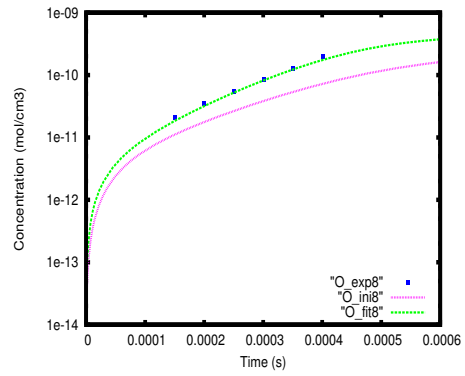


Figure 5.11: Eighth experiment

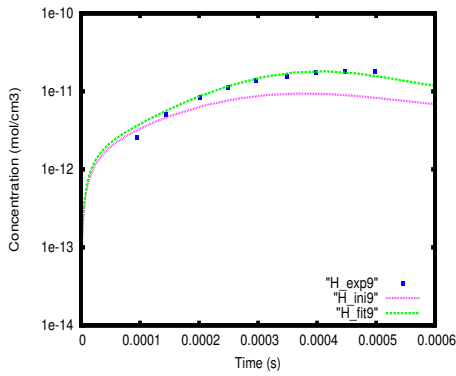


Figure 5.12: Ninth experiment

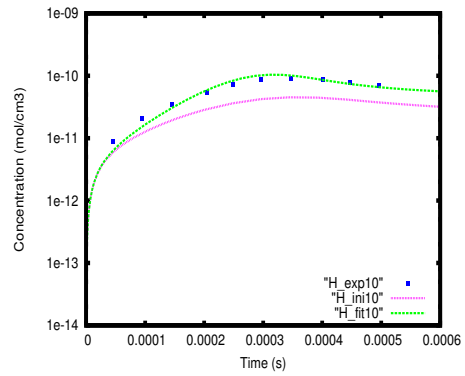


Figure 5.13: Tenth experiment

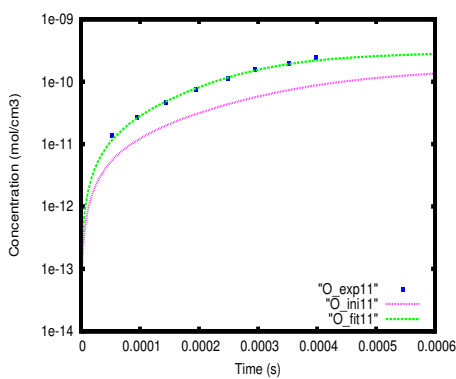


Figure 5.14: Eleventh experiment

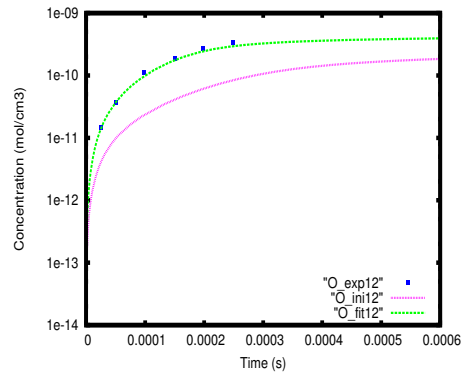


Figure 5.15: Twelfth experiment

A significant amelioration can be easily recognized for all measured profiles. If one assumes that the standard deviation is the same for all experimental

concentrations (e.g. 20 % of the value), the chi-squares norm can be employed according to the formula:

$$X^2 = \frac{1}{v_{dev}^2} d \quad (5.1)$$

whereby $d = 3.15$.

It is then possible to deduce the likelihood that model and experiments are consistent with each other

$$Pr_0(X^2) = \frac{\Gamma(\frac{n_e}{2}, \frac{X^2}{2})}{\Gamma(\frac{n_e}{2})} . \quad (5.2)$$

which has been plotted out as a function of the standard deviation (fig. 5.16).

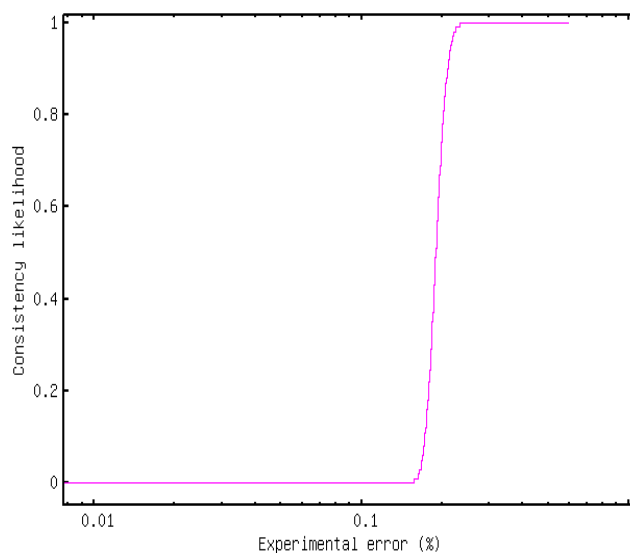


Figure 5.16: Consistency likelihood as function of the standard deviation

For standard deviation values greater than 20%, the probability of consistency becomes superior to 75%, thereby indicating that the reaction mechanism is in good agreement with the experiments. For the kind of free radicals measured, it is likely that the uncertainty would exceed 20%. It is thus legitimate to draw the conclusion that the GRI-mechanism is potentially capable of accounting for these profiles without introducing additional reactions. Since the number of optimized parameters (112) is greater than the number of experimental points (89), the optimization cannot be considered as an estimation of

the parameters. Most involved parameters have an influence on many experimental profiles originally used to optimize and validate the GRI-mechanism 3.0. To estimate their values in such a way that they will also be consistent with Saito's experiments would require a long-lasting large scale optimization including all experiments already considered for the validation of the GRI-mechanism 3.0 and Saito's experiments simultaneously.

Chapter 6

Mechanism reduction

6.1 Motivation

As previously explained, reaction mechanisms covering a large range of pressures and temperatures must include many species and reactions. However, only a limited number of them are going to play a role for the simulation of specific experiments. The potential relevance of mechanism reduction for parameter optimization is twofold:

- it allows to only retain the most important reactions, facilitating then the identification of the most sensitive reactions
- it may allow to suppress reactions playing no significant role, thereby alleviating the computational burden.

The last point is of particular interest because the computational burden is one of the biggest hurdle hindering the application of optimization methods to large scale problems involving numerous experiments as well as many parameters. In order to converge to the global minimum (see chapter 3), optimization methods often needs thousands of iterations, whereby all systems of differential equations corresponding to the experiments must be solved. This may cost a tremendous amount of time if the mechanism comprises thousands of reactions and hundreds of species. As a consequence, methods for reducing mechanisms are indispensable if there are many optimizable parameters and experiments. Methods like surface mapping [51], widely employed in the field of chemical kinetics for parameter estimation/optimization, are in the case of combustion problems crucially dependent on the identification of important and negligible parameters. However, there is no guarantee that removed reactions with the original optimized parameter values will not play a role with the final optimizable parameter values. This may in turn possibly invalidate the results of the optimization. A program for the reduction of reaction

mechanism has therefore been developed during this work, with the scope of evaluating the general applicability of reduction methods to the problems of optimizing and estimating kinetic parameters for combustion mechanisms.

6.2 Overview of existing approaches

Several methods have been developed for the practical reduction of kinetic differential equation systems for a particular set of conditions. They may be divided in two categories: those which preserve the structural integrity of the mechanism and those which do not. According to Androulakis definition [1], we will say that a reduced mechanism maintains the structural integrity of a detailed mechanism if all species and reactions of the reduced mechanism were already present in the initial one. This implies that the chemical description of the system in terms of reaction flux remains the same over the whole reduction process, only those chemical species and reactions which play no significant role for the desired output are removed.

An intuitive method [49] belonging to this class consists of the successive application of a reaction flow analysis to distinguish between slow and fast reactions, followed by a sensitivity analysis carried out only for the slow reactions to identify those which are crucial for the variables of interest. The rapid reactions and the slow reactions with high sensitivity values are then kept within the reduced mechanism.

Other methods imply the stepwise removals of a group of reactions followed by the evaluation of the discrepancies introduced with respect to the original model. For example, Petzold and Zhu [40] reformulated the mechanism reduction as a non-linear integer-programming problem which was itself transformed into a continuous optimization problem solved with a sequential quadratic programming method. Androulakis [26] et al. also formulated the mechanism reduction as a non-linear integer-programming problem which he solved with the help of a branch and bound algorithm.

The methods belonging to the second group modify the structure of the problem either by lumping reactions and species or by resorting to algebraic simplification of the differential equation system underlying the detailed kinetic scheme. The most traditional approaches consist of applying the assumption of steady state to very reactive radicals (which means that the temporal derivatives of their concentrations must remain close to zero over the whole interval) which leads to algebraic relations allowing the simplification of the underlying system of differential equations and the lumping of groups of species and reactions. This approach usually involve skillful kineticists and intuitions [40], although Montgomery et al. [36] have proposed an auto-

mated procedure for doing this. The system of differential equations can also be simplified by considering very fast bidirectional reactions to be in equilibrium. These methods, which consist in fact of a differentiation between slow and rapid modes of the differential equation system, can be replaced by more general frameworks like the ILDM (Intrinsic Low Dimensional Manifolds) [29] or the CSP (Computational Singular Perturbation) [25] methods. However, such methods cannot be employed for parameter estimation since they do not conserve the mathematical structure upon which the detailed chemistry is based. Thus, only the first class of approaches is of interest for the parameter estimation problem at hand. In the following section, an easily implementable method maintaining the structural integrity of the reaction mechanism developed recently will be presented and demonstrated for one concrete example concerning the oxidation of methane CH_4 .

6.3 Description and validation of the program Mechacut

For quickly obtaining a simplified mechanism accurately reproducing the variables of interest resulting from the detailed mechanism, the tool Mechacut has been developed by the author. It relies on the software Homrea for the simulation of homogeneous kinetic systems [18].

As input, it requires the following information:

- the conditions of all experiments considered
- the reaction mechanism
- the thermodynamic data
- the target variables (concentrations or temperature) whose profiles must be reproduced
- the tolerance in terms of relative differences e (say $e = 2\%$)

Like several methods cited above, it is based upon the fact that typically reactions containing species with small concentrations tend to play a minor role for the whole system.

In a first step, for each species k , $k \in \{1 \dots n_S\}$, the greatest molar fraction value over all experiments and time points $C_{k,max}$ is determined. The use of molar fractions instead of concentration units allows the simultaneous consideration of experiments with different orders of magnitude of initial reactant and diluent concentrations. Then, for a given reaction $R : \sum_i v_i R_i = \sum_j v_j P_j$, the greatest molar fractions $C_{k,max}$ of all participating species are compared,

and the species having the lowest (in comparison with the other species of the reaction) value of the greatest molar fractions is identified and the corresponding value is assigned to the reaction. The reactions are then sorted according to this characteristic value in a decreasing order. Therefore, the reactions situated towards the end of the mechanism will typically contain some species having very low concentrations, whereas the reactions located at the beginning will only have species with greater concentrations. There may be however situations where small concentrations of some participating species do not necessarily entail the unimportance of the reaction, especially in the case where the reactants or products include free radicals which usually have low concentrations but do play a crucial role for the whole reaction system.

To discriminate important and unimportant reactions, it is therefore necessary to proceed in a stepwise fashion, removing a group of reactions and accepting the change if the variations of the target variables are less than a pre-defined threshold e .

To introduce flexibility, random numbers are employed to choose the first line of the group to be suppressed $n \in \{1 \dots n_{reac}\}$ and the number of reactions m to be deleted which is included in the interval $\{0 \dots m_{max}\}$. m , the current number of deletable lines, is generated according to an uniform distribution function, whereas n follows a probability law strongly biased towards the end of the interval $\{1 \dots n_{reac}\}$, so as to target most of the time the reactions with minor species.

The current maximum number of lines m_{max} is multiplied by a pre-defined factor a ($a > 1$) if the deletion could be accepted, otherwise (the deletion led to some discrepancies greater than the tolerance) it is multiplied by an other pre-defined factor b ($0 < b < 1$). The maximum number of lines m_{max} is however never allowed to exceed the threshold m_{max}^{max} . A species is suppressed from the input file if it no longer appears in the reaction mechanism either as reactant, product or third body.

In this manner, large numbers of reactions may be deleted at the beginning of the process, as long as unimportant reactions are considered. From a certain point, the deletion of more influential reactions is tried out and rejected what reduces the length of the interval. If the number of failures exceeds a given threshold, the algorithm leaves the probabilistic mode and tries to delete each reaction one by one.

In what follows, an application example is given to illustrate the algorithm and its efficiency. As will be presented in detail in the next chapter, the estimation or optimization of kinetic parameters out of experimental data

requires solving the differential equations systems underlying the simulated variables for many possible combinations of parameters (several thousands of times for a dozen of adjustable parameters). If several experiments are considered simultaneously for extracting the best set of parameters matching the measurements, each simulation for fixed values of the parameters may cost several minutes if the whole reaction mechanism is employed. This situation is clearly not satisfying for practitioners who often must consider different combinations of adjustable parameters before finding the one which will lead to acceptable discrepancies with the experiment: the optimization process will then last a considerable time before either the optimal solution will be found or it may be concluded that the current mechanism is inconsistent with the data. Reaction mechanism simplification techniques offer here an interesting option to considerably reduce the time of each iteration (corresponding to the simulation of all measured variables), thereby leading to significantly shorter CPU time usage for parameter optimization. The GRI-mechanism 3.0 [54] is widely used for simulating the combustion of methane. This reaction mechanism has been reduced using Mechacut for a set of experiments concerning the oxidation of CH_4 whereby the temporal profiles of carbon monoxide CO and hydroxyl OH have been measured. These compounds have been considered as target species, that is the reduced mechanism must reproduce the profiles from the detailed mechanism within a given tolerance ϵ . The conditions of the four chosen experiments are given below. $[\text{CH}_4]$ and $[\text{O}_2]$ denote the molar fractions of methane and oxygen, T the temperature in Kelvin, p the pressure in bar and t corresponds to the duration of the experiment in seconds.

Table 6.1: Experimental conditions considered

Experiment	$[\text{CH}_4]$	$[\text{O}_2]$	$p(\text{bar})$	$T(\text{K})$	$t(\text{s})$
1	0.4%	20%	1.48	1711	6.0e-04
2	0.5%	10%	1.53	1752	6.0e-04
3	0.5%	10%	1.62	1843	6.0e-04
4	0.4%	5%	1.57	1821	6.0e-04

The rest of the mixture is made up of argon. In what follows, the reaction mechanism has been reduced to reproduce the concentration profiles of CO and OH within a tolerance of 2 %. The parameters had the following values: $a = 2$, $b = 0.6$ and $m_{max}^{max} = 150$.

After the end of the procedure, the reduced reaction mechanism contained 172 reactions and 31 species which amounts to a reduction of 59.24% in number of reactions and 18.42% in number of species respectively. To illustrate the accuracy of the reduced model, two characteristic profiles were considered and a comparison between detailed and reduced mechanism used in the simulation is given in figures 6.1 and 6.2.

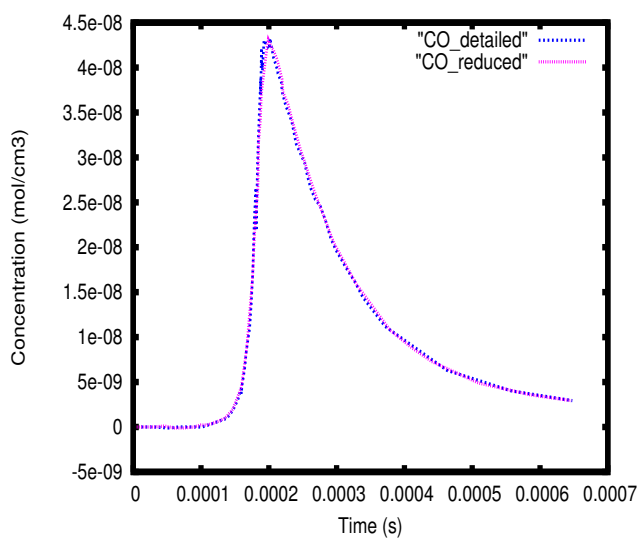


Figure 6.1: Comparison between the detailed and reduced mechanisms for the CO profile of the second experiment

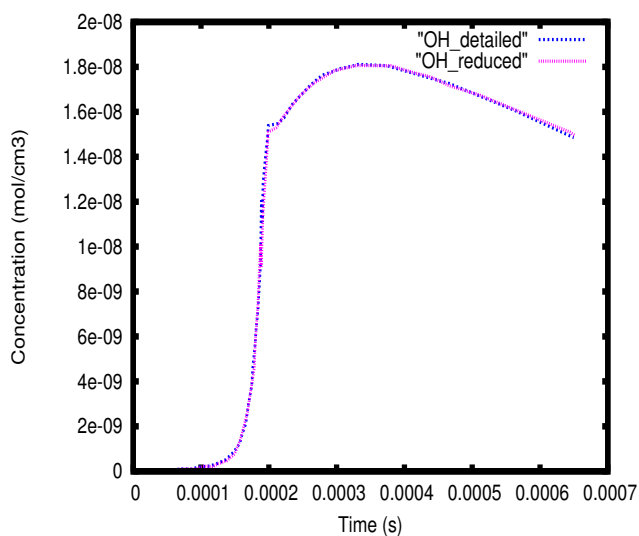


Figure 6.2: Comparison between the detailed and reduced mechanisms for the OH profile of the second experiment

The differences between the two profiles are extremely small and the results are similar for the 6 remaining profiles. A considerable reduction in terms of reactions could thus be reached, showing that many reactions of the GRI-mechanism 3.0 play a negligible role for the evolution of the species CO and

OH during the combustion of methane under the conditions considered here.

6.4 Application to the optimization of large reaction mechanisms

As already explained, the optimization of large reaction mechanisms such as those encountered in combustion is an extremely challenging task in many respects. On the one hand, the presence of numerous parameters having overlapping influences on measured variables hinders the unequivocal determination of parameter value sets. On the other hand, the handling of large mechanisms involves considerable computational times, especially in cases where hundreds of experimental conditions must be simulated at the same time. For a given reaction system, the reduction methods described above may potentially come into play by removing all reactions and species insignificant for the outcomes of interest. The surface mapping approach [51], [46] relies on an even greater approximation in that the whole ODE system is replaced by algebraic (usually polynomial) relations including only the most sensitive reactions. However, there is a-priori no warrant that reduction techniques may be systematically used in such a manner for optimizing complex mechanisms. In fact, the reduction of the mechanism occurs before the beginning of the minimization with the initial, unoptimized parameter values p_0 . It is then conceivable that reactions excluded for p_0 are going to play a more important role for other sets of values p during the optimization so that they may no longer be neglected. The errors adding up in this way may dramatically change the shape of the minimization landscape, thereby creating local minima which do not exist in the true problem. To estimate the extent of these difficulties, the real optimization problem of chapter 5 involving the GRI-mechanism 3.0 was considered. First, the reaction mechanism was reduced two times separately with thresholds of 1% and 2% with respect to the twelve profiles. The pre-exponential factors of the fourteen most important reactions reported in table 6.2 were taken as optimizable variables.

Table 6.2: Reactions chosen for the optimization

Number	Reaction	A	n	E_a
1	$O + CH_3 \rightleftharpoons H + CH_2O$	5.06E+13	0.00	0.00
2	$H + CH_2OH \rightleftharpoons OH + CH_3$	1.65E+11	0.65	-1.18854
3	$OH + CH_3 \rightleftharpoons CH_2 + H_2O$	5.60E+07	1.60	22.6827
4	$OH + CH_3 \rightleftharpoons CH_2(S) + H_2O$	6.44E+17	-1.34	5.930145
5	$OH + CH_2O \rightleftharpoons HCO + H_2O$	3.43E+09	1.18	-1.870695
6	$CH_2 + CH_4 \rightleftharpoons CH_3 + CH_3$	2.46E+06	2.00	34.60995
7	$CH_2(S) + O_2 \rightleftharpoons CO + H_2O$	1.20E+13	0.00	0.00
8	$CH_2(S) + CH_4 \rightleftharpoons CH_3 + CH_3$	1.60E+13	0.00	-2.38545
9	$CH_3 + O_2 \rightleftharpoons O + CH_3O$	3.56E+13	0.00	127.5588
10	$CH_3 + O_2 \rightleftharpoons OH + CH_2O$	2.31E+12	0.00	85.018275
11	$CH_3 + CH_3 \rightleftharpoons H + C_2H_5$	6.84E+12	0.10	44.361
12	$CH_3 + C_2H_6 \rightleftharpoons C_2H_5 + CH_4$	6.14E+06	1.74	43.73325
13	$O + CH_3 \rightarrow H + H_2 + CO$	3.37E+13	0.00	0.00
14	$CH_3 + CH_3 + M(3) \rightleftharpoons C_2H_6 + M(3)$	6.77E+16	-1.18	2.73699
	LOW	3.40E+41	-7.03	11.55897

The reactions were present in all reduced models so that a comparison of the predictions of the complete and reduced models for different values was possible. The simulated profiles are the same as the experimental ones, as reported in table 5.1 in chapter 5. The pre-exponential factors were first varied within a factor of hundred, that is in the interval $[0.01 p_0, 100 p_0]$. This corresponds to a situation whereby the parameters are completely unknown and must be estimated (ideally unequivocally) from experimental data alone. 800 points were randomly generated in this way. For each of those, the relative difference $d = \frac{|m-e|}{e}$ between detailed and reduced mechanism for each concentration at each time point was calculated. The greatest value among those was then identified and related to the corresponding parameter value set. In this way, the number of points whose greatest relative discrepancies d_i are located in a certain interval could be calculated. For example, for the first reduced model (tolerance 1 %) 5 points had d_i included in the interval $[0, 0.01]$. The results for all intervals are reported in figures 6.3 - 6.4.

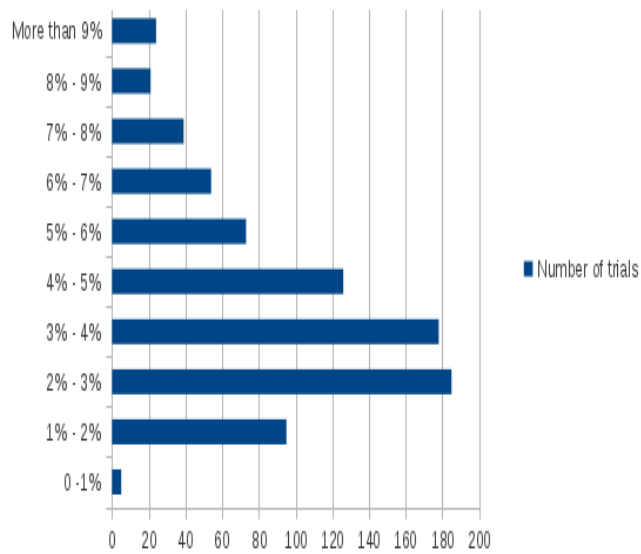


Figure 6.3: Distribution of the maximum error for a reduction tolerance of 0.01

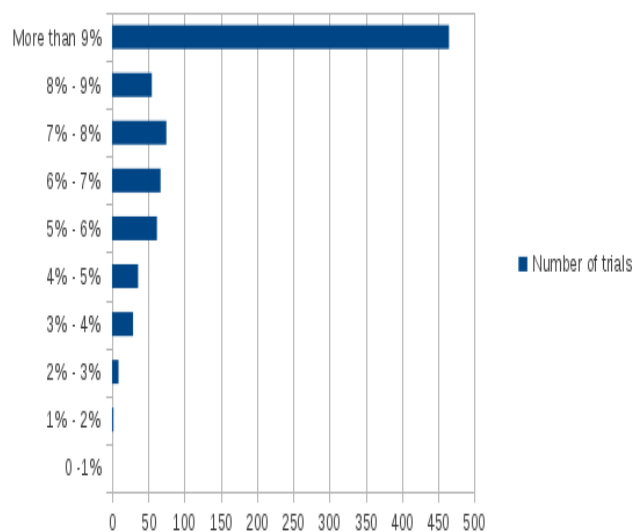


Figure 6.4: Distribution of the maximum error for a reduction tolerance of 0.02

In both cases, the discrepancies at a great number of points are too large for allowing a reliable optimization using the reduced mechanism. Next, the pre-exponential factors were varied within a factor of ten, that is in the interval $[0.1 p_0 \quad 10 p_0]$. This correspond to a situation where the orders of magnitude

of the parameters are already known. The results are given in figures 6.5 - 6.6.

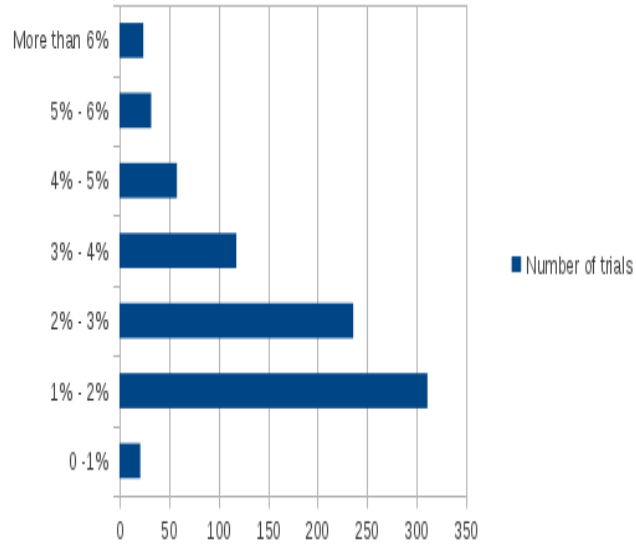


Figure 6.5: Distribution of the maximum error for a reduction tolerance of 0.01

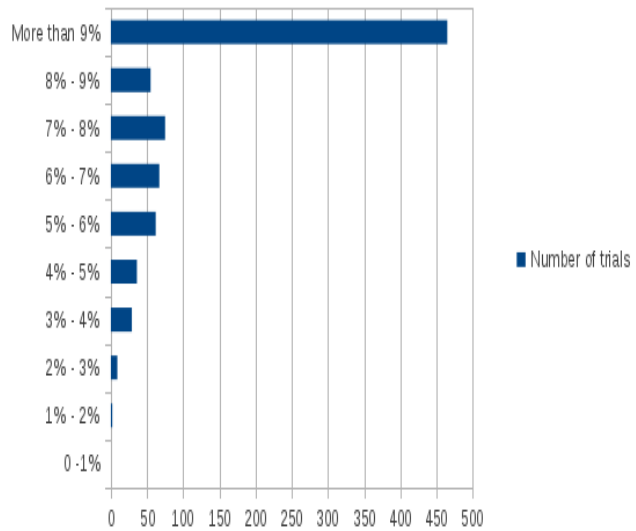


Figure 6.6: Distribution of the maximum error for a reduction tolerance of 0.02

No reliable optimization can be carried out with the second reduced mechanism. The result of the first reduced mechanism remain closer to those of

the detailed one but may still change the optimization landscape. Thirdly, the pre-exponential factors were varied within a factor of four, that is in the interval $[0.25 p_0 \quad 4 p_0]$. The results are given in figures 6.7 - 6.8.

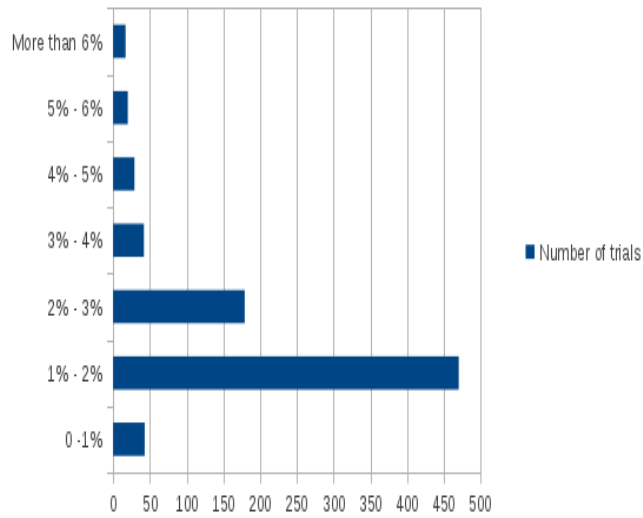


Figure 6.7: Distribution of the maximum error for a reduction tolerance of 0.01

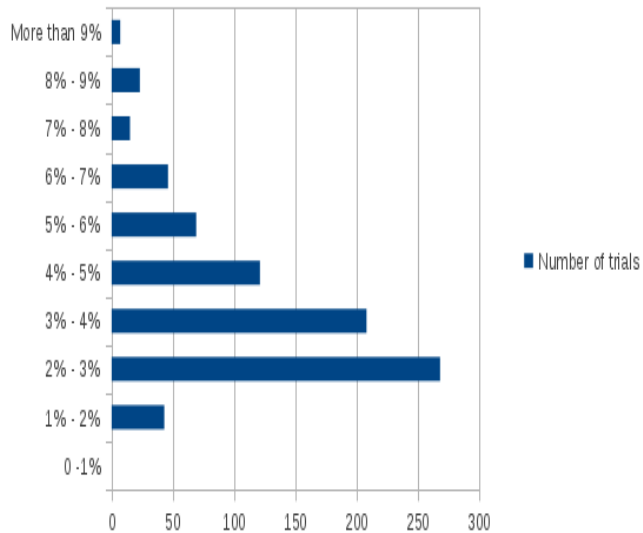


Figure 6.8: Distribution of the maximum error for a reduction tolerance of 0.02

In the first case, most of the discrepancies are small. As a consequence,

the optimization problem should remain the same. For the second reduced mechanism the discrepancies are more important and might modify the optimization landscape. Finally, the pre-exponential factors were varied within a factor of two, that is in the interval $[0.5 p_0 \quad 2 p_0]$ as given in figures 6.9 - 6.10.

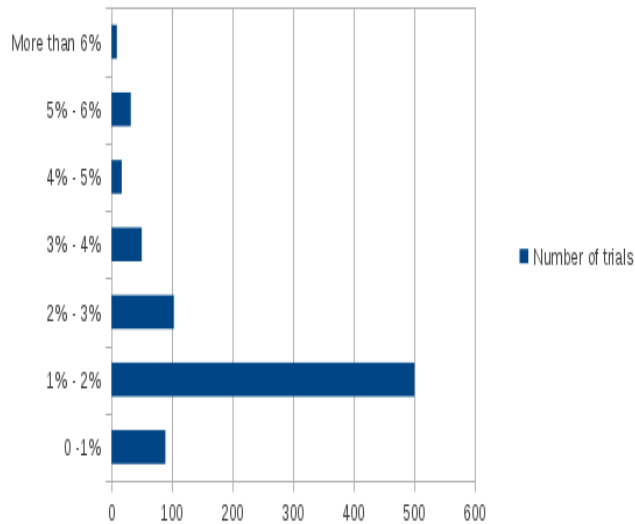


Figure 6.9: Distribution of the maximum error for a reduction tolerance of 0.01

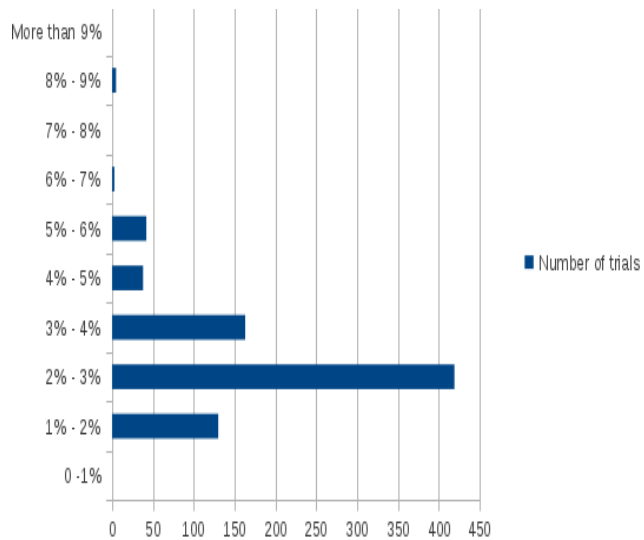


Figure 6.10: Distribution of the maximum error for a reduction tolerance of 0.02

These results suggest that chemical kinetic reduction methods including the surface mapping method [46] may be only reliable when parameters are varied within narrow ranges such as factors two or four and for low values of the tolerance such as 0.01. Otherwise, an error difficult to evaluate is introduced. For the estimation of unknown kinetic parameters, methods relying on solving the underlying ODE systems like Kinefit seem to be more trustworthy than methods relying on reduced models like surface mapping [14] which might be more apt to optimize parameters already known within small intervals of uncertainty.

Chapter 7

Parameter estimation for benzene formation during propargyl pyrolysis

7.1 Relevance for soot formation and characterization of the system

Historically, the formation of particulate matter during pyrolysis and rich-combustion of fuels has been viewed as either owing to the formation and growth of poly-acetylene /polyyne ([4],[5]) or to the appearance and growth of Polycyclic Aromatic Hydrocarbons (PAH) ([13] and [44]) that is compounds which contain at least two benzene-type rings. During the last years, a great deal of experimental and theoretical results ([6], [34],[35], and, [39]) have made it clear that soot is overwhelmingly formed through the aromatic route, and that the polyacetylene route could at most only play a minor role by leading to the formation of certain Polycyclic Aromatic Hydrocarbons (PAH). Soot plays an enormous economical role in modern industrial nations. On the one hand, it is a harmful pollutant capable of penetrating deeply into lungs ([10], [42]) and it may be partially responsible for the decay of the ozone layer [7]. On the other hand, soot may also lead to financial gains through the production of carbon black [19], used for example in automotive tires, and by optimizing the heat exchange in some kinds of burners. Its precursors Polycyclic Aromatic Hydrocarbons (PAHs) have carcinogenic properties both in humans and animals [42] and are a frequent outcome of incomplete combustion. On these grounds, it is primordial for combustion researchers to attain a better comprehension of the chemical and physical processes involved, so that operative conditions minimizing (or sometimes maximizing) PAH and

soot release may be optimized. Starting from aliphatic fuels, the formation of the first aromatic ring (benzene or phenyl radical) has been shown to be a rate limiting step for the formation of growing PAH and eventually of soot itself [33]. Accurate predictions of soot emission in complex industrial systems like car engines and gas turbines require therefore the appearance of the first rings to be accurately described. Historically, this process has mainly been viewed as either the addition of C₂-species with C₄-species (even pathway, [67]) or the recombination of propargyl C₃H₃ radical (odd pathway, [33]). Over the last decades, evidences for the predominance of the odd pathway have accumulated ([22], [33], [56], and [69]), and it is now widely acknowledged that a precise description of its chemistry is a crucial step for the prediction of PAH and particulate matter. In almost every detailed reaction mechanism aiming at simulated PAH and soot formation, the recombination chemistry is lumped into two or three steps involving the recombination of propargyl to form benzene, fulvene and possibly phenyl (see [45], [53], [2] and [41]). To determine accurate parameter values, Scherer [50] carried out a series of shock tube experiments at high temperatures and relatively high pressures to determine coherent rate coefficients for a C₃H₃-subsystem including primary reactions of benzene and phenyl. Nevertheless, recent results from computational chemistry have revealed the involved chemistry to be much more complex and to imply many more species and reactions than previously thought. Miller and Klippenstein [32] carried out a detailed quantum chemical analysis of all species and pathways participating in this transition regime. Their results from their Potential Energy Surface (PES) confirmed that the chemistry is in fact extremely complex, the cyclic compounds being produced through isomerisation of linear C₆H₆-species which themselves are the direct recombination products of propargyl radicals.

7.2 First trial to determine an optimal propargyl-subsystem

7.2.1 Structure of the mechanism

Relying on Miller and Klippenstein results, Tang et al. [59] developed a semi-detailed mechanism with 14 steps aiming at describing the chemistry involved in the C₃H₃-C₃H₃ recombination as shown in table 7.1.

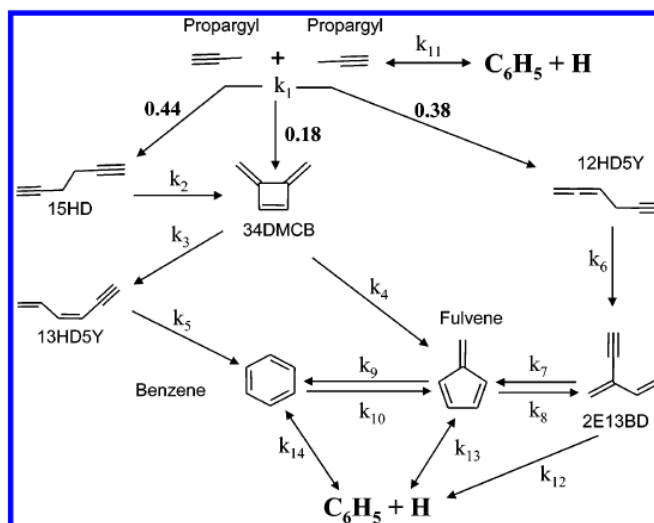


Figure 7.1: A semidetailed kinetic model of propargyl recombination and subsequent C_6H_6 isomerization. 15HD, 1,5-hexadiyne; 1245HT, 1,2,4,5-hexatetraene; 12HD5Y, 1,2-hexadiene-5-yne; 34DMCB, 3,4-dimethylenecyclobutene; 13HD5Y, 1,3-hexadiene-5-yne; 2E13BD, 2-ethynyl-1,3-butadiene. Taken from Tang et al. [59]

The kinetic parameters are given in table 7.1 along with their sources.

Table 7.1: Tang et al. C_3H_3 -mechanism

Number in Fig. 7.1	Reaction	A (mol, s, n cm)	E_a (kJ/mol)	Ref
1	$C_3H_3 + C_3H_3 \rightarrow 15HD$	$4.40E+12$	0.000	[12]
1	$C_3H_3 + C_3H_3 \rightarrow 34DMCB$	$1.80E+12$	0.000	[12]
1	$C_3H_3 + C_3H_3 \rightarrow 12HD5Y$	$3.80E+12$	0.000	[12]
2	$15HD \rightarrow 34DMCB$	$6.50E+10$	139.67	[61]
4	$34DMCB \rightarrow \text{fulvene}$	$1.44E+13$	214.15	T.w.2006
5	$13HD5Y \rightarrow \text{benzene}$	$3.78E+12$	204.36	T.w.2006
6	$12HD5Y \rightarrow 2E13BD$	$2.75E+10$	143.86	[60]
7	$2E13BD \rightarrow \text{fulvene}$	$6.61E+12$	244.34	T.w.2006
9	$\text{fulvene} \rightarrow \text{benzene}$	$9.89E+14$	296.17	T.w.2006
11	$C_3H_3 + C_3H_3 \rightleftharpoons C_6H_5 + H$	$3.67E+26$	28.963	[32]
12	$2E13BD \rightarrow C_6H_5 + H$	$3.09E+43$	496.76	[32]
13	$\text{fulvene} \rightleftharpoons C_6H_5 + H$	$8.51E+24$	474.49	[32]
14	$\text{benzene} \rightleftharpoons C_6H_5 + H$	$5.50E+38$	552.66	[32]
15	$C_3H_3I \rightarrow C_3H_3 + I$	$1.32E+08$	87.470	[60]
16	$I + I \rightarrow I_2$	$1.0E+13$	0.000	[28]
3	$34DMCB \rightarrow 13HD5Y$	$4.10E+12$	211.56	T.w.2006
8	$\text{fulvene} \rightarrow 2E13BD$	$9.12E+15$	346.25	T.w.2006
10	$\text{benzene} \rightarrow \text{fulvene}$	$5.53E+18$	420.35	T.w.2006

T.w.2006 referred to the parameter values optimized by Tang et al. as reported in their article [59]. By convenience, the reaction were reported in

the same order as they appeared in the Homrea mechanism file, whereby a certain format must be respected, but the reaction numbering is the same as in figure 7.1. The species corresponding to the symbols are given in figure 7.1. This was achieved using their recently developed Physically bounded Gauss-Newton method (PGN) [60]. The other reactions kept their original values whereas both pre-exponential factors and activation energies of the numerated reactions were optimized by Tang et al [59].

They considered for that purpose three series of experiments. First, they took their experimental data on the pyrolysis of 1,5-hexadiyne in a shock tube at an average pressure of 25 bar and temperatures varying from 800 K to 1350 K for an initial mole fraction of 42 ppm 1,5-hexadiyne in Argon [61]. They also included the experimental results of their study of propargyl-pyrolysis in a shock tube at an average pressure of 25 bar for temperatures between 720 K and 1340 K for initial mole fractions of 40 ppm and 60 ppm in Argon [58]. In both cases, the profiles of most of the species involving the $C_3H_3 + C_3H_3$ reaction system were reported. They were measured at each temperature after an average reaction time of 1.75 ms. If concentrations at the end of a reaction time are given as a function of the initial temperature, the other parameters (initial concentrations, pressure) are generally constant through the experiments, making it legitimate to represent the model results as curves. However, this was not the case of the experiments considered here. In effect, the pressure, reaction time, and initial concentrations vary over the experiments. Consequently, the data were always represented with a set of points in this chapter. Finally, Tang et al. considered experimental data of an older study of 1,5-Hexadiyne at atmospheric pressure for temperatures between 250 K and 600 K. Since the purpose of the present work concerns experimental conditions reigning in combustion systems such as car engines, only the two first series of experiments were taken into consideration. The readers is referred to [59] for the comparison between the experimental profiles and those stemming from their optimized model. It was verified with Kinfite that the values coming out of their optimization methods really correspond to local minima. The four optimizations techniques of Kinfite were employed for optimizing the same parameters as the authors (that is the pre-exponential factors and activation energies of the seven reactions denoted by T.w.2006 in table 7.1) with respect to the pyrolysis experiment series of 1,5-hexadiyne and propargyl, but no improvement could be achieved. The evolution of the distance as function of separately varied parameters indicates that the values are already optimal. The fourth reaction is characterized by strong slopes at the local minimum, as can be visualized in figures 7.2 and 7.3 describing respectively the evolution of the pre-exponential factor A_4 (s^{-1}) and activation energy $E_{a,4}$ (kJ/mol) of the fourth reaction of figure 7.1, that is $34DMCB \rightarrow$

fulvene.

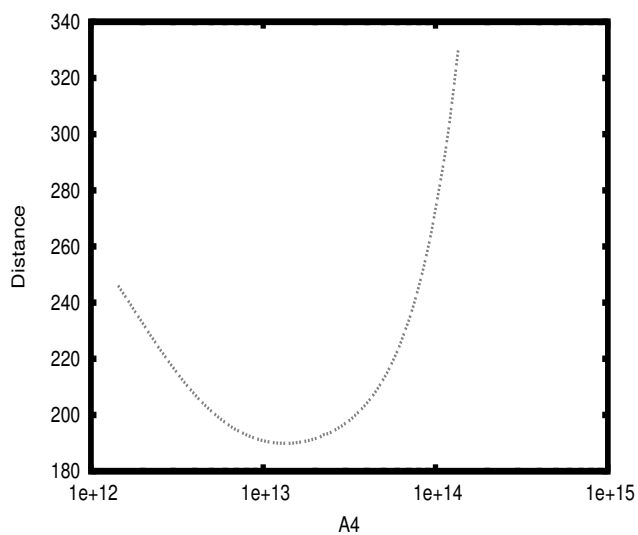


Figure 7.2: Distance as a function of A_4 (s^{-1})

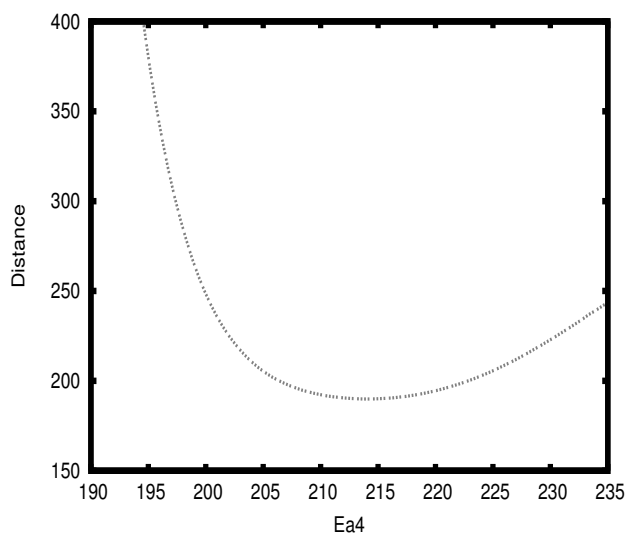


Figure 7.3: Distance as a function of $E_{a,4}$ (kJ mol^{-1})

The slopes for the other reactions are not so strong as is well illustrated in figures 7.4 and 7.5 for the fifth reaction $13\text{HD}5\text{Y} \rightarrow \text{benzene}$.

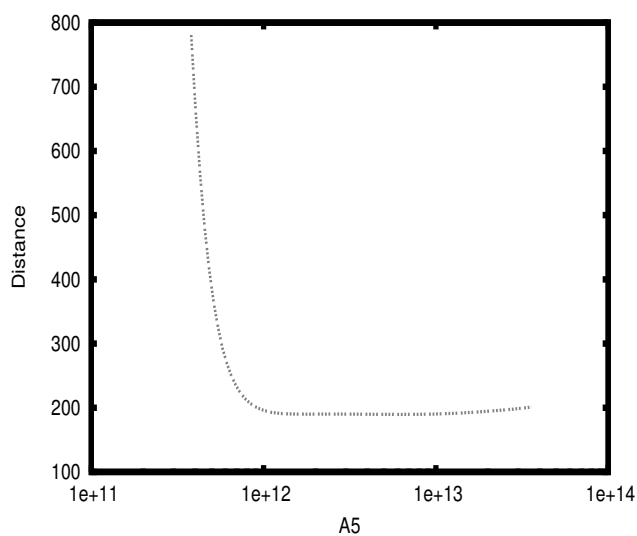


Figure 7.4: Distance as a function of A_5 (s^{-1})

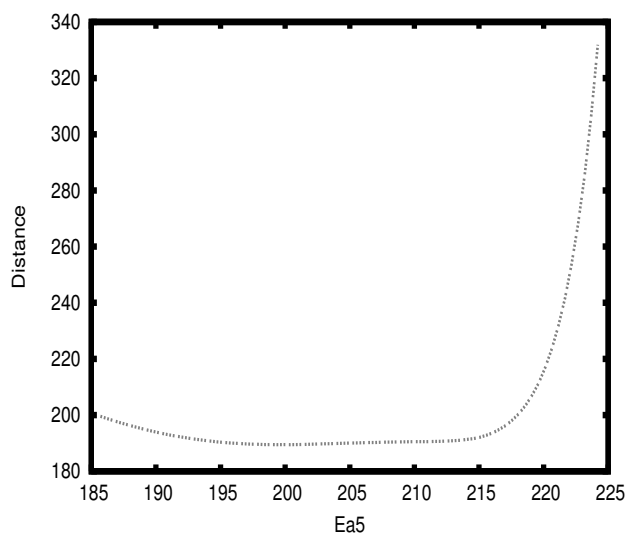


Figure 7.5: Distance as a function of $E_{a,5}$ (kJ mol^{-1})

In such cases the minimum is not unequivocally determined by the experimental data, as explained in section 4.4. This may be the case because the third series of experiments at atmospheric pressure was not considered. Alternatively, additional information in the form of other profiles or thermodynamic properties can be included in the parameter estimation problem in order to

reduce the uncertainties. What is more, the work of the authors rely on four assumptions:

- It was assumed that optimizing separately the reaction rates of forward and backward reactions would automatically lead to thermodynamically consistent results. However, due to the lack of information illustrated above, there is no guarantee this will hold true,
- Owing to the lack of thermodynamic data, the authors further supposed that the reverse steps of most reactions play no role. There is yet no warrant that it will turn out to be the case under all relevant conditions,
- Other reaction steps between the isomers were neglected. They may be however necessary for the mechanism to capture the chemistry really taking place, as indicated in a subsequent publication of the authors [31],
- the authors assumed that the decomposition of C_3H_3 towards smaller hydrocarbon than C_6 -species plays a negligible role. This appears warranted for temperature inferior to 1200 K as Scherer showed in his work [50].

If both the reaction mechanism and the thermodynamic data are consistent, the automatic computation of the reverse reactions of such uni-directional steps should have no influence on the results from the model. A set of consistent and reliable thermodynamic data for each participating species was provided by Dr. Elke Goos, Institute of Combustion Technology, DLR, German Aerospace Center, Stuttgart, Germany. Two derived reaction mechanisms were built up on this ground. Both of them include the thermodynamically defined reverse steps of all uni-directional reactions. As can be seen in figure 7.1, four optimized reaction steps were the reverse of one another, namely:

- R7 ($2E13BD \rightarrow \text{fulvene}$) and R8 ($\text{fulvene} \rightarrow 2E13BD$),
- R9 ($\text{fulvene} \rightarrow \text{benzene}$) and R10 ($\text{benzene} \rightarrow \text{fulvene}$).

In the first mechanism (Ma), the reaction rate coefficients for the forward reactions R7 and R9 were kept whereas the rates of the reverse reactions R8 and R10 were systematically calculated through use of thermochemistry. Likewise, the second mechanism (Mb) used the reaction rates of R8 and R10 as forward coefficients and calculated the rates of reactions R7 and R9 as

reverse reactions through the thermodynamic data. Both mechanisms are represented in figure 7.6.

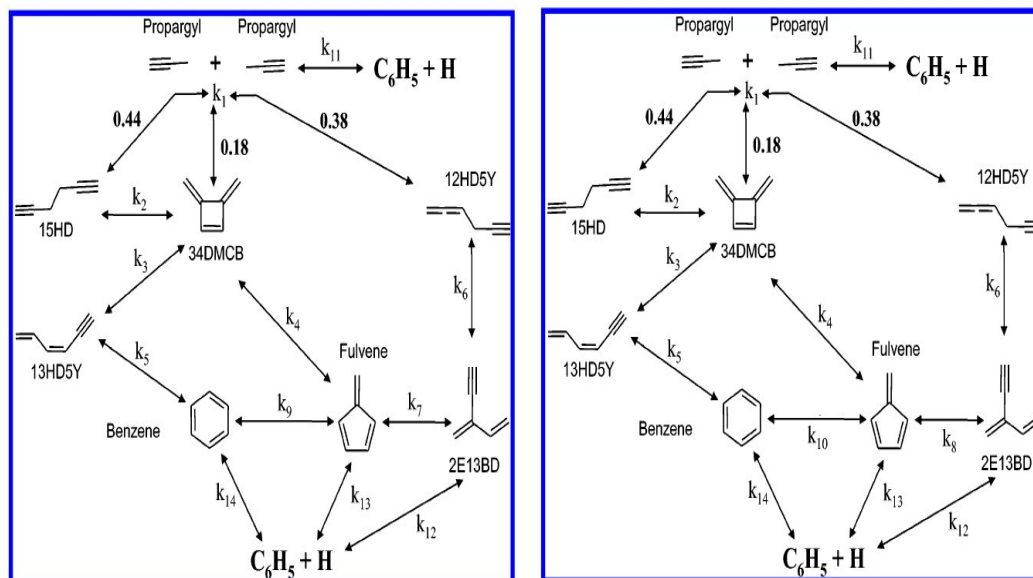


Figure 7.6: New mechanisms Ma(left) and Mb (right)

Given the accuracy of the thermodynamic data, if Tang et al's optimized reaction mechanism has the true kinetic data the results from their mechanism should be the same as those given by the mechanisms Ma and Mb. In what follows, the pyrolysis of 1,5-hexadiene is referred to as the first experiment ("exp1") whereas the second experiment ("exp2") denotes the pyrolysis of propargyl. Neither mechanism Ma nor Mb have been optimized to rematch all profiles.

7.2.2 Comparison between Tang's mechanism and mechanisms Ma and Mb

For five profiles, 13HD5Y, 15HD, 34DMCB for the pyrolysis of 1,5-hexadiene ([61]) and 15HD and C3H3I for the pyrolysis of propargyl ([58]), the differences between the three models are small or even insignificant. This is well illustrated by the profiles of 15HD and 34DMCB for the pyrolysis of 15HD in figures 7.7 and 7.8 .

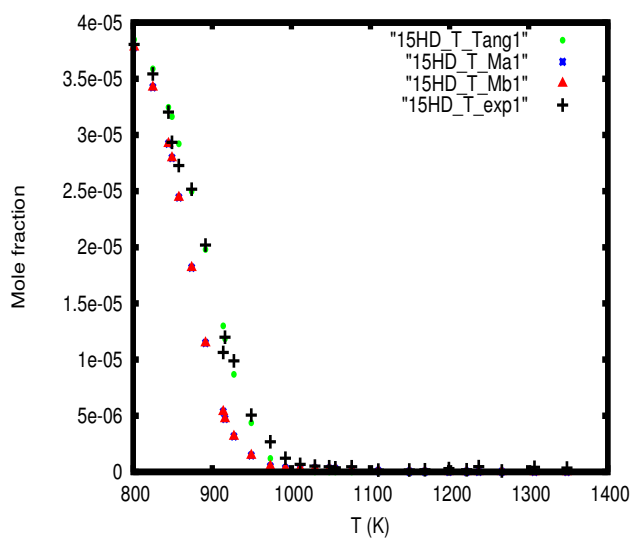


Figure 7.7: 15HD-profile for its pyrolysis

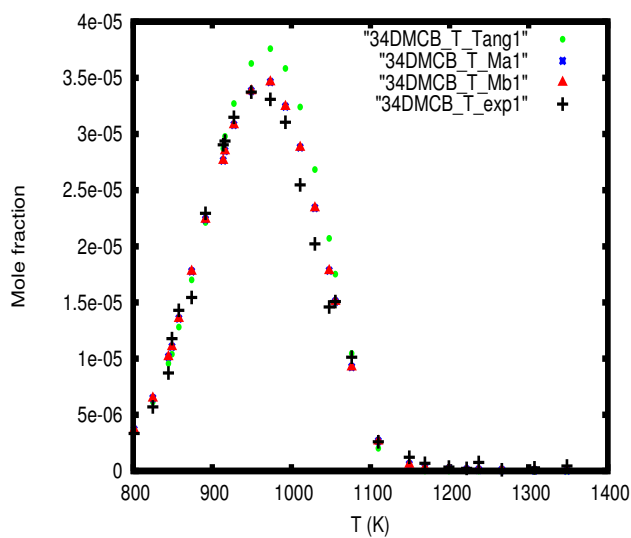


Figure 7.8: 34DMCB-profile for the pyrolysis of 1,5-Hexadyine

For these profiles, models Ma and Mb give exactly the same result and the curves cannot be distinguished. For the profiles of 12HD5Y, 13HD5Y and 34DMCB (pyrolysis of propargyl), the differences are moderate (figures 7.9 and 7.10).

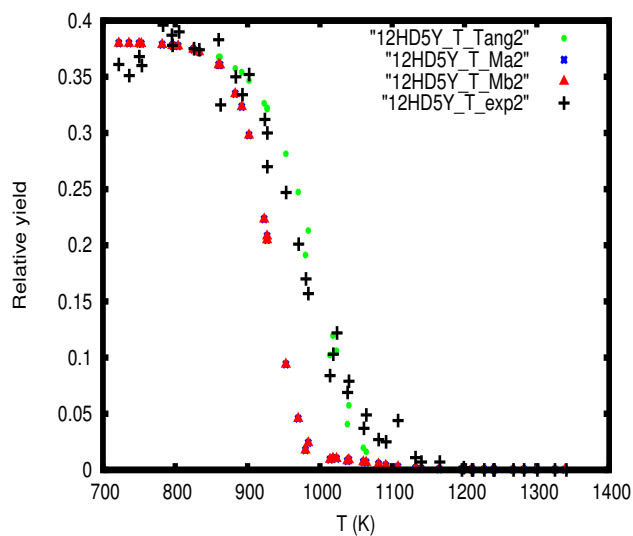


Figure 7.9: 12HD5Y-profile for C₃H₃-pyrolysis

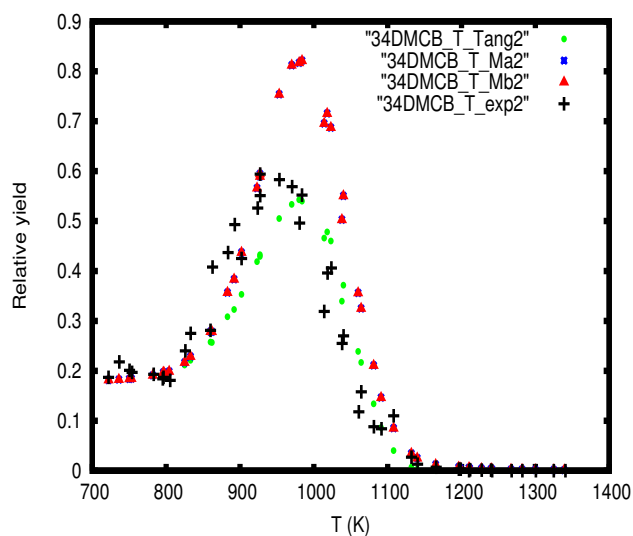


Figure 7.10: 34DMCB-profile for C₃H₃-pyrolysis

2E13BD and fulvene profiles for 15HD and C₃H₃ pyrolysis, respectively, are characterized by great discrepancies between the models as shown in figures 7.11 - 7.13.

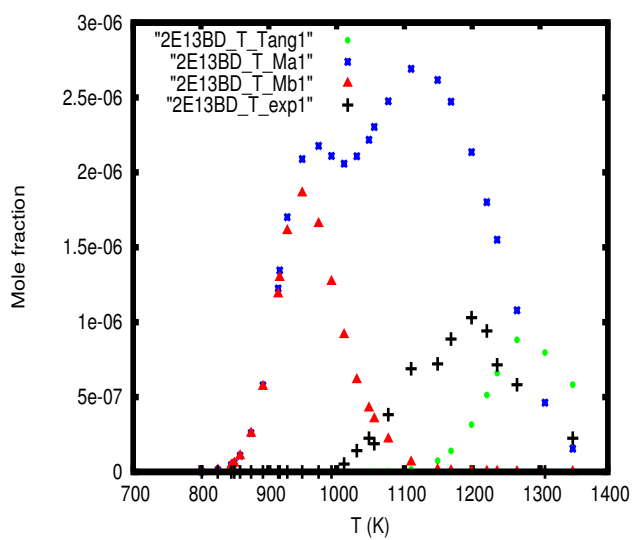


Figure 7.11: 2E13BD-profile for 15HD-pyrolysis

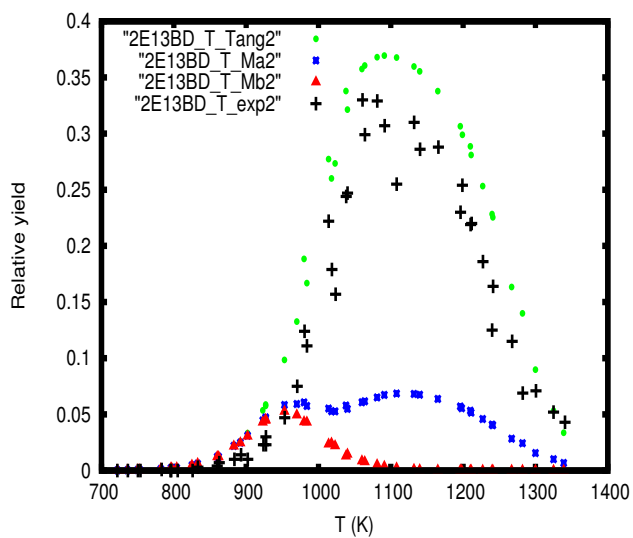


Figure 7.12: 2E13BD-profile for C_3H_3 -pyrolysis

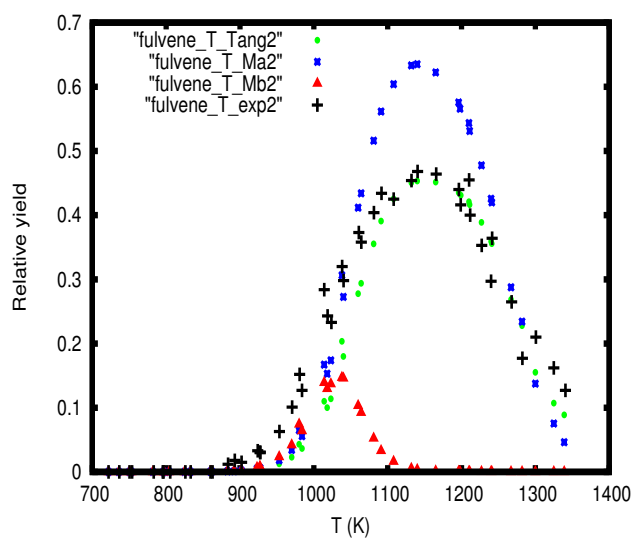


Figure 7.13: Fulvene-profile for C3H3-pyrolysis

In both pyrolysis experiments, the discrepancies between model Ma and model Mb are big for benzene. Whereas the profile Ma is relatively close to the profile from Tang et al., Mb produces considerably erroneous results as shown in figures 7.14 and 7.15.

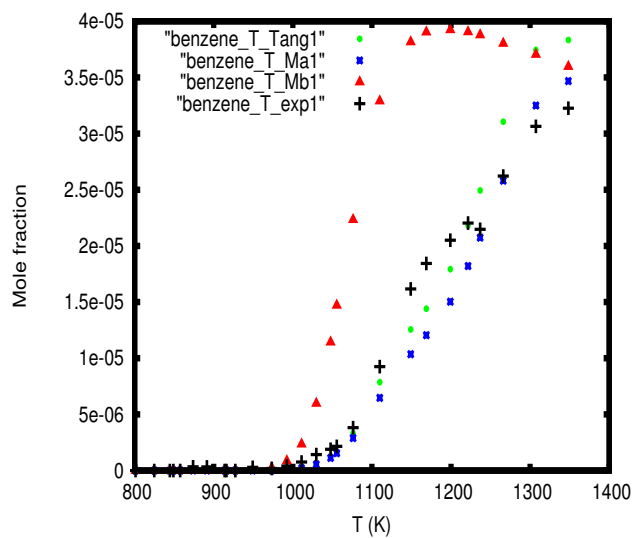


Figure 7.14: Benzene-profile for 15HD-pyrolysis

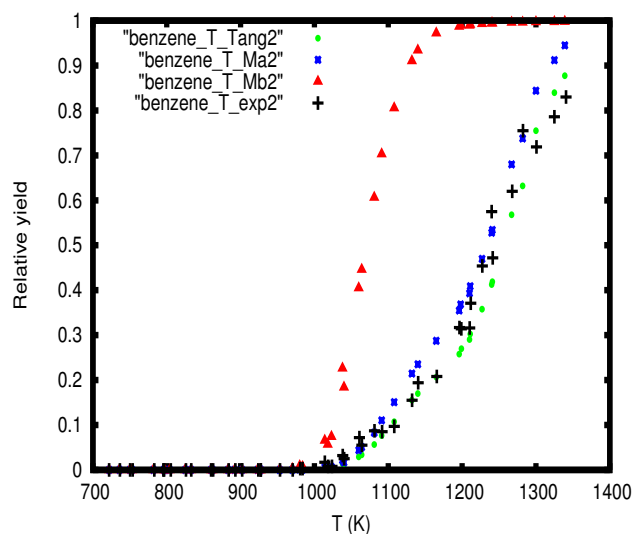


Figure 7.15: Benzene-profile for C_3H_3 -pyrolysis

The three species characterized by the greatest differences (benzene, fulvene and 2E13BD) are the ones involved in the four optimizable reactions (R7-R10) which are the reverse of each others. The consideration of the species thermodynamic data leads thus to considerable differences for the three models. This shows that the kinetic coefficients optimized separately by Tang et al. are inconsistent with the available thermodynamic information. As a consequence, it is desirable to determine a new thermodynamically consistent mechanism in order to enable reliable inclusions into PAH and soot models.

7.3 Optimization of the mechanism Ma

Since Ma is closer to the experiments, it has been chosen as starting point for the optimization. The greatest discrepancies concern the profiles of 2E13BD during the pyrolyses of 1,5-hexadiene and propargyl as shown in figures 7.11 and 7.12. The other profiles are relatively in good agreement with the thermodynamically consistent mechanism Ma. In all following sections, the four optimization methods were employed but solely the results of the one with the smallest discrepancies are shown. The optimized parameters are not reported if it is obvious that the optimized model is largely inconsistent with the experimental measurements.

7.3.1 Use of the chi-squares Norm

First, the weighted chi-squares norm (designated here as norm 1) (see 3.1.2) has been employed, whereby the standard deviations were proportional to the measurements (equation 3.1.2):

$$d = \sum_{i=1}^N \frac{n_{mean}}{n_i} \sum_{j=1}^{n_i} \left(\frac{m_{i,j} - e_{i,j}}{e_{i,j}} \right)^2.$$

For each profile, only those experimental values greater than 5% of the greatest value of the profile were considered, because due to both experimental uncertainties and numerical errors, the other values had proven to be unreliable and to lead to incoherent results.

Optimization of the seven isomerisation reaction

In the first place, the seven isomerisation reactions were optimized using pre-exponential factors, temperature coefficients and activation energies.

Reaction	A	n	E_a (kJ/mol)
15HD =34DMCB	6.50E+10	0.00	139.61
34DMCB =fulvene	1.44E+13	0.00	214.06
13HD5Y =benzene	3.78E+12	0.00	204.27
12HD5Y =2E13BD	2.75E+10	0.00	146.31
2E13BD =fulvene	6.61E+12	0.00	244.24
fulvene =benzene	9.89E+14	0.00	294.92
34DMCB =13HD5Y	4.10E+12	0.00	211.47

Since the initial values have not been precisely determined by Tang et al., large variation intervals were allowed for all parameters. The bounds are defined by $\frac{A_{ini}}{A_{min}} = \frac{A_{max}}{A_{ini}} = 100$, $n_{max} - n_{ini} = n_{ini} - n_{min} = 1.70$, and $E_{a,max} - E_{a,ini} = E_{a,ini} - E_{a,min} = 20 \text{ kJ mol}^{-1}$. Despite such a broad search width, negligible improvements were reached globally. All profiles except those of 2E13BD remain almost unchanged, as well illustrated by the profile of 13HD5Y-profile for propargyl pyrolysis (figure 7.16).

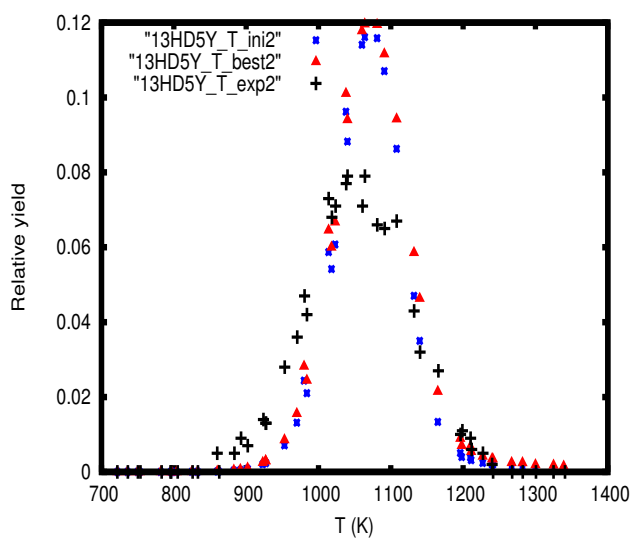


Figure 7.16: 13HD5Y-profile for propargyl pyrolysis

Whereas the profile of 2E13BD was improved for the pyrolysis of 1,5-hexadiene, it was worsend for the pyrolysis of C_3H_3 , as shown in figures 7.17 and 7.18 respectively.

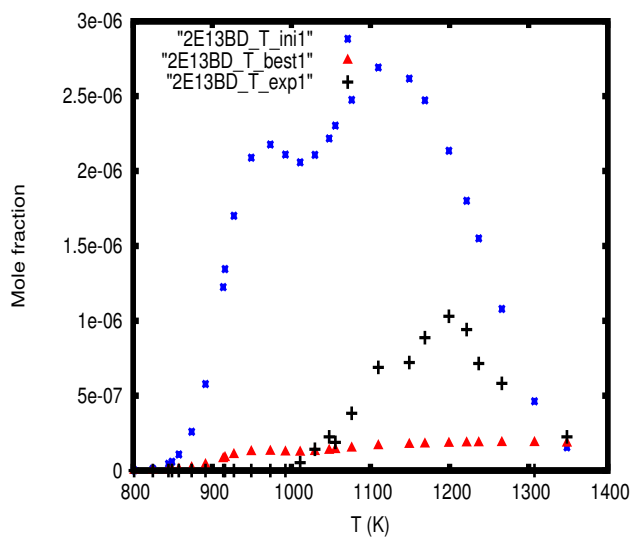


Figure 7.17: 2E13BD-profile for 15HD-pyrolysis

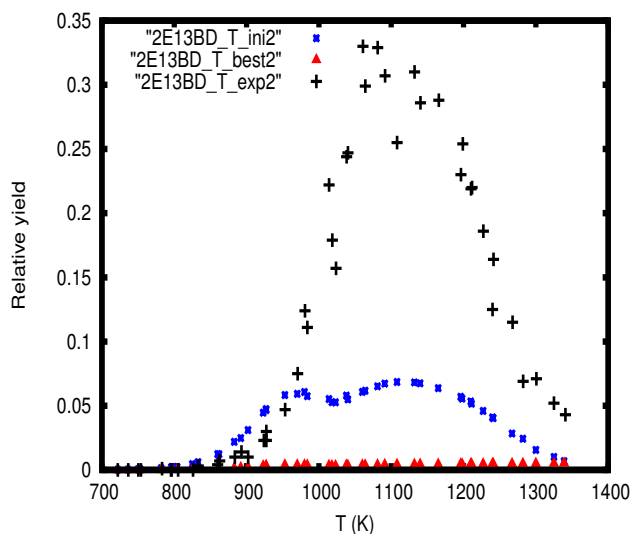


Figure 7.18: 2E13BD profile for propargyl pyrolysis

This situation is due to the nature of the chi-square norm defined above: due to the absence of information about the experimental errors, it has been assumed they are proportional to the measurement values. As a consequence, each term of the chi-squares sum consists of the difference between the values from the model and those from the experiment divided by the experimental values. Considering the initial parameter values, the predictions of Ma are considerably higher for the 2E13BD profile during the pyrolysis of 1,5-hexadiene than the experimental values. On the contrary, the predictions of the model are lower than the experimental values of 2E13BD during the pyrolysis of propargyl in such a way that the term $\frac{m_{i,j} - e_{i,j}}{e_{i,j}}$ never exceed the value 1. However this term takes on great values, often more than 100, for 2E13BD profile during the pyrolysis of 1,5-hexadiene. As a consequence, the optimization methods have tried to lower 2E13BD profile during the pyrolysis of 15HD without giving much consideration to the other profiles, including the one of 2E13BD during C_3H_3 pyrolysis. It is clear that the mechanism Ma optimized in this way is inconsistent with the experimental data.

Optimization of the seven isomerisation reaction and three recombination reactions

A reaction significance analysis (see 3.2.4) was carried out and showed that the three propargyl recombination steps play a crucial role for the concentration of 2E13BD. Consequently, a new optimization was started with the three C_3H_3 recombination reactions alongside the six isomerisation reactions

already considered. The profiles of 2E13BD for the pyrolyses of 1,5-hexadiene and pyrolysis are better predicted by the current optimized model than by the old one (see figures 7.19 and 7.20).

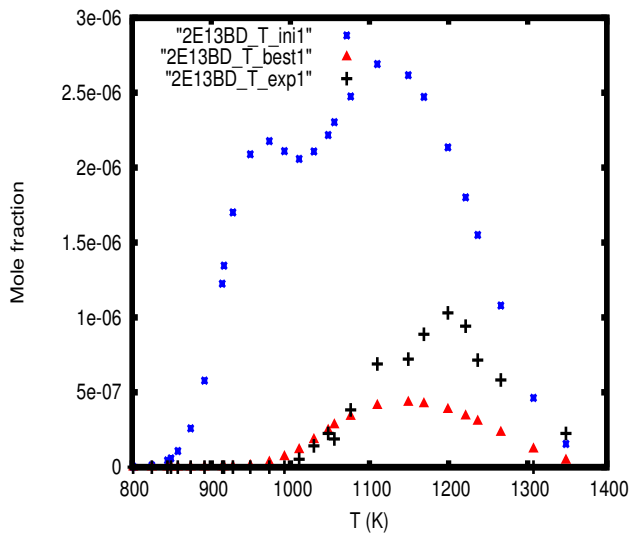


Figure 7.19: 2E13BD-profile for 15HD-pyrolysis

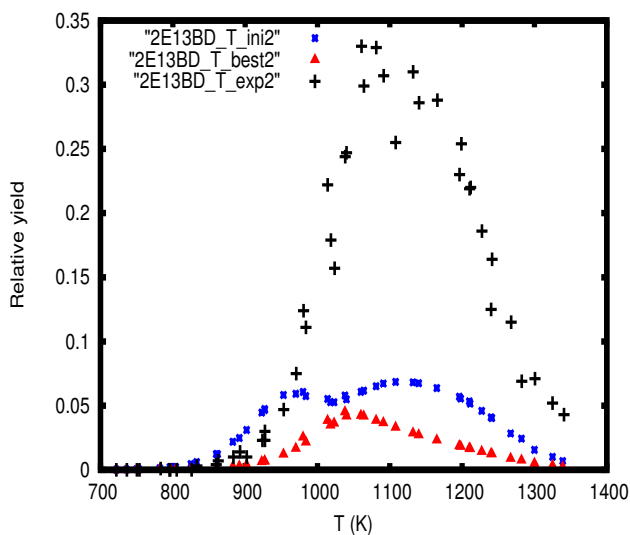


Figure 7.20: 2E13BD-profile for propargyl pyrolysis

The prediction of the optimized model are almost identical with those of the initial model for the profiles of 13HD5Y and benzene for 1,5-hexadiene and

propargyl pyrolyses as exemplified by figure 7.21.

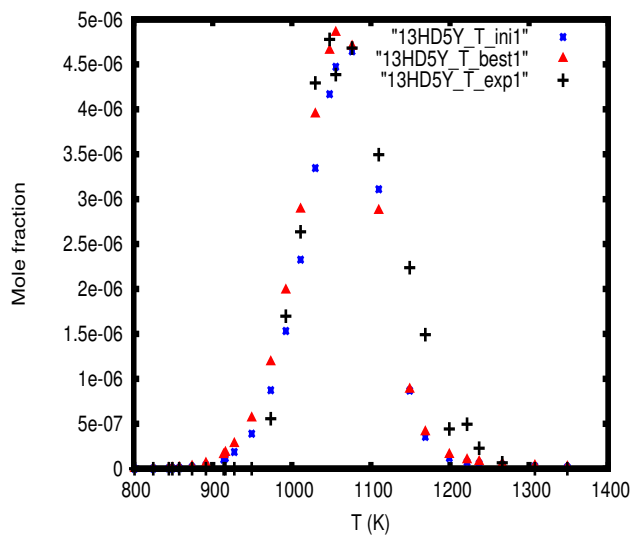


Figure 7.21: 13HD5Y profile for 1,5-hexadiene pyrolysis

The predictions of 15HD profile for its own pyrolysis and of C_3H_3I also for its own pyrolysis were slightly improved, as shown in figures 7.22 and 7.23.

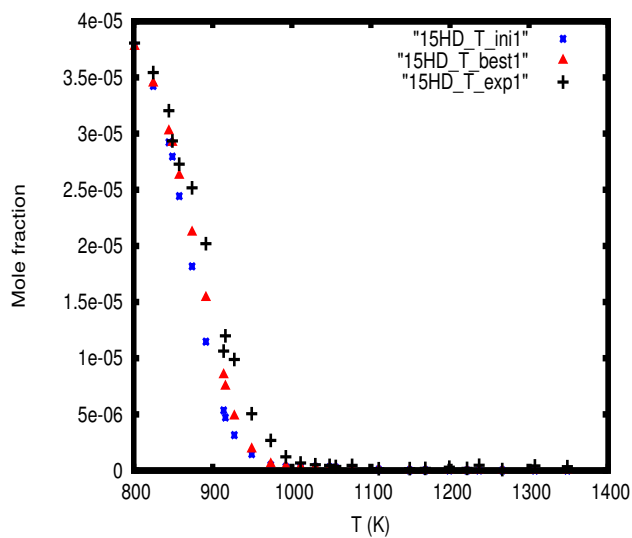


Figure 7.22: 15HD profile for its own pyrolysis

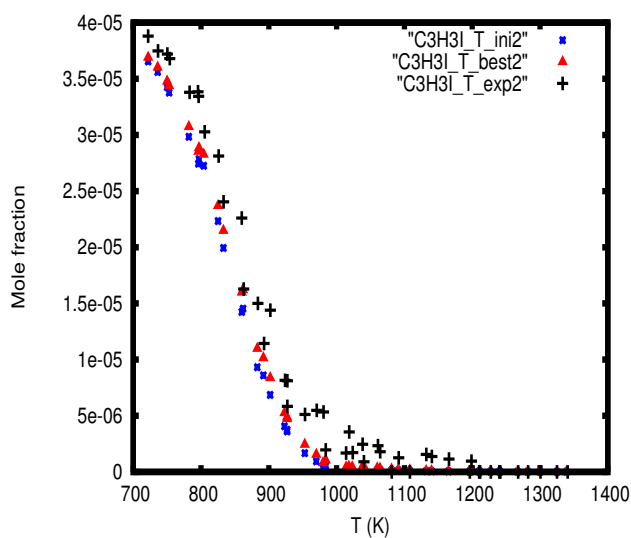


Figure 7.23: C_3H_3I profile for its own pyrolysis

The profile of 34DMCB for C_3H_3I pyrolysis is much better predicted by the optimized mechanism than by the initial one (figure 7.26).

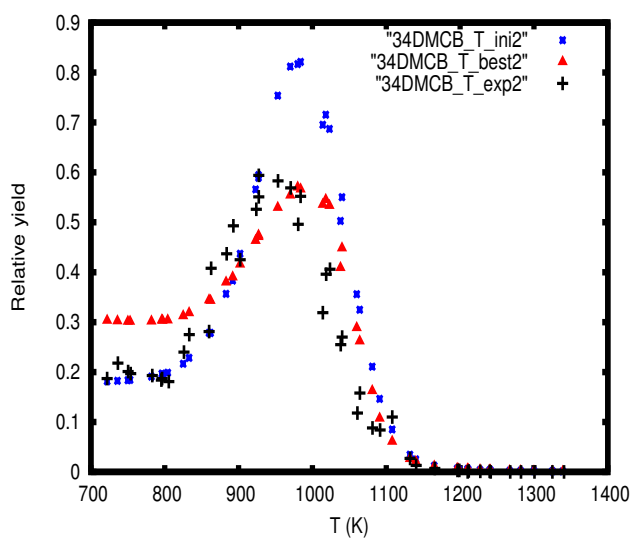


Figure 7.24: 34DMCB profile for the pyrolysis of propargyl

The predictions are slightly worse for the profiles of 12HD5Y for propargyl pyrolysis and 34DMCB for 1,5-hexadiyne pyrolysis (figures 7.25 and 7.26).

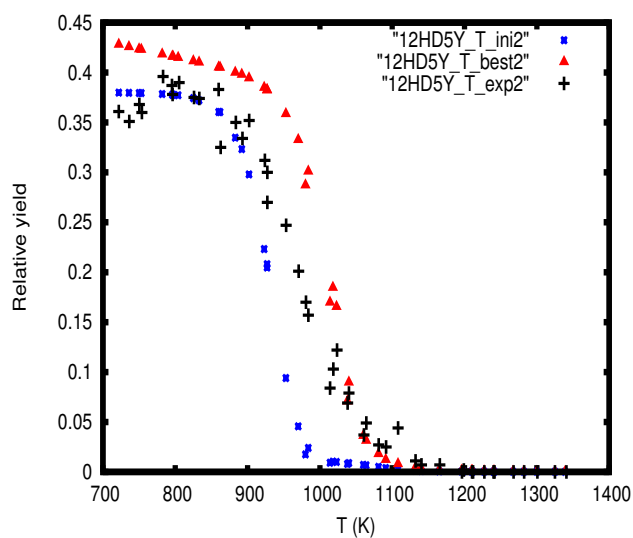


Figure 7.25: 12HD5Y profile for the pyrolysis of propargyl

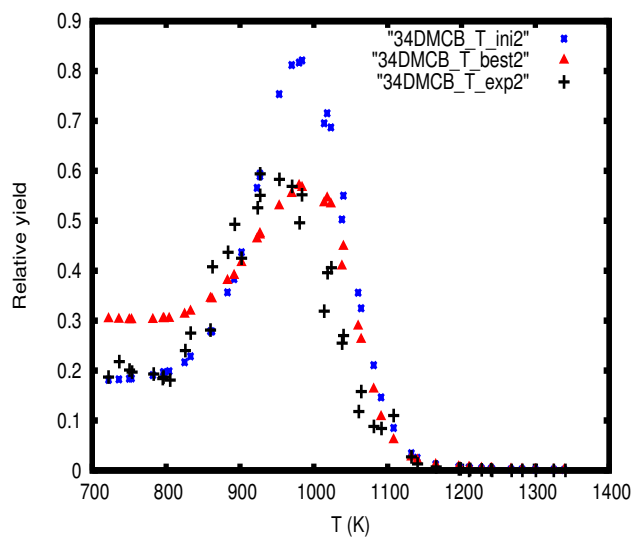


Figure 7.26: 34DMCB profile for the pyrolysis of 1,5-hexadiene

The predictions are considerably worsened for 15HD profile for the pyrolysis of propargyl as shown in figure 7.27.

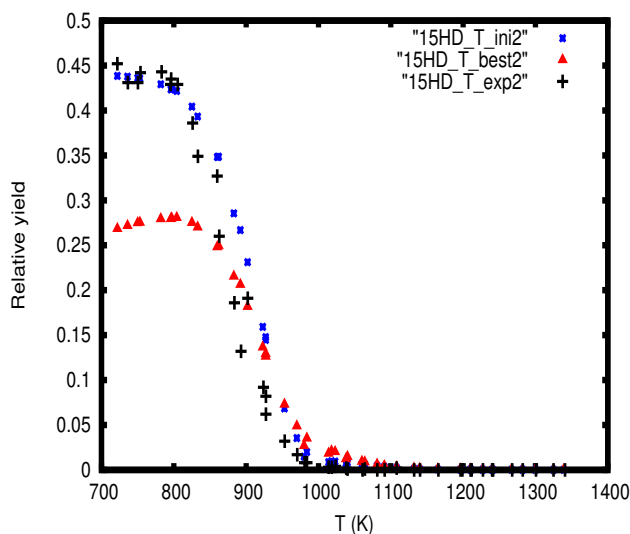


Figure 7.27: 15HD profile for the pyrolysis of propargyl

It is evident that the optimized model is in disagreement with the experiments.

7.3.2 Use of a new customized norm

As explained above, if the standard deviations are proportional to the experimental measurements (provided they are not too small), the chi-squared norm tend to reduce the values from the model at all cost whenever they are higher. To overcome this problem, a new relative least-squares norm (designated here as norm 2) was defined:

$$d = \sum_{i=1}^N \frac{n_{mean}}{n_i} \sum_{j=1}^{n_i} \left(\frac{m_{i,j} - e_{i,j}}{\max(e_{i,j}, m_{i,j})} \right)^2, \quad (7.1)$$

where N is the number of profiles whereas n_i is the number of experimental points for the i -th profile. For each profile, only those experimental values greater than 5% of the greatest value of the profile were considered.

Optimization of the six isomerisation reaction

As previously, the six isomerisations were optimized simultaneously which led to a similar result as with the previous norm.

Optimization of the six isomerisation reaction and three recombination reactions

The same reactions than in 7.3.1 were optimized with norm 2. This time, a satisfactory agreement was attained. The profiles of 2E13BD were hugely improved.

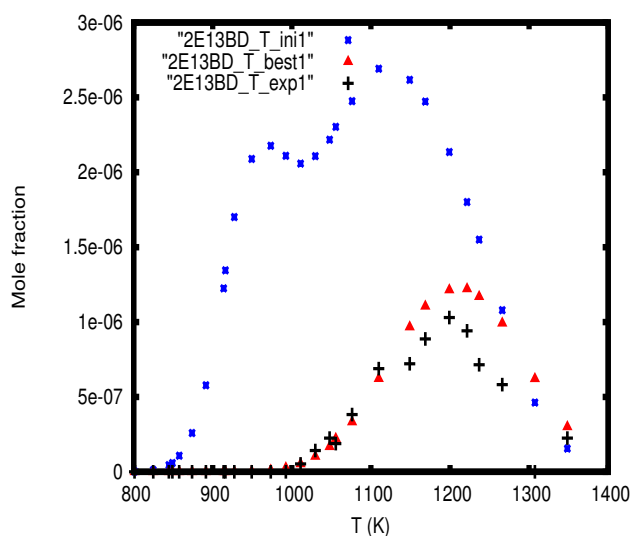


Figure 7.28: 2E13BD-profile for Hexadyine-pyrolysis

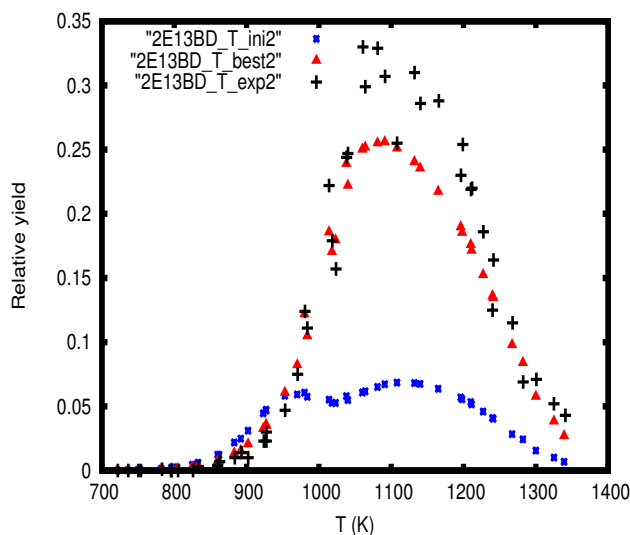


Figure 7.29: 2E13BD-profile for C₃H₃-pyrolysis

The profiles of $^{13}\text{HD5Y}$ and $^{34}\text{DMCB}$ during the pyrolysis of propargyl were also better predicted.

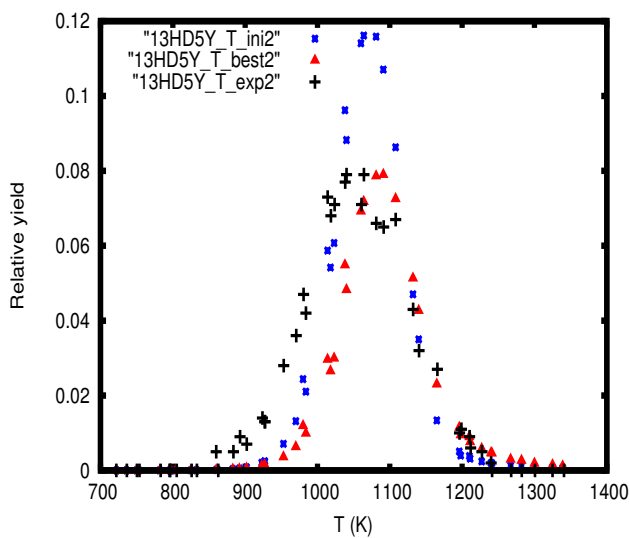


Figure 7.30: $^{13}\text{HD5Y}$ -profile for C_3H_3 -pyrolysis

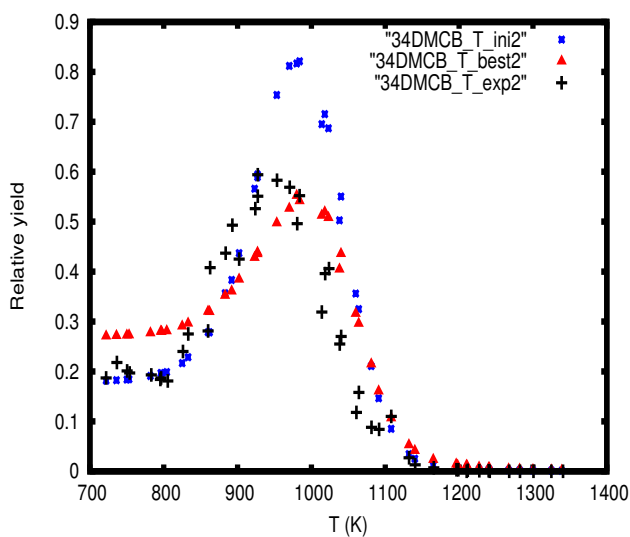


Figure 7.31: $^{34}\text{DMCB}$ -profile for C_3H_3 -pyrolysis

However, the prediction of ^{15}HD during the pyrolysis of propargyl was slightly worse.

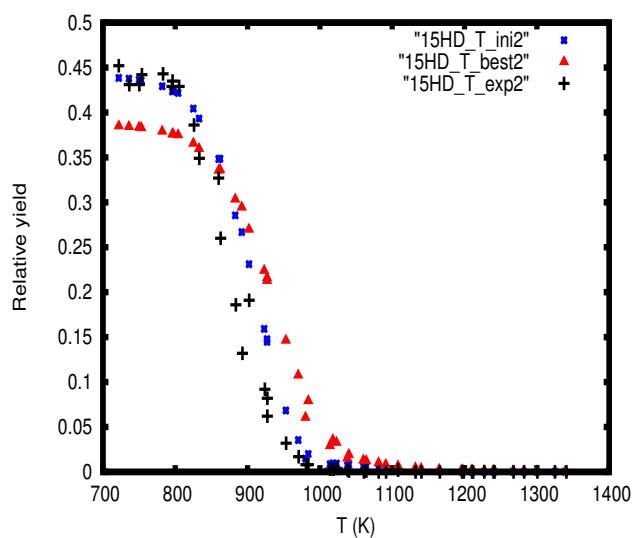


Figure 7.32: 15HD-profile for C3H3-pyrolysis

Globally, the optimized mechanism is in good agreement the experiments. Unfortunately, the reaction rates of the propargyl recombination steps have been reduced by several orders of magnitude by the optimizing methods.

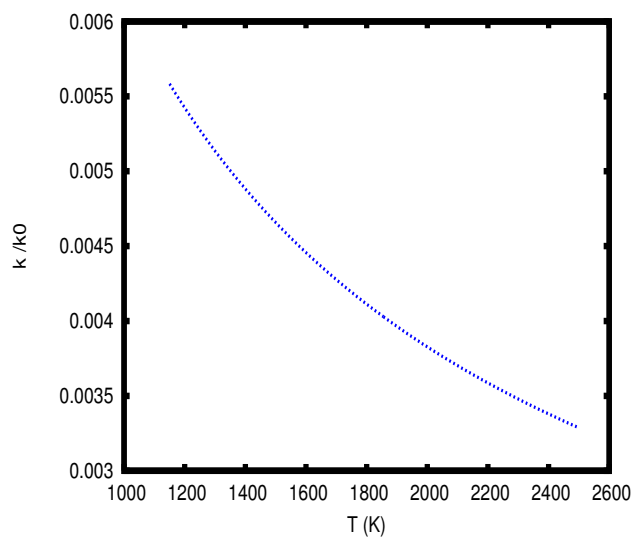


Figure 7.33: Ratio k/k_0 for $C_3H_3 + C_3H_3 = 15HD$

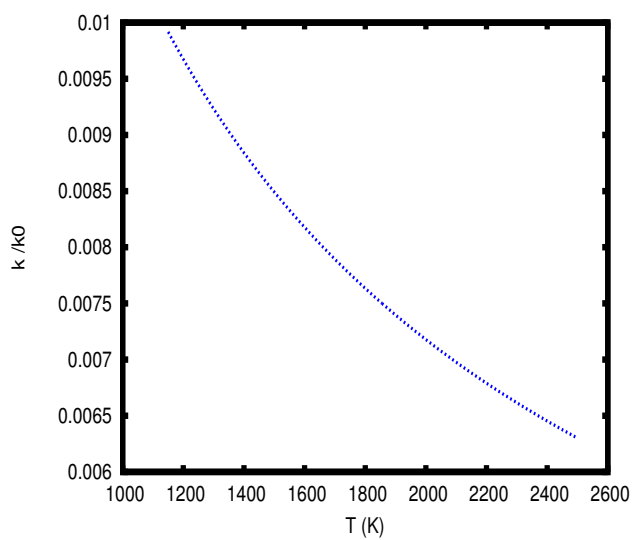


Figure 7.34: Ratio k/k_0 for $C_3H_3 + C_3H_3 = 34DMCB$

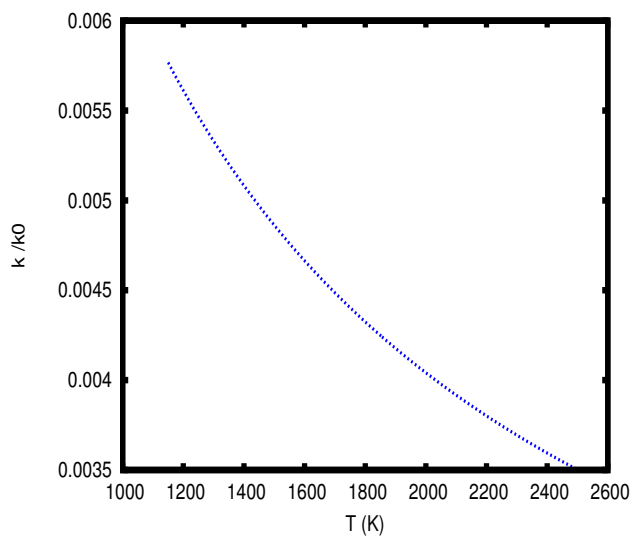


Figure 7.35: Ratio k/k_0 for $C_3H_3 + C_3H_3 = 12HD5Y$

At the same time, the rates of the isomerisation reactions are only slightly modified, as shown in figures 7.36 and 7.37.

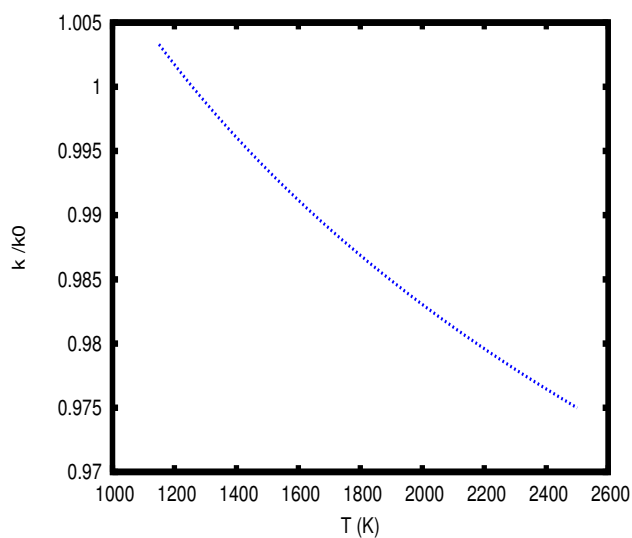


Figure 7.36: Ratio k/k_0 for 15HD = 34DMCB

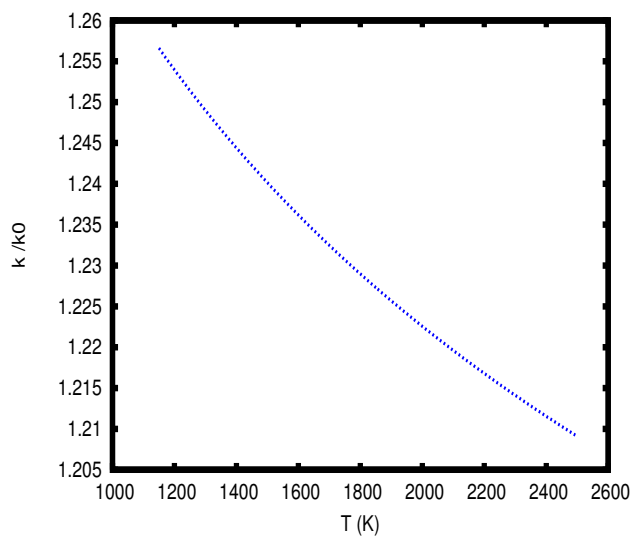


Figure 7.37: Ratio k/k_0 for 34DMCB = fulvene

Since the reaction rate coefficient of the propargyl recombination is known within a factor ten [59], the values lowered by a factor greater than hundred (figures 7.33 - 7.35) are unphysical. The same optimization was carried out with bounds equal to ten for the three recombination reaction rate coefficients k_i , but only a negligible improvement could be achieved in comparison with the initial values. Such a situation often comes up in parameter estimation

problems of all kinds: a satisfactory agreement can only be reached if some parameters take on unrealistic values, which shows that the underlying model is erroneous.

7.3.3 Successive optimization of Ma

In this part, all recombination and isomerization reactions (reactions 1 and 2-10, respectively, see figure 7.1) were optimized using norm 1 (see 7.3.1) within very large intervals, defined in the following way:

$$\frac{A_0}{1000} \leq A \leq 1000A_0$$

$$n_0 - 2.7 \leq n \leq n_0 + 2.7$$

$$E_{a,0} - 50 \leq E_a \leq E_{a,0} + 50$$

and for the first three recombination reactions

$$\frac{k_0}{10} \leq k \leq 10k_0.$$

Despite such extremely wide intervals, all optimized solutions had physically meaningful values, as shown later.

Optimization of Mechanism Ma to the pyrolyses of 1,5-hexadiene alone

First, the mechanism Ma was optimized with the experimental results of the pyrolysis of 1,5-hexadiene only. An excellent agreement was achieved.

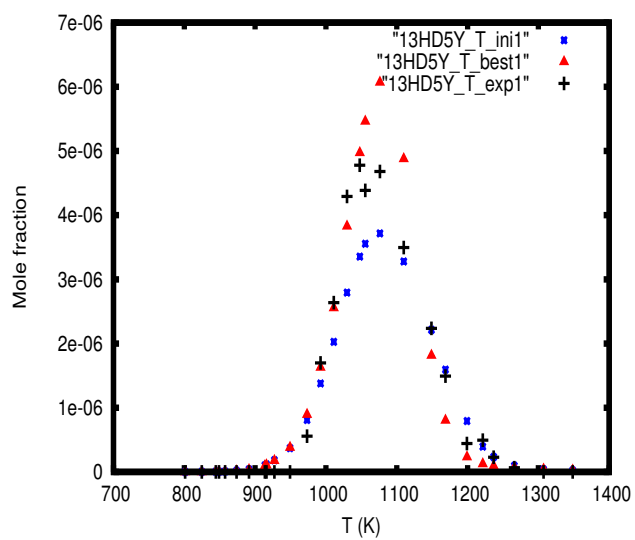


Figure 7.38: 13HD5Y profile for the pyrolysis of 1,5-Hexadyine

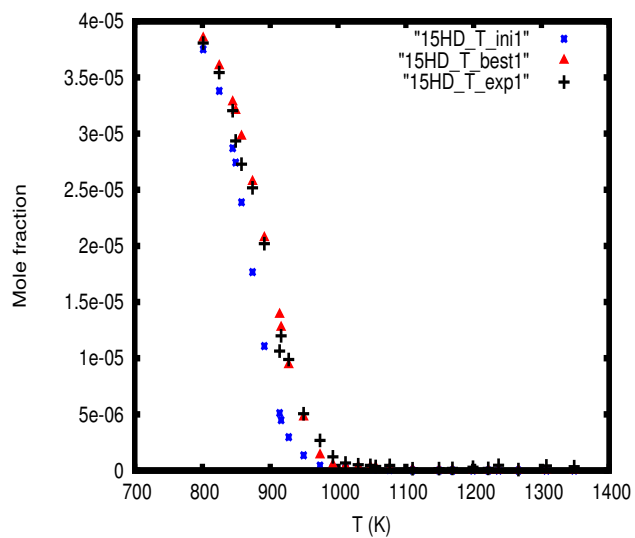


Figure 7.39: 15HD profile for the pyrolysis of 1,5-Hexadyine

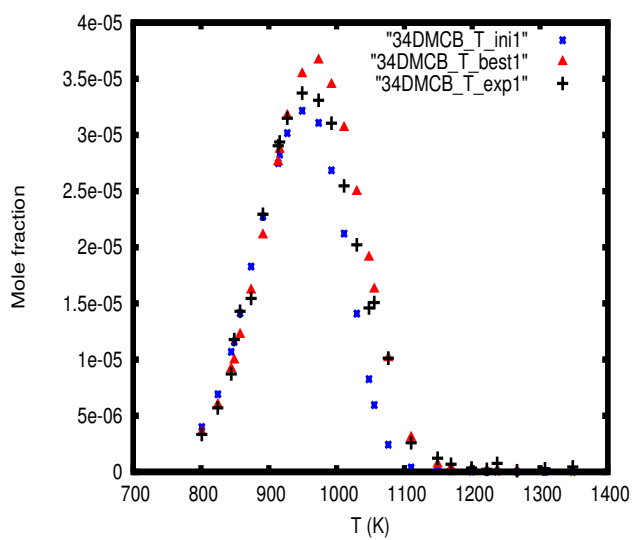


Figure 7.40: 34DMCB profile for the pyrolysis of 1,5-Hexadyine

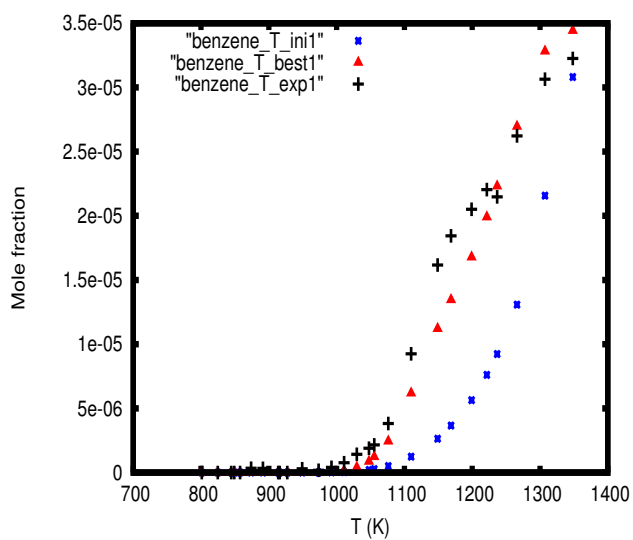


Figure 7.41: Benzene profile for the pyrolysis of 1,5-Hexadyine

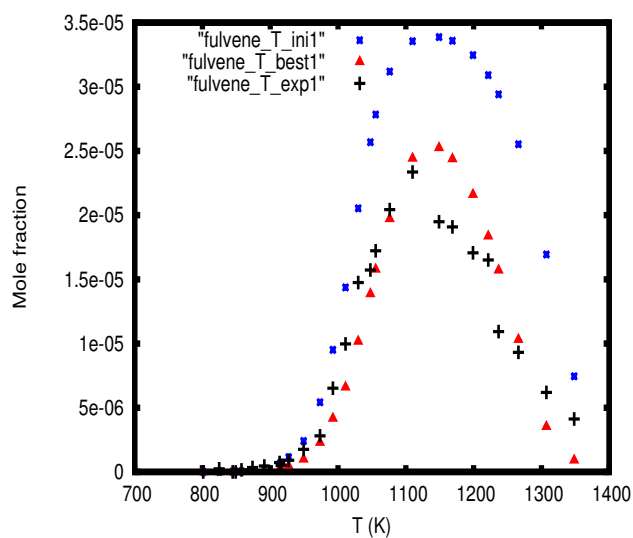


Figure 7.42: Fulvene profile for the pyrolysis of 1,5-Hexadiene

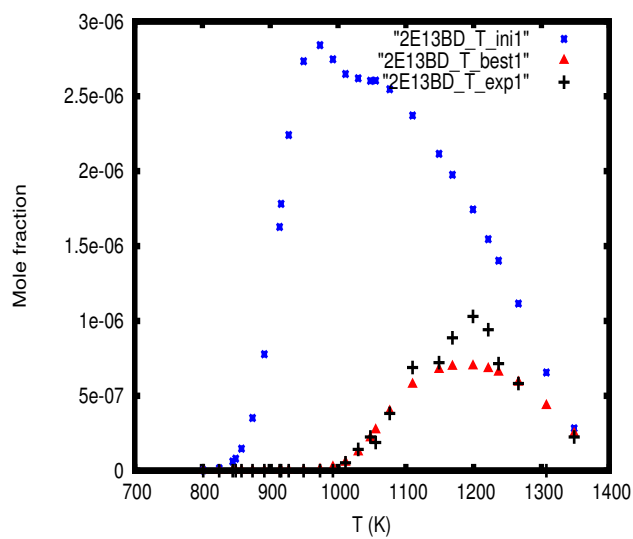


Figure 7.43: 2E13BD profile for the pyrolysis of 1,5-Hexadiene

The profile of 2E13BD was considerably better predicted and poses an interesting problem for the optimized model of Tang et al which, by convenience, is given once again in figure 7.44.

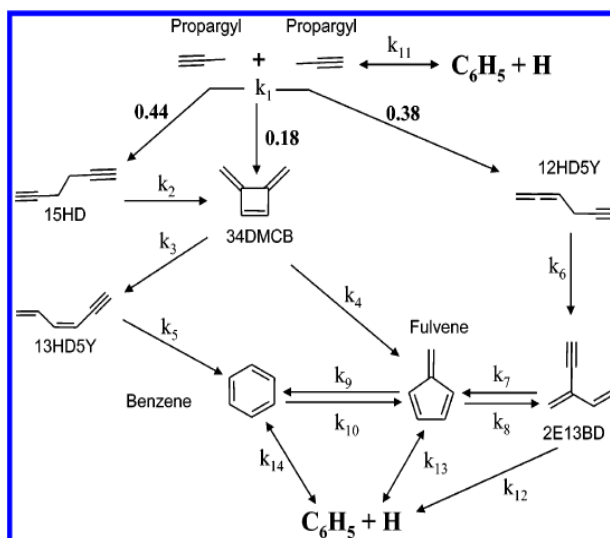


Figure 7.44: Reproduction of Tang's mechanism, added for the sake of clarity. 15HD, 1,5-hexadiyne; 1245HT, 1,2,4,5-hexatetraene; 12HD5Y, 1,2-hexadiene-5-yne; 34DMCB, 3,4-dimethylenecyclobutene; 13HD5Y, 1,3-hexadiene-5-yne; 2E13BD, 2-ethynyl-1,3-butadiene. Taken from Tang et al. [59]

According to Tang's model, during the pyrolysis of 1,5-hexadiyne, 2E13BD can only be produced from fulvene through reaction 8. This possibility itself is rejected by the authors in a previous publication [61], owing to the fact that the thermal excitation under their conditions is not high enough to drive fulvene back to 2E13BD. But since this was the only possibility in their mechanism, their optimization method forced the coefficients of the isomerization Fulvene \rightarrow 2E13BD to produce 2E13BD in order to better fit the experimental profile, thereby creating a physically meaningless step. On the contrary, the mechanism Ma (see figure 7.6) optimized in this way here includes the reverses of the isomerization reactions, therefore enabling the formation of C_3H_3 from 15HD and 34DMCB (reverse of reaction 1) and the reaction of the propargyl radicals appearing in this manner towards 12HD5Y. However, this route towards 12HD5Y and 2E13BD may not be the only reaction pathway involved. In effect, Tranter et al. [61] pointed out that an isomerization step between 15HD and 12HD5Y could not be excluded. Likewise, Miller et al. [31] found an apparent isomerization between 12HD5Y and 34DMCB which predominantly removed 12HD5Y. As guaranteed by the optimization methods of Kinfite, the optimized reaction rate coefficients of the three recombination steps were kept within a factor 10 from their original values, as shown in figures 7.45 - 7.47 representing reactions $C_3H_3 + C_3H_3 \rightarrow 15HD$, $C_3H_3 + C_3H_3 \rightarrow 34DMCB$ and $C_3H_3 + C_3H_3 \rightarrow 12HD5Y$ respectively.

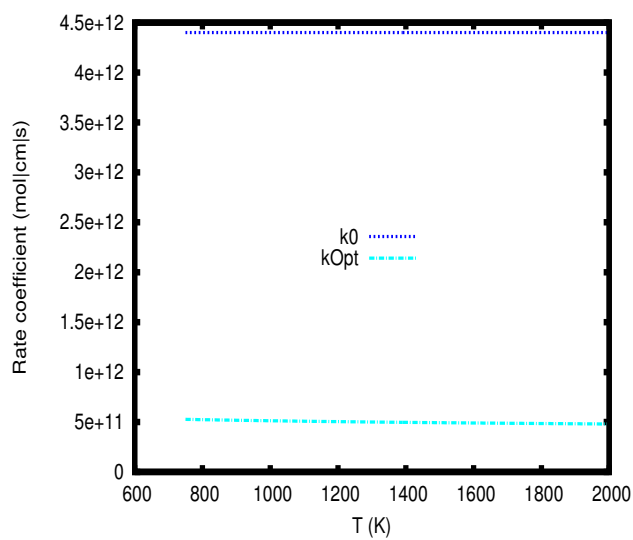


Figure 7.45: Initial and optimized rate coefficients for $C_3H_3 + C_3H_3 \rightarrow 15HD$.

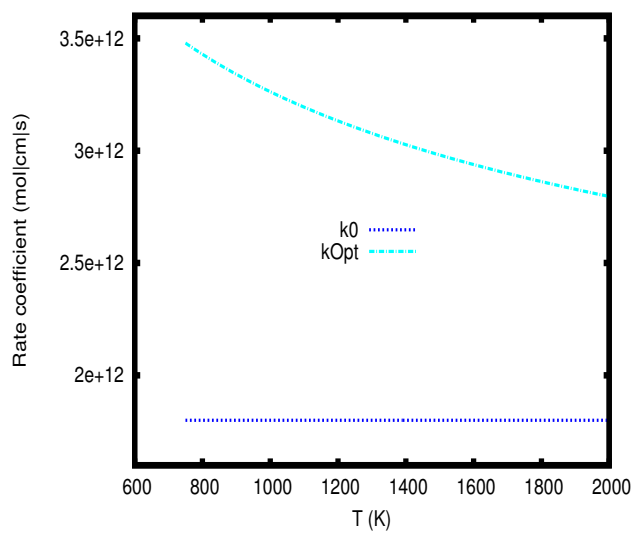


Figure 7.46: Initial and optimized rate coefficients for $C_3H_3 + C_3H_3 \rightarrow 34DMCB$.

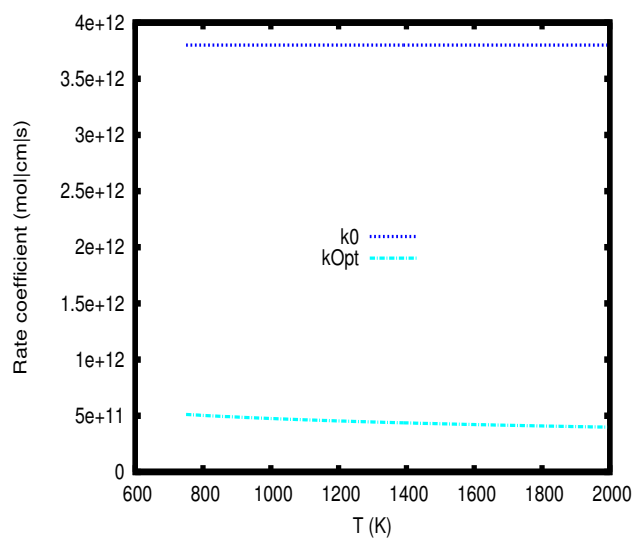
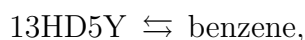
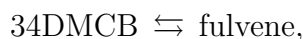
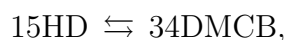


Figure 7.47: Initial and optimized rate coefficients for $C_3H_3 + C_3H_3 \rightarrow 12HD5Y$.

It makes sense that the reaction rate coefficient of $C_3H_3 + C_3H_3 \rightarrow 15HD$ is reduced since it allows greater quantity of propargyl to be produced through the reverse reaction. However, there is no obvious explanation for the increase of the rate coefficient of $C_3H_3 + C_3H_3 \rightarrow 34DMCB$ and the decrease of the rate coefficient of $C_3H_3 + C_3H_3 \rightarrow 12HD5Y$ since this should increase the formation of 12HD5Y. In spite of the absence of bounds, the reaction rate coefficients of all isomerization reactions had realistic optimized values, as is exemplified in figures 7.48 - 7.51 corresponding to the reactions



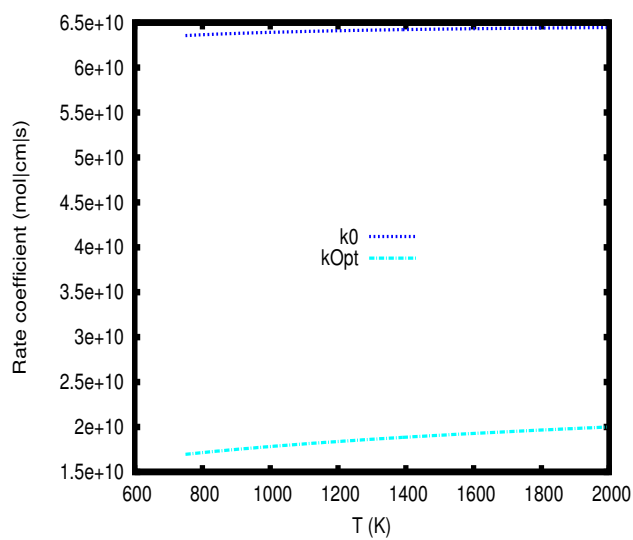


Figure 7.48: Initial and optimized rate coefficients for $15\text{HD} \rightleftharpoons 34\text{DMCB}$.

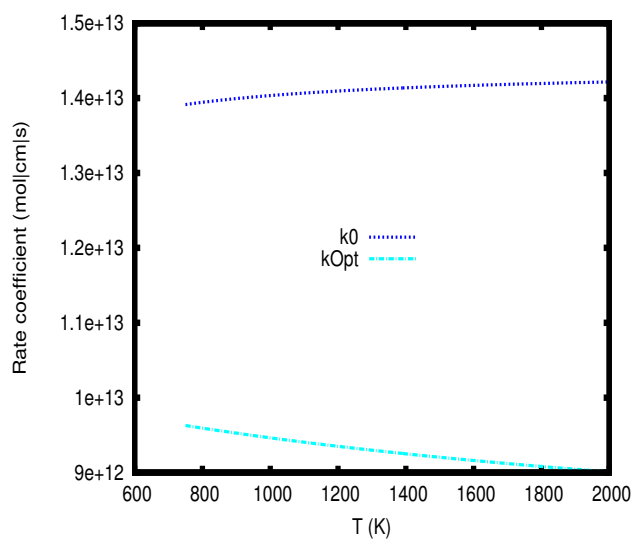


Figure 7.49: Initial and optimized rate coefficients for $34\text{DMCB} \rightleftharpoons \text{fulvene}$.

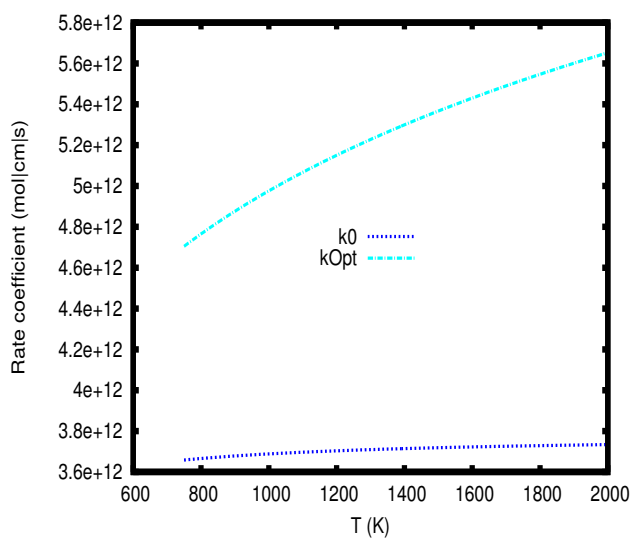


Figure 7.50: Initial and optimized rate coefficients for $13\text{HD}5\text{Y} \rightleftharpoons \text{benzene}$.

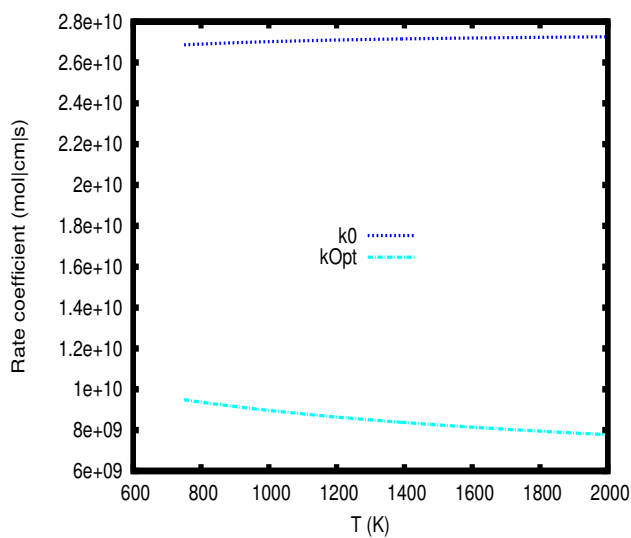


Figure 7.51: Initial and optimized rate coefficients for $12\text{HD}5\text{Y} \rightleftharpoons 2\text{E}13\text{BD}$.

Such physically meaningful results are encouraging because they seem to indicate that the experiments are at least partially captured by the mechanism Ma. If the system did not correspond to the model, one would have expected parameters to take on unrealistic values.

Prediction of the newly optimized mechanism for 1,5-hexadiene pyrolysis on propargyl pyrolysis

The reaction mechanism Ma has been optimized independently from the pyrolyses of propargyl and is now being employed for the simulation of the propargyl experiments. Four profiles remain relatively well predicted although no improvement was achieved. They are the profiles of 13HD5Y, benzene, C3H3I, and fulvene (see figures 7.52 - 7.53). *Sp*_T_new2 designates the temperature-dependent concentration of the species Sp predicted by the newly optimized mechanism.

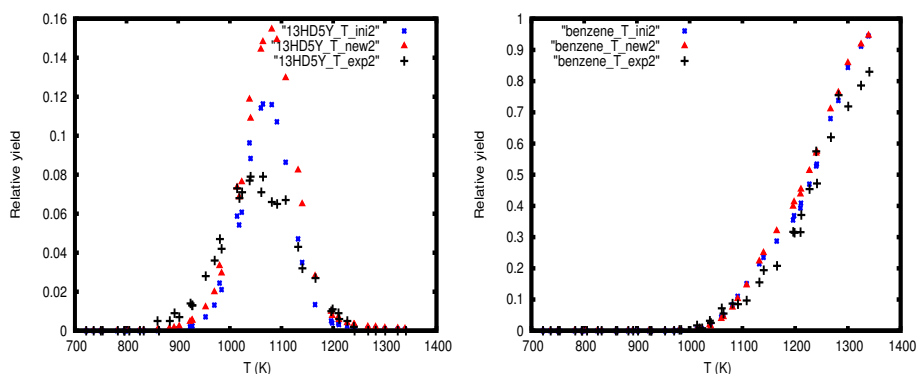


Figure 7.52: 13HD5Y and benzene profiles for the pyrolysis of propargyl

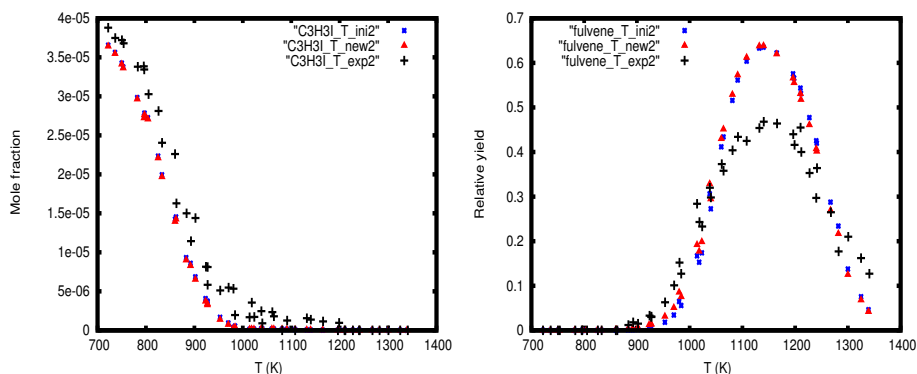


Figure 7.53: C3H3I and fulvene profiles for the pyrolysis of propargyl

The four remaining profiles 2E13BD, 12HD5Y, 15HD, and 34DMCB, are characterized by gigantic discrepancies (figures 7.54 - 7.55).

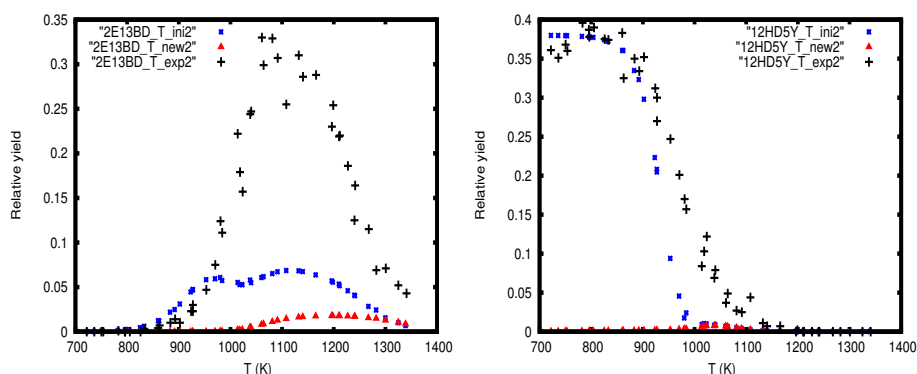


Figure 7.54: 2E13BD and 12HD5Y profiles for the pyrolysis of propargyl

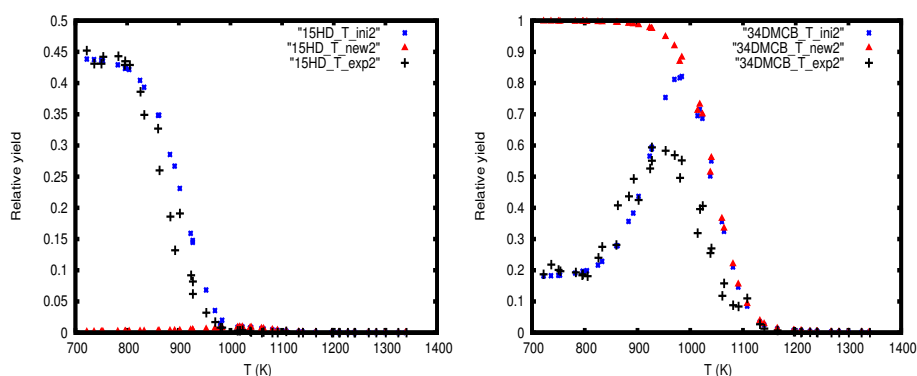


Figure 7.55: 15HD and 34DMCB profile for the pyrolysis of propargyl

It was the hope of the author that a system at least valid for 1,5-hexadiene pyrolyses could be found in this manner, but this proved not possible. The extent of the differences is by far too great to be attributed to unknown reaction pathways playing a role for propargyl pyrolysis but not for 1,5-hexadiene pyrolysis. The optimization problem of this sub-section was underdetermined in that many sets of reasonable parameter values could lead to an agreement with the 1,5-hexadiene experiments alone. If no further information from propargyl experiments is introduced, an almost perfect fit having nothing to do with reality was attained. This shows the importance to always include as much experimental information as possible while carrying out an optimization. The same optimization was then started with inclusion of the pyrolyses of propargyl. No significant improvement was achieved in comparison with the initial concentration values, neither with norm 1 nor with norm2.

7.4 Addition of two isomerization reactions to the mechanism Ma

As it has been shown previously, the greatest discrepancies between the model predictions and the experiments concern the profile of 2E13BD, which is formed from 12HD5Y. The reaction mechanism of Tang et al. [59] and the mechanism Ma do not include however all potentially important reaction pathways related to 12HD5Y. Tranter et al. [61] pointed out that an isomerization step between 15HD and 12HD5Y could not be excluded. Likewise, Miller et al. [31] found an apparent isomerization between 12HD5Y and 34DMCB which predominantly removed 12HD5Y. Thus those two steps were added in order to start a new optimization. The initial parameters of $15\text{HD} \rightleftharpoons 12\text{HD5Y}$ were the same as those of $15\text{HD} \rightleftharpoons 34\text{DMCB}$, namely $A_0 = 6.50\text{E}+10 \text{ s}^{-1}$, $n_0 = 0.00$ and $E_{a,0} = 139.61 \text{ kJ mol}^{-1}$. Since the true values are unknown, large variation intervals were allowed:

$$6.5\text{E}+07 \leq A \leq 6.5\text{E}+13 \text{ s}^{-1},$$

$$-2.7 \leq n \leq 2.7,$$

$$0 \leq E_a \leq 1.9\text{E}+02 \text{ kJ mol}^{-1}.$$

Similarly, the initial parameters of $34\text{DMCB} \rightleftharpoons 12\text{HD5Y}$ were set equal to those of $34\text{DMCB} \rightleftharpoons 13\text{HD5Y}$, namely $A_0 = 4.10\text{E}+12 \text{ s}^{-1}$, $n_0 = 0.00$ and $E_{a,0} = 211.46805 \text{ kJ mol}^{-1}$. The parameters were also allowed to vary within large bounds:

$$4.1\text{E}+09 \leq A \leq 4.1\text{E}+15 \text{ s}^{-1},$$

$$-2.7 \leq n \leq 2.7,$$

$$0 \leq E_a \leq 261.47 \text{ kJ mol}^{-1}.$$

As in the previous sections, the following inequalities had to hold for all other parameters:

$$\frac{A_0}{1000} \leq A \leq 1000A_0,$$

$$n_0 - 2.7 \leq n \leq n_0 + 2.7,$$

$$E_{a,0} - 50 \leq E_a \leq E_{a,0} + 50 \text{ kJ mol}^{-1},$$

and for the first three recombination reactions additional constraints were

$$\frac{k_0}{10} \leq k \leq 10k_0.$$

In spite of the absence of bounds, the optimized rate coefficients of all isomerization steps are included within a factor ten from the initial values for all

considered temperatures. The optimization improved the predictions of the profiles of 2E13BD, 13HD5Y, benzene and fulvene for the pyrolysis of 1,5-hexadiene; benzene and fulvene for the pyrolysis of propargyl, as reported in figures 7.56 - 7.58.

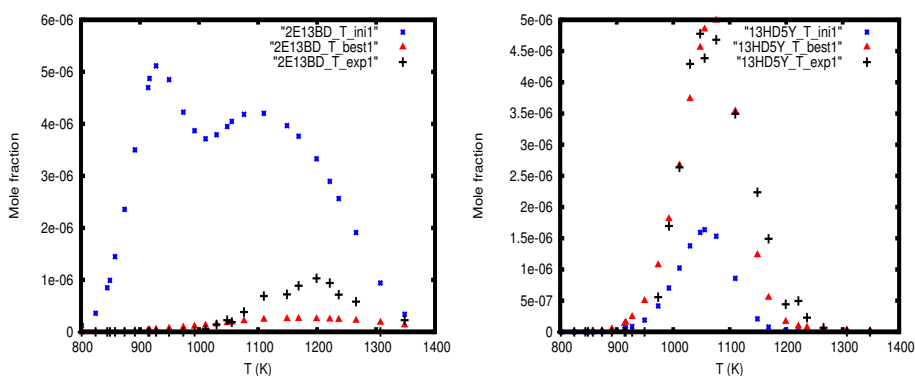


Figure 7.56: 2E13BD and 13HD5Y profiles for the pyrolysis of 1,5-Hexadiene

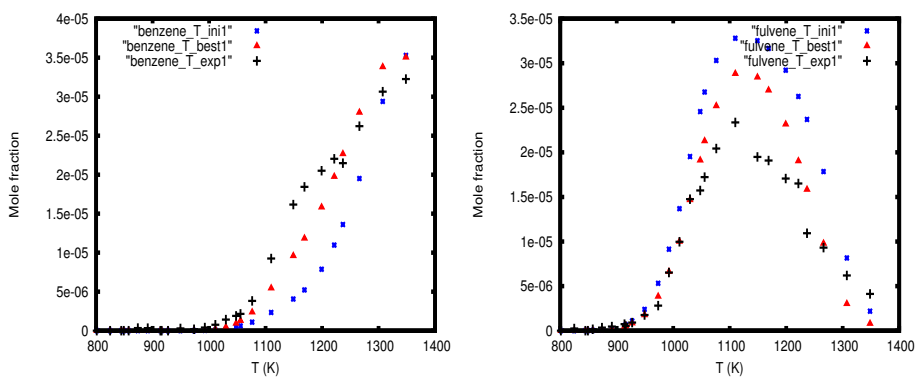


Figure 7.57: Benzene and fulvene profiles for the pyrolysis of 1,5-Hexadiene

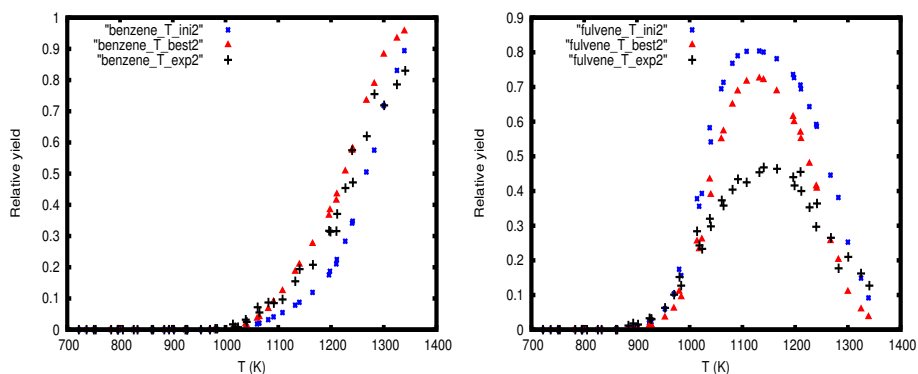


Figure 7.58: Benzene and fulvene profiles for the pyrolysis of propargyl

The quality of the predictions was unchanged for the profiles of 12HD5Y, 15HD and C3H3I for the pyrolysis of propargyl and for the profile of 34DMCB for the pyrolysis of 1,5-hexadiene. The optimization made the predictions of the profiles of 2E13BD, 13HD5Y and 34DMCB for the pyrolysis of propargyl worse, as shown in figures 7.59 and 7.60.

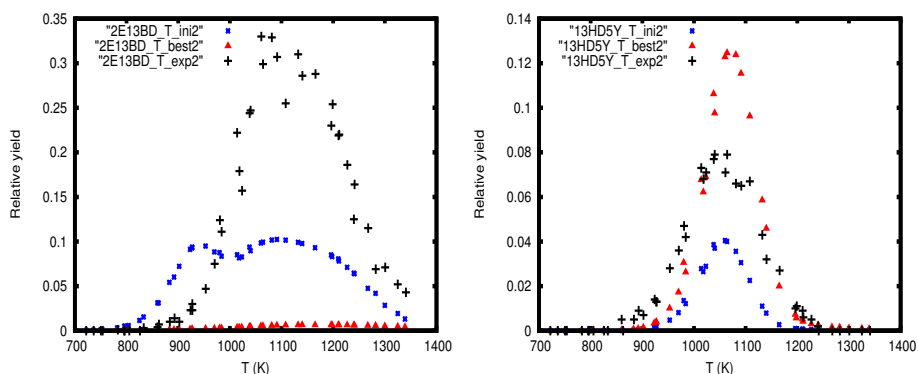


Figure 7.59: 2E13BD and 13HD5Y profiles for the pyrolysis of propargyl

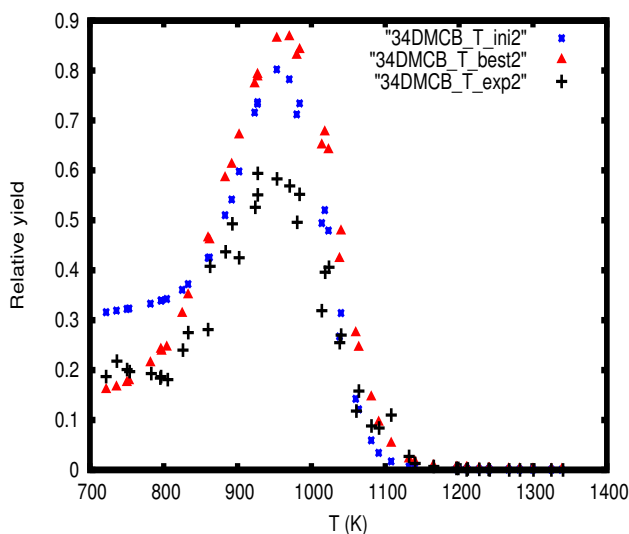


Figure 7.60: 34DMCB-profile for C₃H₃-pyrolysis

It is clear that the optimized model is not in agreement with the experiments.

7.5 Conclusion of the optimization trials

After having carried out wide-ranging experiments about the pyrolysis of 1,5-hexadiene [61] and then propargyl [58], Tang et al. assumed that a semi-detailed mechanism consisting of 14 reaction steps would be sufficient to accurately describe the chemistry underlying the C₃H₃ system [59]. Since the kinetic coefficients were largely unknown, they decided to optimize them against their own experimental data. The resulting model was in fairly good agreement with the set of experimental data. However, their model is unphysical for two reasons:

1. they carried out their optimization independently from thermochemistry, the inclusion of reliable thermodynamic coefficients (7.2.2) showed some reaction rates to be thermodynamically inconsistent,
2. their mechanism can only account for the formation of 2E13BD during the pyrolysis of 1,5-hexadiene by transforming fulvene molecules into 2E13BD, which is physically very unlikely (see 7.3.3).

During the present work, it has been tried to determine a physically meaningful reaction mechanism consistent with all experimental data about the C₃H₃ system at higher temperatures (700 K - 1400 K). A new reaction mechanism

(Ma) accounting for the thermochemistry was built based on the mechanism of Tang et al (see 7.2.1). Since the agreement of Ma with the experiments was already good for many profiles, *the initial expectation* was that the re-optimization of the isomerization reaction parameters would be enough to match the experimental observations. The greatest discrepancies concerned the profiles of 2E13BD: for the pyrolysis of 1,5-hexadiene, the concentration increase is too strong and too early, for the pyrolysis of propargyl the concentration remains too low. The optimization of all isomerisation reactions within large intervals failed to improve the situation. Optimal profiles in agreement with the experiments could be obtained while optimizing at the same time the three recombination reactions, but only by imposing unrealistically low values for the reaction rate coefficients. The recombination and isomerization reaction parameters could be successfully adapted to the profiles of 1,5-hexadiene pyrolysis. The model optimized in this way failed however to accurately predict the measurements from propargyl pyrolysis. The addition of two additional isomerization reactions which were optimized along with the other reactions considered previously failed to lead to results consistent with the experiments. This shows that *contrarily to the initial expectation*, the C_3H_3 reaction system is more complex than the reaction steps proposed by Tang et al [59]. Further experimental investigations are required in order to resolve the problems involved here. Shock tube pyrolysis experiments of 12HD5Y and 2E13BD should prove extremely valuable to bring up the information necessary for understanding the yet unknown reaction pathways.

Chapter 8

Conclusion

The use of detailed reaction mechanisms in combustion chemistry has brought up a substantial gain of conceptual and practical knowledge. Once suitable elementary reactions have been found, the determination of accurate parameters in agreement with the experiments lies at the very core of the undertaking. Over the recent decades, methods from computational chemistry have become more widely utilized but often lead to considerable uncertainties. Therefore experimental measurements remain extremely relevant for the estimation of chemical kinetic parameters.

The traditional approach has been to choose experimental conditions in such a way that only a few reactions play a role and an analytical solution of the underlying system of ordinary differential equations is possible. In this manner, concentrations and other variables like ignition delay times can be expressed as analytical functions of the parameters p , which then define the value of the distance $d(p)$ between the experimental results and the model predictions. This distance itself may be minimized by differentiating it, thereby determining the optimal values of the parameters within the measurement uncertainties. The main shortcoming of this method is the extreme difficulty or even impossibility to isolate many elementary reactions in a way that would enable an analytical solution.

The use of numerical optimization methods relying on the solution of the ODE systems describing the experiments is a natural and legitimate extension of the approach followed by kineticists for decades.

In the present work, the package Kinefit has been developed for the optimization of kinetic parameters. It relies on the software Homrea for the numerical solution of the ODE systems describing homogeneous combustion systems whereby variables only depend on time. The distance $d(p)$ can then be numerically calculated, and four optimization methods were implemented to minimize it: a genetic algorithm, an adaptive random search, and two

trust-region based methods, Broyden-C-G and Condor.

To verify the reliability of the minimization methods, parameter estimation problems were constructed using the $\text{H}_2 - \text{O}_2$ part of the GRI-mechanism 3.0 [54]. Artificial experimental data were generated using the initial values of the parameters, some of which were then modified in a such a way to introduce discrepancies between model and experiment. It was then checked that the optimization methods are capable of retrieving the perfect agreement existing for the initial parameter values. One cause of oscillations of the distance $d(p)$ and local minima was identified, it is the exponential decrease of concentrations related to self-ignition phenomenon. Optimization problems based on six experiments with respectively three profiles were constructed. The optimization methods were first validated for problems without self ignition. It was shown that they can reliably identify optimal parameter sets for problems involving respectively 6 pre-exponential factors, six pre-exponential factors located on bounds while using the penalty terms and 6 pre-exponential factors, temperature coefficients and activation energies. The optimization methods were then validated for problems where a significant amount of oscillations come up. All methods were able to solve a problem involving seven parameters, all methods except one could solve a problem with 7 temperature coefficients and activation energies. All optimization methods failed for a complex problem involving seven pre-exponential factors, temperature coefficients and activation energies.

The GRI-mechanism 3.0 with its initial values leads to considerable discrepancies with real experiments involving the pyrolysis of CH_3 and C_2H_6 [47]. Through the program package Kinefit it was shown that these experiments do not refute the GRI-mechanism since a good agreement could be achieved with realistic parameter values.

Methods for reducing reaction mechanisms are frequently employed in the context of chemical kinetic optimization and can be relevant for problems related to soot formation, which involve the use of large reaction mechanisms. Consequently, a mechanism reduction program was developed in C++ and validated during this work. The reliability of reduction methods for parameter optimization was investigated with an example involving the previous experiments of CH_3 and C_2H_6 pyrolysis. The results indicate that parameters must be varied within narrow intervals for the reliable use of reaction mechanism reduction methods.

Since propargyl C_3H_3 is an important species for the formation of soot and its precursors PAH [50], [33], Kinefit was used to optimize a semi-detailed reaction mechanism accounting for the pyrolyses of the propargyl radical and 1,5-hexadiene [59]. A good agreement with all experimental profiles could only be attained by strongly decreasing the reaction rate coefficients of propar-

gyl recombination reactions. The optimized values are unlikely because they contradict numerous measurements and theoretical calculations of the global C_3H_3 recombination rate coefficient. This shows that several reaction steps are probably unknown and that further experimental investigations of the system are needed.

Bibliography

- [1] I.P. Androulakis. Kinetic mechanism reduction based on an integer programming approach. *AIChE Journal*, 46(2): 361, 2000.
- [2] J. Appel, H. Bockhorn, and M. Frenklach. *Proc. Combust. Inst.*, 28: 1519, 2000.
- [3] P.W. Atkins. *Physical Chemistry*. Freeman, New York, fifth edition, 1996.
- [4] Krestinin A.V. Kinetic model of soot formation from acetylene in different mixtures at temperatures higher than 1600 k. *Chim. Phys. Reports.*, 6(3): 342, 1987.
- [5] Krestinin A.V. Polyne model of soot formation process. *Proc. Combust. Inst.*, 27: 1557, 1998.
- [6] M. Balthasar and M. Frenklach. Detailed kinetic modeling of soot aggregate formation in laminar premixed flames. *Combust. Flame.*, 140: 130, 2005.
- [7] S. Bekki. On the possible role of aircraft-generated soot in the middle latitude ozone depletion. *Journal of Geophysical Research*, 102(10):751, 1997.
- [8] A. Burcat. *Combustion Chemistry., Chapter Thermochemical Data for Combustion*. Springer-Editions, New York, first edition, 1984.
- [9] M. Carlier, C. Corre, R. Minetti, J-F. Pauwels, M. Ribaucour, and L-R. Sochet. Autoignition of butane: a burner and a rapid compression machine study. *Proc. Combust. Inst.*, 23(4): 1753, 1990.
- [10] W.D. Dockery. Epidemiologic evidence of cardiovascular effects of particulate air pollution. *Environ. Health Perspect.*, 109(4): 483, 2001.

- [11] W.D. Docvkery. Epidemiologic evidence of cardiovascular effects of particulate air pollution. *Environement Health Perspectives*, 109(4): 483, 2001.
- [12] R. X. Fernandes, H. Hippler, and M. Olzmann. *Proc. Combust. Inst.*, 30: 1033, 2005.
- [13] M. Frenklach and H. Wang. *Detailed Kinetic Modelling of Soot Particle Formation*. Springer, New York, 1994.
- [14] Michael Frenklach. Process informatics for combustion chemistry. *31-th International Symposium on Combustion, Heidelberg*, page 1, 2006.
- [15] W.C. Gardiner. *Gas-Phase Combustion Chemistry*. Springer, New York, first edition, 2000.
- [16] Luther K. Troe J. Gilbert, J. Theory of thermal unimolecular reactions in the fall-off range. ii. weak collision rate constants. *Ber. Bunsenges. Phys. Chem.*, 87: 169, 1983.
- [17] R. Q. Gonzales. *Evaluation of a Detailed Reaction Mechanism for Partial and Total Oxidation of C1-C4 Alkanes*. PhD thesis, University of Heidelberg, 2007.
- [18] C. Heghes. *Soot Formation Modeling during Hydrocarbon Pyrolysis and Oxidation behind Shock Waves*. PhD thesis, University of Heidelberg, 2006.
- [19] G.L. Heller. Vortex reactor for carbon black manufacture. *US Patent*, 3,490,869: 1970.
- [20] J. C. Ianni. A comparison of the bader-deuffhard and the cash-karp runge-kutta integrators for the gri-mech 3.0 model based on the chemical kinetics code kintecus. *Second MIT Conference on Computational Fluid and Solid Mechanics*, page 1368, 2003.
- [21] R.J. Kee, F.M. Rupley, and J.A. Miller. Janaf thermochemical tables. *Sandia Report*, page 1, 1987.
- [22] R.D. Kern, H.J. Singh, and C.H. Wu. Thermal decomposition of 1,2 butadiene. *Int. J. Chem. Kinet.*, 20: 731, 1988.
- [23] V.V. Kislov and Mebel A.M. An ab initio g3-type/statistical theory study of the formation of indene in combustion flames. ii. the pathways originating from reactions of cyclic c5 species-cyclopentadiene and

- cyclopentadienyl radicals. *Journal of Physical Chemistry A*, 112: 700, 2008.
- [24] S. Koerkel. *Numerische Methoden fr Optimale Versuchsplanungsprobleme bei nichtlinearen DAE-Modellen*. PhD thesis, University of Heidelberg, 2002.
- [25] S.H. Lam. Using csp to understand complex chemical kinetics. *Combustion, Science and Technology*, 89: 375, 1993.
- [26] L. Liang, J.G. Stevens, J.T. Farrell, P.T. Huynh, I.P. Androulakis, and M. Ierapetritou. An adaptive approach for coupling detailed chemical kinetics and multidimensional cfd. *5th US Combustion Meeting- Paper C09*, page 1, 2007.
- [27] A.E. Lutz, R.J. Kee, and J.A. Miller. Senkin: A fortran program for predicting homogeneous gas phase chemical kinetics with sensitivity analysis. *SAND87-8248*, Sandia National Laboratories, page 4, 1988.
- [28] S.H. Luu and J. Troe. Intermolecular energy transfer in the photoisomerization of cycloheptatriene. *Ber. Bunsenges. Phys. Chem.*, 77:325, 1973.
- [29] U. Maas and S.B. Pope. Simplifying chemical kinetics: Intrinsic low-dimensional manifolds in composition space. *Combustion and Flame*, 88: 239, 1992.
- [30] J. V. Michael and K. P. Lim. Shock tube techniques in chemical kinetics. *Annu. Rev. Phys. Chem.*, 44: 429, 1993.
- [31] C.H Miller, W. Tang, R.S. Tranter, and K. Brezinsky. Shock tube pyrolysis of 1,2,4,5-hexatetraene. *J. Phys. Chem. A*, 110: 3605, 2006.
- [32] J. A. Miller and S. Klippenstein. *S. J. J. Phys. Chem. A*, 107: 7783, 2003.
- [33] J.A. Miller and C.F.. Melius. Kinetic and thermodynamic issues in the formation of aromatic compounds in flames of aliphatic fuels. *Combustion and Flame*, 91: 21, 1992.
- [34] P. Minutolo, G. Gambi, A. DAlessio, A. DAnna, and M. V. Johnston. Optical and spectroscopic characterization of rich premixed flames across the soot formation threshold. *Combust. Sci. Tech.*, 101: 311, 1994.

- [35] P. Mitchell and M. Frenklach. Particle aggregation with simultaneous surface growth. *Phys. Rev. E*, 67(6): 1, 2003.
- [36] C. J. Montgomery, M.A. Cremer, J.-Y. Chen, C.K. Westbrook, and L.Q. Maurice. Reduced chemical kinetic mechanisms for hydrocarbon fuels. *Journal of Propulsion and Power*, 18(01): 2002.
- [37] I. I. Naydenova. *Soot Formation Modeling during Hydrocarbon Pyrolysis and Oxidation behind Shock Waves*. PhD thesis, University of Heidelberg, 2007.
- [38] M.A. Oehlschlaeger, D.F. Davidson, and R.K. Hanson. Shock tube measurements of ethane, propane, and butane decomposition using laser absorption of CH_3 . *WSSCI Fall 2003 Meeting*, page 2003.
- [39] B. Oktem, M. P. Tolocka, B. Zhao, H. Wang, and M. V. Johnston. Chemical species associated with the early stage of soot growth in laminar premixed ethylene-oxygen-argon flame. *Combust. and Flame*, 142: 364, 2005.
- [40] L. Petzold and W. Zhu. Model reduction for chemical kinetics: An optimization approach. *AIChE Journal*, 45(4): 869, 1999.
- [41] C. J. Pope and J. A. Miller. *J. A. Proc. Combust. Inst.*, 28: 1519, 2000.
- [42] C.A. Pope, R.T. Burnett, M.J. Thun, E.E Valle, D. Krewski, K. Ito, and G.D Thurston. Lung cancer, cardiopulmonary mortality, and long-term exposure. *American Medical Association (JAMA)*, 287: 1132, 2002.
- [43] W.H. Press, B.P. Flannery, S. Teukolsky, and W.T. Vetterling. *Numerical Recipes: The Art of Scientific Computing*. Press Syndicate of the University of Cambridge, Cambridge, first edition, 1989.
- [44] H. Richter, S. Granata, W.H. Green, and J.B. Howard. Detailed modelling of PAH and soot formation in a laminar premixed benzene/oxygen/argon low-pressure flame. *Proc. Combust. Inst.*, 30: 1397, 2005.
- [45] H. Richter and J. B. Howard. Formation and consumption of single-ring aromatic hydrocarbons and their precursors in premixed acetylene, ethylene and benzene flames. *Phys. Chem. Chem. Phys.*, 4: 2038, 2002.
- [46] T. Russi, A. Packard, R. Feeley, and M. Frenklach. Sensitivity analysis of uncertainty in model prediction. *J. Phys. Chem. A.*, 112(12): 2579, 2008.

- [47] K. Saito, R. Ito, T. Kakumoto, and A. Imamura. The initial process of the oxidation of the methyl radical in reflected shock waves. *The Journal of Physical Chemistry*, 90(7): 1422, 1986.
- [48] A. Saltelli, M. Ratto, S. Tarantola, and F. Campolongo. Sensitivity analysis for chemical models. *Chemical Review C, American Chemical Society*, Published on Web, 2004.
- [49] A. Saylam, M. Ribaucour, M. Carlier, and R. Minetti. Reduction of detailed kinetic mechanisms using analyses of rate and sensitivity of reactions: Application to iso-octane and n-heptane. *Proceedings of the European Combustion Meeting 2005*, page 1, 2005.
- [50] S. Scherer. *Untersuchung pyrolytischer Reaktionen des Russvorläufermolekuls Propargyl im Stosswellenrohr*. PhD thesis, University of Stuttgart, 2001.
- [51] N. Shenvi, J. M. Geremia, and H. Rabitz. Nonlinear kinetic parameter identification through map inversion. *J. Phys. Chem. A*, 106: 12315, 2002.
- [52] A. B. Singer, J. W. Taylor, P. I. Barton, and W. H. Green. Global dynamic optimization for parameter estimation in chemical kinetics. *J. Phys. Chem. A.*, 110: 971, 2006.
- [53] M. S. Skjoeth-Rasmussen, P. Glarborg, M. Oestberg, J. T. Johannessen, H. Livbjerg, A. D. Jensen, and T.S. Christensen. Detailed modeling of pah and soot formation in a laminar premixed benzene/oxygen/argon low-pressure flame. *Combustion and Flame*, 136: 91, 2004.
- [54] G.P. Smith et.al. Gri-mechanism 3.0. www.me.berkeley.edu/gri-mech.
- [55] H.S. Soyhan, F. Mauss, and C. Sorousbay. Chemical kinetic modeling of combustion in internal combustion engines using reduced chemistry. *Combustion Science and Technology*, 174(11,12): 73, 2002.
- [56] S. E. Stein, J. A. Walker, M. M. Suryan, and A. Fahr. A new path of benzene in flames. *Proc. Comb. Inst.*, 23: 85, 1991.
- [57] D.R. Stull and H. Prophet. Janaf thermochemical tables. *Department of Commerce, Washington DC Technical Report*, page 1, 1971.
- [58] W. Tang, R.S. Tranter, and K. Brezinsky. Isomeric product distributions from the self-reaction of propargyl radicals. *J. Phys. Chem. A*, 109: 6056, 2005.

- [59] W. Tang, R.S. Tranter, and K. Brezinsky. An optimized semidetailed submechanism of benzene formation from propargyl recombination. *J. Phys. Chem. A*, 110: 2165, 2006.
- [60] Weiyong Tang, Libin Zhang, Andreas.A. Linninger, Robert S. Tranter, and Brezinsky. Solving kinetic inversion problems via a physically bounded gauss-mewton (pgn) method. *Industrial and Engineering Chemistry Research*, 44(10): 3626, 2005.
- [61] R.S. Tranter, W Tang, K.B. Anderson, and K. Brezinsky. Shock tube study of thermal rearrangement of 1,5-hexadiyne over wide temperature and pressure regime. *J. Phys. Chem. A*, 108: 3406, 2004.
- [62] J. Troe. Predictive possibilities of unimolecular rate theory. *The Journal of Physical Chemistry*, 83: 114, 1979.
- [63] J. Troe. *Ber. Bunsenges. Phys. Chem.*, 87: 161, 1983.
- [64] B. Unterreiner, M. Sierka, and R. Ahlrichs. Reaction pathways for growth of polycyclic aromatic hydrocarbons under combustion conditions, a dft study. *Phys. Chem. Chem. Phys.*, 26(4-6): 565, 2004.
- [65] V. Vasudevan, D. F. Davidson, and R. K. Hanson. Shock tube measurements of toluene ignition times and oh concentrations time histories. *Proceedings of the Combustion Institute*, 30: 1155, 2005.
- [66] A. Violi, Sarofim A.F., and Truong T.N. Quantum mechanical study of molecular weight growth process by combination of aromatic molecules. *Combustion and Flame*, 126: 1506, 2001.
- [67] H. Wang and M. Frenklach. A detailed kinetic modeling study of aromatics formation in laminar premixed acetylene and ethylene flames. *Combustion and Flame*, 110: 173, 1997.
- [68] J. Warnatz, U. Maas, and R.W. Dibble. *Combustion: Physical and Chemical Fundamentals, Modeling and Simulation, Experiments, Pollutant Formation*. Springer-Editions, Berlin, third edition, 2001.
- [69] P.R. Westmoreland, A.M. Dean, J.B. Howard, and J.P. Longwell. Forming benzene in flames by chemically activated isomerization. *J. Phys. Chem.*, 93: 8171, 1989.

- [70] T. Zeuch. *Reaktionskinetik von Verbrennungsprozessen in der Gasphase: Spektroskopische Untersuchungen der Geschwindigkeit, Reaktionsprodukte und Mechanismen von Elementarreaktionen und die Modellierung der Oxidation von Kohlenwasserstoffen mit detaillierten Reaktionsmechanismen*. PhD thesis, University of Goettingen, 2003.
- [71] I. GY. Zsely, J. Zador, and T. Turanyi. On the similarity of the sensitivity functions of methane combustion models. *Combustion Theory and Modelling*, 9(4): 721, 2005.

List of Figures

2.1	Thermodynamic data of oxygen	13
2.2	Energy profile of an elementary reaction	15
2.3	Scheme of a typical shock tube, Karlsruhe institute for technology, http://www.ipc.uni-karlsruhe.de/mol/84.php	20
4.1	Distance between the modified model and the experiment as function of the first parameter	45
4.2	$[\text{H}_2\text{O}_2](A_1)$ at the 21-th time point	45
4.3	$[\text{H}_2\text{O}_2](A_1)$ at the 38-th time point	46
4.4	$[\text{H}_2\text{O}_2](A_1)$ at the 63-th time point	46
4.5	$[\text{H}_2\text{O}_2](A_1)$ at the 65-th time point	47
4.6	$[\text{H}_2\text{O}_2](t)$	48
4.7	$[\text{H}_2\text{O}_2](t)$	48
4.8	$[\text{H}_2\text{O}_2](t)$	49
4.9	$d(A_1)$	51
4.10	$d(A_2)$	51
4.11	$d(A_3)$	52
4.12	$d(A_4)$	52
4.13	$d(A_5)$	53
4.14	$d(A_6)$	53
4.15	OH, 1-st experiment	54
4.16	H_2O_2 , 4-th experiment	54
4.17	H_2O , 6-th experiment	55
4.18	Compared performances of the optimization techniques	56
4.19	Compared performances of the optimization techniques	58
4.20	Compared performances of the optimization techniques	60
4.21	$d(A_1)$	62
4.22	$d(A_2)$	62
4.23	$d(A_3)$	63
4.24	$d(A_4)$	63
4.25	$d(A_5)$	64
4.26	$d(A_6)$	64

4.27	$d(A_7)$	65
4.28	OH-profile for the second experiment	66
4.29	H_2O_2 -profile for the second experiment	66
4.30	H_2O_2 -profile for the fourth experiment	67
4.31	Compared performances of the optimization techniques	68
4.32	Bobyqa, H_2O_2 -profiles, 1-st experiment	69
4.33	Bobyqa, H_2O_2 -profiles, 4-st experiment	70
4.34	Bobyqa, OH-profile, 5-th experiment	70
4.35	Bobyqa, H_2O -profile, 3-rd experiment	71
4.36	Condor, H_2O -profile, 1-st experiment	71
4.37	Condor, H_2O_2 -profile, 3-rd experiment	72
4.38	Condor, OH-profile, 6-th experiment	72
4.39	Compared performances of the optimization techniques	73
4.40	Condor, OH-profile, 1-th experiment	75
4.41	Condor, OH-profile, 3-rd experiment	75
4.42	Condor, H_2O_2 -profile, 5-th experiment	76
4.43	Condor, H_2O_2 -profile, 6-th experiment	76
4.44	Condor, OH-profile, 2-th experiment	77
4.45	Condor, H_2O_2 -profile, 2-nd experiment	78
4.46	Condor, OH-profile, 2-nd experiment	79
4.47	Compared performances of the optimization techniques	81
4.48	Distance as function of n_3	83
4.49	Distance as function of A_4	83
4.50	Distance as function of A_5	84
4.51	Distance as function of A_6	84
4.52	Distance as function of A_1	85
4.53	Distance as function of n_2	85
4.54	CO-profile optimized by the GA	86
4.55	C_2H_4 -profile optimized by the GA	86
4.56	Distance as function of A_1	87
4.57	Distance as function of n_2	88
5.1	Q_1 for $O + CH_3 \rightleftharpoons H + CH_2O$	97
5.2	Q_2 for $O + CH_2O \rightleftharpoons OH + HCO$	98
5.3	Q_3 for $O + C_2H_6 \rightleftharpoons OH + C_2H_5$	98
5.4	First experiment	99
5.5	Second experiment	99
5.6	Third experiment	99
5.7	Fourth experiment	99
5.8	Fifth experiment	99
5.9	Sixth experiment	99

5.10	Seventh experiment	100
5.11	Eighth experiment	100
5.12	Ninth experiment	100
5.13	Tenth experiment	100
5.14	Eleventh experiment	100
5.15	Twelvth experiment	100
5.16	Consistency likelihood as function of the standard deviation .	101
6.1	Comparison between the detailed and reduced mechanisms for the CO profile of the second experiment	108
6.2	Comparison between the detailed and reduced mechanisms for the OH profile of the second experiment	108
6.3	Distribution of the maximum error for a reduction tolerance of 0.01	111
6.4	Distribution of the maximum error for a reduction tolerance of 0.02	111
6.5	Distribution of the maximum error for a reduction tolerance of 0.01	112
6.6	Distribution of the maximum error for a reduction tolerance of 0.02	112
6.7	Distribution of the maximum error for a reduction tolerance of 0.01	113
6.8	Distribution of the maximum error for a reduction tolerance of 0.02	113
6.9	Distribution of the maximum error for a reduction tolerance of 0.01	114
6.10	Distribution of the maximum error for a reduction tolerance of 0.02	114
7.1	A semidetailed kinetic model of propargyl recombination and subsequent C ₆ H ₆ isomerization. 15HD, 1,5-hexadiyne; 1245HT, 1,2,4,5-hexatetraene; 12HD5Y, 1,2-hexadiene-5-yne; 34DMCB, 3,4-dimethylenecyclobutene; 13HD5Y, 1,3-hexadiene-5-yne; 2E13BD, 2-ethynyl-1,3-butadiene. Taken from Tang et al. [59]	118
7.2	Distance as a function of A_4 (s ⁻¹)	120
7.3	Distance as a function of $E_{a,4}$ (kJ mol ⁻¹)	120
7.4	Distance as a function of A_5 (s ⁻¹)	121
7.5	Distance as a function of $E_{a,5}$ (kJ mol ⁻¹)	121
7.6	New mechanisms Ma(left) and Mb (right)	123
7.7	15HD-profile for its pyrolysis	124
7.8	34DMCB-profile for the pyrolysis of 1,5-Hexadiyne	124

7.9	12HD5Y-profile for C3H3-pyrolysis	125
7.10	34DMCB-profile for C3H3-pyrolysis	125
7.11	2E13BD-profile for 15HD-pyrolysis	126
7.12	2E13BD-profile for C ₃ H ₃ -pyrolysis	126
7.13	Fulvene-profile for C3H3-pyrolysis	127
7.14	Benzene-profile for 15HD-pyrolysis	127
7.15	Benzene-profile for C ₃ H ₃ -pyrolysis	128
7.16	13HD5Y-profile for propargyl pyrolysis	130
7.17	2E13BD-profile for 15HD-pyrolysis	130
7.18	2E13BD profile for propargyl pyrolysis	131
7.19	2E13BD-profile for 15HD-pyrolysis	132
7.20	2E13BD-profile for propargyl pyrolysis	132
7.21	13HD5Y profile for 1,5-hexadiyne pyrolysis	133
7.22	15HD profile for its own pyrolysis	133
7.23	C ₃ H ₃ I profile for its own pyrolysis	134
7.24	34DMCB profile for the pyrolysis of propargyl	134
7.25	12HD5Y profile for the pyrolysis of propargyl	135
7.26	34DMCB profile for the pyrolysis of 1,5-hexadiyne	135
7.27	15HD profile for the pyrolysis of propargyl	136
7.28	2E13BD-profile for Hexadiyne-pyrolysis	137
7.29	2E13BD-profile for C3H3-pyrolysis	137
7.30	13HD5Y-profile for C3H3-pyrolysis	138
7.31	34DMCB-profile for C3H3-pyrolysis	138
7.32	15HD-profile for C3H3-pyrolysis	139
7.33	Ratio k/k_0 for C3H3 +C3H3 =15HD	139
7.34	Ratio k/k_0 for C3H3 +C3H3 =34DMCB	140
7.35	Ratio k/k_0 for C3H3 +C3H3 = 12HD5Y	140
7.36	Ratio k/k_0 for 15HD = 34DMCB	141
7.37	Ratio k/k_0 for 34DMCB = fulvene	141
7.38	13HD5Y profile for the pyrolysis of 1,5-Hexadiyne	143
7.39	15HD profile for the pyrolysis of 1,5-Hexadiyne	143
7.40	34DMCB profile for the pyrolysis of 1,5-Hexadiyne	144
7.41	Benzene profile for the pyrolysis of 1,5-Hexadiyne	144
7.42	Fulvene profile for the pyrolysis of 1,5-Hexadiyne	145
7.43	2E13BD profile for the pyrolysis of 1,5-Hexadiyne	145
7.44	Reproduction of Tang's mechanism, added for the sake of clarity. 15HD, 1,5-hexadiyne; 1245HT, 1,2,4,5-hexatetraene; 12HD5Y, 1,2-hexadiene-5-yne; 34DMCB, 3,4-dimethylenecyclobutene; 13HD5Y, 1,3-hexadiene-5-yne; 2E13BD, 2-ethynyl-1,3-butadiene. Taken from Tang et al. [59]	146
7.45	Initial and optimized rate coefficients for C ₃ H ₃ + C ₃ H ₃ → 15HD.147	

7.46	Initial and optimized rate coefficients for $C_3H_3 + C_3H_3 \rightarrow$ 34DMCB.	147
7.47	Initial and optimized rate coefficients for $C_3H_3 + C_3H_3 \rightarrow$ 12HD5Y.	148
7.48	Initial and optimized rate coefficients for $15HD \rightleftharpoons 34DMCB$	149
7.49	Initial and optimized rate coefficients for $34DMCB \rightleftharpoons$ fulvene.	149
7.50	Initial and optimized rate coefficients for $13HD5Y \rightleftharpoons$ benzene.	150
7.51	Initial and optimized rate coefficients for $12HD5Y \rightleftharpoons 2E13BD$	150
7.52	13HD5Y and benzene profiles for the pyrolysis of propargyl	151
7.53	C3H3I and fulvene profiles for the pyrolysis of propargyl	151
7.54	2E13BD and 12HD5Y profiles for the pyrolysis of propargyl	152
7.55	15HD and 34DMCB profile for the pyrolysis of propargyl	152
7.56	2E13BD and 13HD5Y profiles for the pyrolysis of 1,5-Hexadyne 154	
7.57	Benzene and fulvene profiles for the pyrolysis of 1,5-Hexadyne	154
7.58	Benzene and fulvene profiles for the pyrolysis of propargyl	155
7.59	2E13BD and 13HD5Y profiles for the pyrolysis of propargyl	155
7.60	34DMCB-profile for C3H3-pyrolysis	156

List of Tables

2.1	Recombination reactions	16
2.2	Recombination reaction	19
4.1	Initial conditions	44
4.2	Modified reactions for the example which causes oscillations .	44
4.3	Initial conditions	50
4.4	Optimized parameters	55
4.5	Chosen parameters	56
4.6	Chosen parameters	57
4.7	Optimized parameters	57
4.8	Chosen parameters	59
4.9	Optimized parameters	59
4.10	Optimized rate coefficients at 1000 K	60
4.11	Initial conditions	61
4.12	Optimized parameters	65
4.13	Chosen parameters	68
4.14	Optimized parameters	69
4.15	Modified parameters	74
4.16	Optimized parameters	74
4.17	Modified parameters	77
4.18	Optimized parameters	78
4.19	Optimized reaction rate coefficients	80
4.20	Optimized parameters	82
4.21	Initial conditions	87
5.1	Initial conditions	91
5.2	Reactions chosen for the optimization	92
6.1	Experimental conditions considered	107
6.2	Reactions chosen for the optimization	110
7.1	Tang et al. C ₃ H ₃ -mechanism	118